Reviews in Mineralogy & Geochemistry
Vol. 56, pp. 431-493, 2004

Allanite and Other REE-Rich Epidote-Group Minerals

Reto Gieré
Institut für Mineralogie, Petrologie und Geochemie
Universität Freiburg
Albertstrasse 23b
D-79104 Freiburg, Germany
giere@uni-freiburg.de

Sorena S. Sorensen
Department of Mineral Sciences
National Museum of Natural History
Smithsonian Institution
Washington, D.C. 20560, U.S.A.
sorena@volcano.si.edu

INTRODUCTION

Epidote-group minerals rich in rare earth elements (REE), in particular allanite, are common accessory phases in igneous, metamorphic, metasomatic, and sedimentary rocks. Small amounts of REE are present in most epidote-group minerals, but in allanite—and the related minerals dissakisite, ferriallanite, dollaseite, khristovite and androsite—the REE are essential structural constituents. An important characteristic of REE-rich epidote-group minerals is that their octahedrally coordinated M sites contain major amounts of divalent cations. This paper summarizes literature data for these minerals and discusses their chemistry, occurrence, phase relations, and petrologic and geologic significance. The chapter emphasizes allanite, because it is the most common and best-studied of the REE-rich epidote-group minerals.

MINERAL CHEMISTRY AND NOMENCLATURE

Epidote-group minerals contain isolated silicon tetrahedra and corner-sharing groups of two tetrahedra, and are thus assigned to the disilicate or sorosilicate structural family (for a detailed description of the structure, see Franz and Liebscher 2004). The epidote-group structural formula is $A_2M_3(SiO_4)(Si_2O_7)(O,F)(OH)$, or in a simplified form $A_2M_3Si_3O_{11}(O,F)(OH)$, in which A = Ca, Sr, Pb^{2+}, Mn^{2+}, Th, REE^{3+}, and U, and M = Al, Fe^{3+}, Fe^{2+}, Mn^{3+}, Mn^{2+}, Mg, Cr^{3+}, and V^{3+} (Deer et al. 1986). There are two structurally different A sites, A(1) and A(2), with different coordination numbers, and there are three different M sites, M(1), M(2), and M(3), which are all octahedrally coordinated (Ueda 1955; Dollase 1971).

In epidote-group minerals, trivalent REE are accommodated in the A sites, which in endmember epidote both contain Ca. The incorporation of REE^{3+} is commonly charge balanced by a divalent cation (Fe^{2+}, Mn^{2+}, Mg) substituted for a trivalent one in the M sites (Table 1). In an attempt to clarify the nomenclature of the REE-dominant members of the

1529-6466/04/0056-0010$10.00

Table 1. Idealized formulae for clinozoisite, epidote, and piemontite, and for the REE-rich epidote-group minerals

	A(1)	A(2)	M(1)	M(2)	M(3)	T	O(4)	
Clinozoisite	Ca^{2+}	Ca^{2+}	Al^{3+}	Al^{3+}	Al^{3+}	Si_3O_{11}	O	OH
Epidote	Ca^{2+}	Ca^{2+}	Al^{3+}	Al^{3+}	Fe^{3+}	Si_3O_{11}	O	OH
Piemontite	Ca^{2+}	Ca^{2+}	Al^{3+}	Al^{3+}	Mn^{3+}	Si_3O_{11}	O	OH
Allanite	Ca^{2+}	REE^{3+}	Al^{3+}	Al^{3+}	Fe^{2+}	Si_3O_{11}	O	OH
Dissakisite	Ca^{2+}	REE^{3+}	Al^{3+}	Al^{3+}	Mg^{2+}	Si_3O_{11}	O	OH
Ferriallanite	Ca^{2+}	REE^{3+}	Fe^{3+}	Al^{3+}	Fe^{2+}	Si_3O_{11}	O	OH
Oxyallanite	Ca^{2+}	REE^{3+}	Al^{3+}	Al^{3+}	Fe^{3+}	Si_3O_{11}	O	O
Dollaseite	Ca^{2+}	REE^{3+}	Mg^{2+}	Al^{3+}	Mg^{2+}	Si_3O_{11}	F	OH
Khristovite	Ca^{2+}	REE^{3+}	Mg^{2+}	Al^{3+}	Mn^{2+}	Si_3O_{11}	F	OH
Androsite	Mn^{2+}	REE^{3+}	Mn^{3+}	Al^{3+}	Mn^{2+}	Si_3O_{11}	O	OH

epidote group, Ercit (2002) proposed the (unnecessary) term "allanite subgroup" for all REE-dominant varieties. Because Y is commonly found in allanite, in the rest of this chapter the abbreviation "REE" will include it.

The chemical data presented here were extracted from the literature (see Reference List) to produce a database for allanite and the other REE-rich epidote-group minerals. The database contains more than 1700 chemical analyses, comprising both older data obtained primarily via wet-chemical techniques and newer data obtained mostly by electron probe microanalysis. If Fe^{2+} and Fe^{3+} have been directly analyzed, we have used those values for the calculation of the molar values of each component in allanite. For all other cases, we have estimated Fe^{2+}/Fe^{3+} by normalizing the analysis to 12.5 oxygens and 8 cations. The database includes a large number of unpublished electron microprobe analyses provided by Dr. James Beard, Virginia Museum of Natural History (personal communication; 2004) as well as some of our own unpublished data. Literature sources containing data used in the diagrams of this chapter, but not referred to in the text, are provided in the Reference List and specially marked by an asterisk.

Allanite

Allanite, which is named after the Scottish mineralogist Thomas Allan (1777-1833), can be represented by the idealized formula $CaREEAl_2Fe^{2+}Si_3O_{11}O(OH)$. It is related to epidote by the coupled substitution

$$REE^{3+} + Fe^{2+} \leftrightarrow Ca^{2+} + Fe^{3+} \quad (1)$$

(Khvostova 1963; Ploshko and Bogdanova 1963) and to clinozoisite by

$$REE^{3+} + Fe^{2+} \leftrightarrow Ca^{2+} + Al^{3+} \quad (2)$$

Allanite and ferriallanite (Kartashov et al. 2002) are the only members of the epidote group in which Fe^{2+} is an essential constitutent (Table 1).

The structure of allanite is almost identical to that of other epidote-group minerals (Ueda 1955; Pudovkina and Pyatenko 1963; Dollase 1971; see also Franz and Liebscher 2004). It consists of two sets of chains of edge-sharing octahedra (M sites) arranged parallel to [010]. One of these is a composite chain that consists of M(1) octahedra with greatly distorted M(3) sites attached on alternate sides along its length (Fig. 1a). The other chain contains the M(2) octahedra, which are occupied only by Al (Dollase 1971, 1973). The chains are cross-linked by two types of tetrahedral (T) sites, i.e., by isolated SiO_4 tetrahedra and by corner-sharing

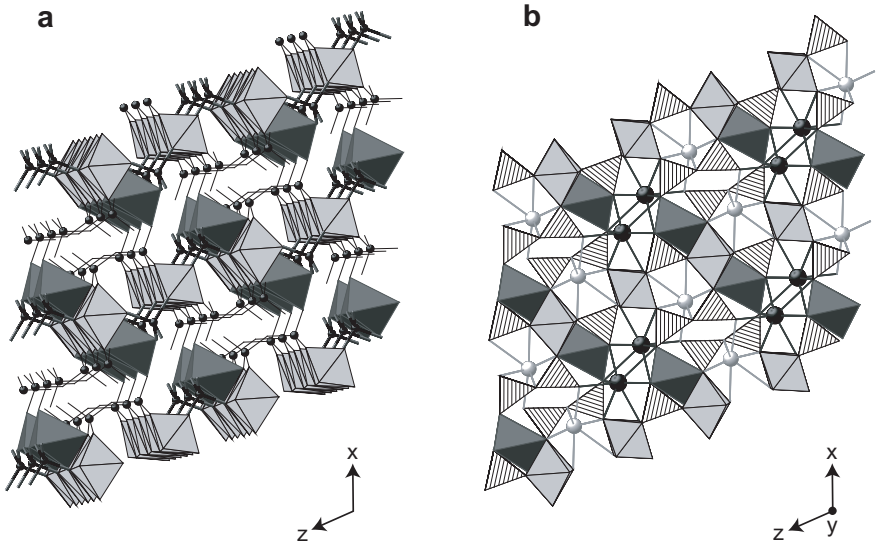

Figure 1. Crystal structure of allanite, drawn with CrystalMaker® using data from Dollase (1971). The structure consists of chains of edge-sharing octahedra, which are parallel to [010]: M(1) and M(2) sites are the light gray octahedra; M(3) octahedra are shown as dark octahedra. These chains are linked by single SiO_4 tetrahedra and double-tetrahedral groups (Si_2O_7). **a)** Simplified diagram showing M and T sites only, viewed slightly off the b axis: Si(3) forms an isolated SiO_4 group (shown as sphere with stick bonds); Si(1) and Si(2) share an oxygen, forming an Si_2O_7 group (shown as spheres with wire bonds). **b)** View parallel to the b axis: the SiO_4 and the Si_2O_7 groups are both shown as striated tetrahedra. The large cavities in the framework contain Ca^{2+} (small light gray spheres) and REE^{3+} (black spheres) in 9-fold and 11-fold coordination by oxygen, respectively.

pairs of tetrahedral groups (Si_2O_7). The A(1) and A(2) sites reside between the chains and the cross-links (Fig. 1b). In allanite, the A(1) site is occupied by Ca and is 9-fold coordinated, as it is in other epidote-group minerals, but the coordination polyhedron is less regular than in epidote. The A(2) site is 11-fold coordinated in allanite and contains the REE^{3+} (Dollase 1971). Nearly all Fe^{2+} occupies the distorted M(3) positions, but some Fe^{2+} may be present in the M(1) site (Dollase 1973). Even though the REE^{3+} typically enter the A(2) site, extended X-ray absorption fine structure spectra of Er^{3+} and Lu^{3+} environments in synthetic epidotes were interpreted as evidence of smaller REE accommodated in other sites, i.e., Er^{3+} in the A(1) site and Lu^{3+} in the M(3) octahedron (Cressey and Steel 1988). This conclusion, however, has not been corroborated by other data. The unit cell of allanite (Table 2) is larger than those of the clinozoisite-epidote series, and the volume increases with the REE and Fe contents (Fig. 2; Kumskova and Khostova 1964; Bonazzi and Menchetti 1995). This volume increase is correlated with the increase in the *b* value of the unit cell that results from incorporation of REE (Fig. 2) and Fe. Bonazzi and Menchetti (1995) showed that the presence of REE^{3+} decreases the unit-cell parameters *c* and β (Fig. 2). These authors derived equations that can be used to estimate the number of REE and Fe atoms per formula unit in allanite:

$$REE = 1.19 \times (115.41 - \beta) + 2.74 \times (10.160 - c) \quad (3)$$

$$Fe_{total} = 13.22 \times (b - 5.571) - 1.32 \times REE \quad (4)$$

The most common species in the allanite group is allanite-(Ce), which was first described by Thomson (1810). As is commonly observed in REE-rich minerals, however, other REE

Table 2. Lattice parameters, crystal system and space group for allanite and other REE-rich epidote-group minerals

	Epidote	**Allanite-(Ce) ***	**Dissakisite-(Ce)**	**Ferriallanite-(Ce)**	**Oxyallanite ****	**Dollaseite-(Ce)**	**Khristovite-(Ce)**	**Androsite-(La)**
Unit Cell Parameters								
a (Å)	8.914	8.927	8.905	8.962	8.893	8.934	8.903	8.896
b (Å)	5.640	5.761	5.684	5.836	5.683	5.721	5.748	5.706
c (Å)	10.162	10.150	10.113	10.182	10.369	10.176	10.107	10.083
β (°)	115.4	114.77	114.62	115.02	115.75	114.31	113.41	113.88
V (Å^3)	461.5	474.0	465.3	482.6	472.0	474.0	474.6	468.0
Z	2	2	2	2	2	2		2
Crystal System	monoclinic	monoclinic	monoclinic	monoclinic	monoclinic	monoclinic	monoclinic	monoclinic
Space Group	$P2_1/m$	$P2_1/m$	$P2_1/m$	$P2_1/m$		$P2_1/m$	$P2_1/m$	$P2_1/m$
Reference	Dollase (1971)	Dollase (1971, 1973)	Rouse and Peacor (1993)	Kartashov et al. (2002)	Dollase (1973)	Peacor and Dunn (1988)	Pautov et al. (1993)	Bonazzi et al. (1996)

* Allanite from Pacoima Canyon

** Allanite from Pacoima Canyon, CA, heat-treated in air for 118 h at 680°C. $Fe^{2+}/(Fe^{2+}+Fe^{3+}) = 0.12$

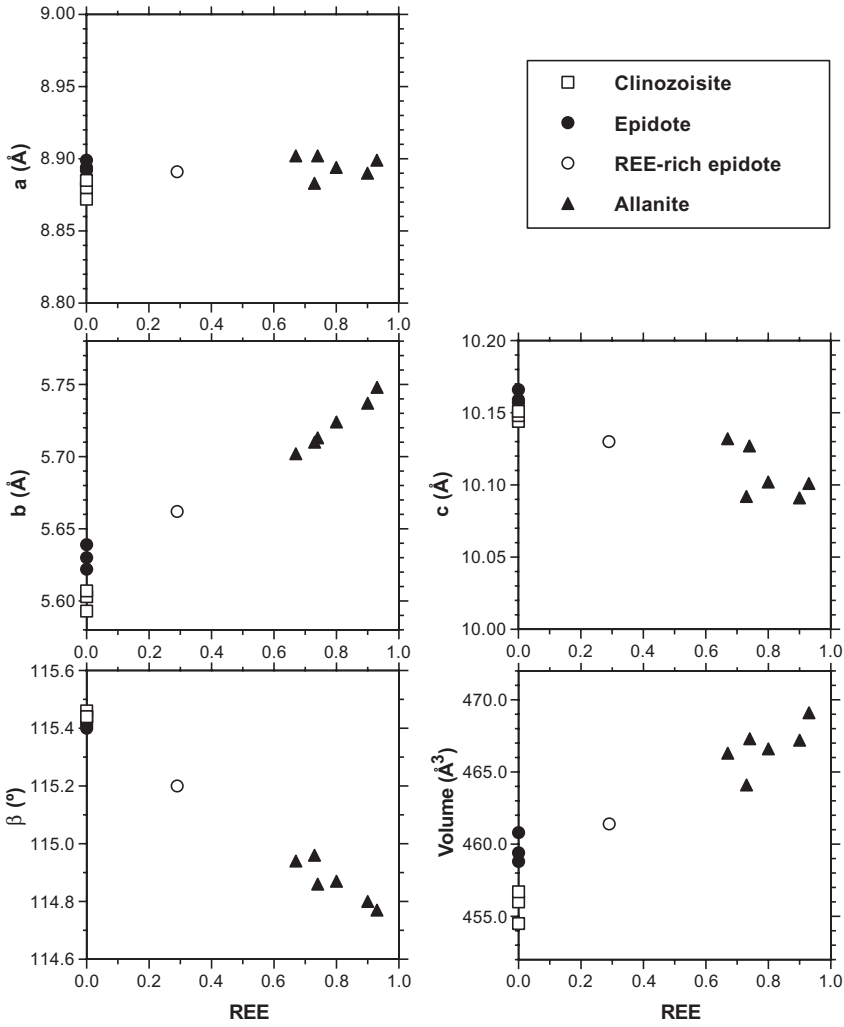

Figure 2. Change in values of the unit-cell parameters *a*, *b*, *c*, and β and of the unit-cell volume of allanite as a function of REE content (in atoms per formula unit). For comparison, the respective values for clinozoisite and epidote are shown. All data from Bonazzi and Menchetti (1995).

may predominate in certain specimens (e.g., Bayliss and Levinson 1988). La-dominant and Y-dominant allanite were reported in the literature before the introduction by Levinson (1966) of the currently valid nomenclature for rare earth minerals (Hutton 1951a,b; Zhirov et al. 1961; Neumann and Nilssen 1962; Semenov and Barinskii 1958, Hugo 1961). These species are now known as allanite-(La) and allanite-(Y), respectively. Additional occurrences of allanite-(La) and allanite-(Y) have been reported more recently (e.g., Pan and Fleet 1991; Peterson and MacFarlane 1993).

Allanite typically contains small amounts of Th and U and thus may be used as a geochronometer (see below). The presence of isotopes that emit α-particles, however, may lead to the partial or complete transformation of allanite from a crystalline to a metamict

state, in which the mineral is more susceptible to alteration (see below). The name orthite was introduced to emphasize a difference in habit from the characteristic tabular form of allanite: it has been used to describe crystals with prismatic habits, yet considerable degrees of alteration and hydration (Deer et al. 1986). This nomenclature, however, is not consistent with the occurrence of isotropic and birefringent varieties of both unaltered and altered hydrated allanite (Deer et al. 1986). Hutton (1951b) suggested that the name orthite be discontinued, and indeed it is no longer in use. The term "allanite", however, has been used quite loosely and inconsistently mainly because: 1) there is still no IMA-approved nomenclature in place for the epidote-group minerals; and 2) REE-rich epidote typically also contains substantial amounts of Th. The latter means that an analysis with REE+Th > 0.5 atoms per formula unit may be called allanite by some authors, whereas others would restrict the name for analyses with REE > 0.5 atoms per formula unit. In this review, we use the former definition. The term "REE-rich epidote" is applied to minerals in which REE are present in weight percent quantities.

Individual physical properties of allanite range widely (Table 3; see also Deer et al. 1986) because the mineral exhibits considerable compositional variability (Ploshko and Bogdanova 1963; Hickling et al. 1970) and various degrees of metamictization (e.g., Zenzén 1916; Tempel 1938; Lima de Faria 1964; Pavelescu and Pavelescu 1972). The refractive indices, birefringence, and density, for example, increase with REE and Fe contents (Tempel 1938; Nesse 2004). The density of metamict allanite is considerably less than that of the crystalline equivalents (see below). Extensive miscibility between epidote-clinozoisite and allanite was pointed out by V.M. Goldschmidt nearly 100 years ago (see comment in Goldschmidt and Thomassen 1924) and later suggested by large suites of analyses (Khvostova 1963; Deer et al. 1986; Pan and Fleet 1990; Grew et al. 1991; Carcangiu et al. 1997). This conclusion is also documented by Figures 3 and 4, which display analyses of epidote-group minerals with widely variable REE contents. The plotted data further demonstrate that epidote-group minerals are in many cases characterized by M-site Me^{2+} contents that exceed the theoretical value of 1 Me^{2+} per formula unit for allanite. It should also be stressed that the plotted data represent analyses of minerals that formed at different pressure and temperature conditions and in a wide variety of geologic environments.

Allanite is a common accessory phase in granite, granodiorite, monzonite, syenite, and granitic pegmatite (e.g., Dollase 1971, 1973; Deer et al. 1986; Buda and Nagy 1995; Broska et al. 2000), and is found in diorite and gabbro as well (Kosterin et al. 1961). Allanite has also been found as phenocrysts in acid volcanic rocks (Izett and Wilcox 1968; Duggan 1976; Brooks et al. 1981; Mahood and Hildreth 1983; Chesner and Ettlinger 1989). The mineral occurs in different types of schist, gneiss, and amphibolite, as well as in metavolcanic rocks and metacarbonates of various metamorphic grades, including those metamorphosed at high-pressure and ultrahigh-pressure conditions (Sakai et al. 1984; Deer et al. 1986; Sorensen 1991; Banno 1993; Cappelli et al. 1993; Smulikowski and Kozlowski 1994; Bingen et al. 1996; Braun 1997; Pan 1997; Gieré et al. 1998; Liu et al. 1999; Ferry 2000; Boundy et al. 2002; Hermann 2002; Spandler et al. 2003; Wing et al. 2003). Detrital allanite is a minor constituent of heavy mineral sands, such as those in Idaho, eastern Greenland, and in Arctic submarine deposits (Frye 1981; Dayvault et al. 1986), and has been observed as detrital grains in clastic sedimentary rocks, such as the Torridonian arkoses (Exley 1980). The mineral also occurs in substantial quantities in the stratiform copper deposit of Talate n'Ouamane, Morocco, where it is associated with various Cu sulfides (Demange and Elsass 1973). Metasomatic allanite has been reported from many geological environments (Gieré 1996; Sorensen 1991), including: limestone skarn (Rudashevskiy 1969; Pavelescu and Pavelescu 1972; Gieré 1986; Smith et al. 2002); altered granite (Ward et al. 1992); altered lujavrite (Coulson 1997); regional metamorphosed calc-silicate rocks (Sargent 1964); carbonate veins (Olson et al. 1954; Peterson and MacFarlane 1993); quartz veins (Banks et al. 1994); and in various other hydrothermal settings, including Alpine clefts (e.g., Exley 1980; Weiss 2002; Weiss and Parodi

2002). As already pointed out by Goldschmidt and Thomassen (1924), allanite is, together with monazite, the main host, and thus repository, of light REE (LREE) in the continental crust (see also Gromet and Silver 1983; Bea 1996).

In some granite pegmatites, alkali granite environments and skarns, allanite occurs in abundances that approach economic potential (Mariano 1989; Möller 1989). Allanite has been mined at the Mary Kathleen uranium deposit in Queensland, where it occurs in a skarn consisting of small uraninite grains in a decussate mass of allanite and apatite (80–90% of the ore; Hawkins 1975; Maas et al. 1987). During the period of 1956 to 1982, approximately 10,000 tons of U and 200,000 tons of REE-oxides were extracted from the Mary Kathleen ore (Scott and Scott 1985). Considerable potential for mining of allanite as a source of LREE exists also in other areas (Hugo 1961; Ehlmann et al. 1964; O'Driscoll 1988; Heinrich and Wells 1980; Halleran and Russell 1996).

Dissakisite

Dissakisite is the Mg-analogue of allanite, with the ideal formula $CaREEAl_2MgSi_3O_{11}O(OH)$. This endmember was described as a new species in the epidote group by Grew et al. (1991), but allanite with $Mg/(Mg+Fe^{2+}) > 0.5$ has long been known (Meyer 1911; Geijer 1927; Hanson and Pearce 1941, Kimura and Nagashima 1951; Khvostova and Bykova 1961; Treolar and Charnley 1987; Enami and Zang 1988). The name is from the Greek for "twice over," because this Mg-analogue of allanite was, in essence, described twice. Even though additional occurrences of dissakisite have been reported recently (Zakrzewski et al. 1992; de Parseval et al. 1997; Yang and Enami 2003), the mineral is relatively rare. It occurs as an accessory constituent of Si-undersaturated, Mg-and Ca-rich metamorphic rocks, including metacarbonate rock, skarn, garnet lherzolite, and spinel peridotite. At the Trimouns talc-chlorite deposit in the French Pyrenees, dissakisite-(Ce) is associated with bastnäsite; it is the most abundant of all REE minerals which formed from fluids within geodes in dolomite rocks (de Parseval et al. 1997). Dissakisite is related to epidote via the substitution

$$REE^{3+} + Mg^{2+} \leftrightarrow Ca^{2+} + Fe^{3+} \quad (5)$$

and to clinozoisite by

$$REE^{3+} + Mg^{2+} \leftrightarrow Ca^{2+} + Al^{3+} \quad (6)$$

Substitution (6) was suggested by Enami and Zang (1988), who described allanite with up to 6.2 wt% MgO (dissakisite) in garnet-corundum rocks, which are characterized by an extremely high Al_2O_3/SiO_2 value as well as by high MgO and CaO contents. Although there is no *a priori* reason to rule out complete miscibility between epidote-clinozoisite and dissakisite, there are few data that demonstrate this relationship (Fig. 4). Grew et al. (1991) pointed out that this lack of data might reflect a more limited extent of solid solution in the Mg-rich, than in the Fe-rich system.

The unit cell of dissakisite-(Ce) is slightly smaller than that of allanite-(Ce) (Table 2; Rouse and Peacor 1993). The color of dissakisite is much paler, its pleochroism weaker, and its density less, than those of allanite (Table 3).

Ferriallanite

This mineral was discovered in an alkaline granite pegmatite from Mount Ulyn Khuren, which is part of the Khaldzan Buragtag peralkaline granite massif in the Mongolian Altai (Kartashov et al. 2002). Ferriallanite has the idealized formula $CaREEFe^{3+}AlFe^{2+}Si_3O_{11}O(OH)$ and is the Fe^{3+}-analogue of allanite (Table 1). The mineral from the type locality is Ce-dominant and thus described as ferriallanite-(Ce). It exhibits both the highest density and birefringence of all REE-rich epidote-group minerals (Table 3).

The structure of ferriallanite shows all the characteristics of monoclinic epidote, and is almost identical to that of allanite (Fig. 1). The reader interested in the atomic parameters

Table 3. Physical properties of allanite and other REE-rich epidote-group minerals

	Allanite-(Ce) *	Dissakisite-(Ce)	Ferriallanite-(Ce)	Oxyallanite	Dollaseite-(Ce)	Khristovite-(Ce)	Androsite-(La)
Indices of Refraction							
α	1.690 - 1.813	1.735	1.825		1.715	1.773	
β	1.700 - 1.857	1.741	1.855		1.718	1.790	
γ	1.706 - 1.891	1.758	1.880		1.733	1.803	
n	1.53 - 1.70, when metamict						1.877 **
Birefringence δ	0.013 - 0.036	0.023	0.055		0.018	0.030	
Optic Axial Angle							
$2V_Z$ (calculated)		64.2°	83°				
$2V_Z$ (measured)	40 - 123°	62°				83°	
Optic Sign	(+) or (−)	(+)	(−)			(−)	
Dispersion	r > v; distinct	r < v; medium	r < v; strong			r < v; medium	
Color	brown to black	yellow-brown	black, opaque or translucent		brown	brown to dark brown	brown-red, transparent
Streak	gray	white	brown			light brown	
Luster	vitreous, resinous to submetallic	vitreous	resinous			vitreous	vitreous

Pleochroism	Z ≥ Y > X	weak; X < Y = Z	Z > Y > X			strong; Y > Z >> X	very strong
X	pale olive-green to reddish brown	pale brown	greenish gray			very light yellow	pale orange-brown
Y	dark brown to brownish yellow	light yellow-brown	brown			dark reddish brown	
Z	greenish brown to dark reddish brown	light yellow-brown	dark red-brown			brown	deep brown-red
Density (g/cm^3)							
ρ (measured)	3.5 - 4.2; when metamict, as low as 2.7	3.75	4.22		3.9	4.05	>4.03
ρ (calculated)		3.97 - 4.02				4.11	4.21
Mohs Hardness	5-6$^1/_2$		6			5	
Cleavage	{001} imperfect; {100} and {110} poor	not observed	not observed			not observed	
Type Locality	Qeqerssuatsiaq, Aluk, South Greenland	Balchen Mountain, E Antarctica	Mount Ulyn Khuren, Altai, Mongolia	Experimental run product	Ostanmossa Mine, Norberg, Sweden	Inyl'chek Massif, Tien-shan, Kirgiziya	Petalon Mountain, Andros Island, Greece
References	Deer et al. (1986), Anthony et al. (1995), Zenzén (1916)	Grew et al. (1991)	Kartashov et al. (2002)	Dollase (1973)	Geijer (1927)	Sokolova et al. (1991); Pautov et al. (1993)	Bonazzi et al. (1996)

* large ranges due to compositional variation

** mean refractive index (calculated)

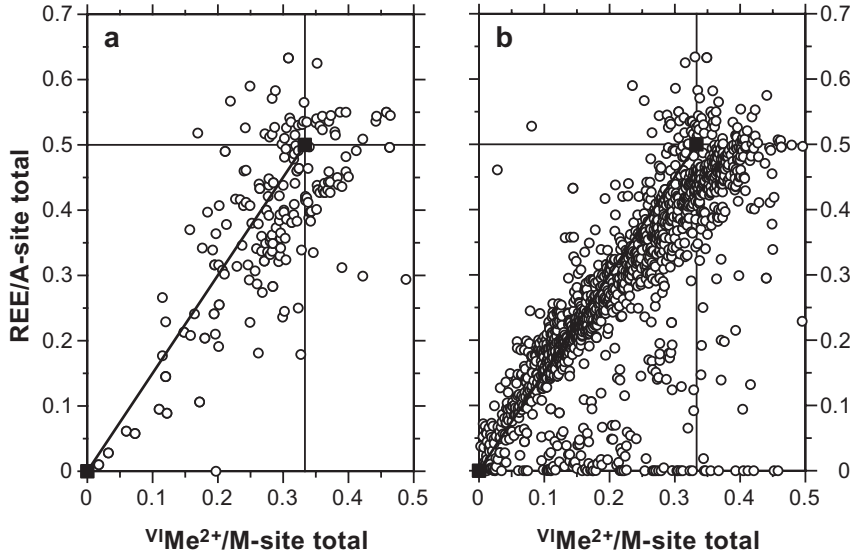

Figure 3. Fraction of REE in the A sites vs. fraction of Me^{2+} in the M sites, showing continuous substitutions along a join between the projected compositions (marked by full squares) of ideal clinozoisite or epidote, and ideal allanite or dissakisite. **a)** analyses, where Fe^{2+} and Fe^{3+} have been analyzed (n = 215), **b)** samples, for which Fe^{2+}/Fe^{3+} was calculated (n = 1521). Diagram is based on Figure 37 of Khvostova (1962).

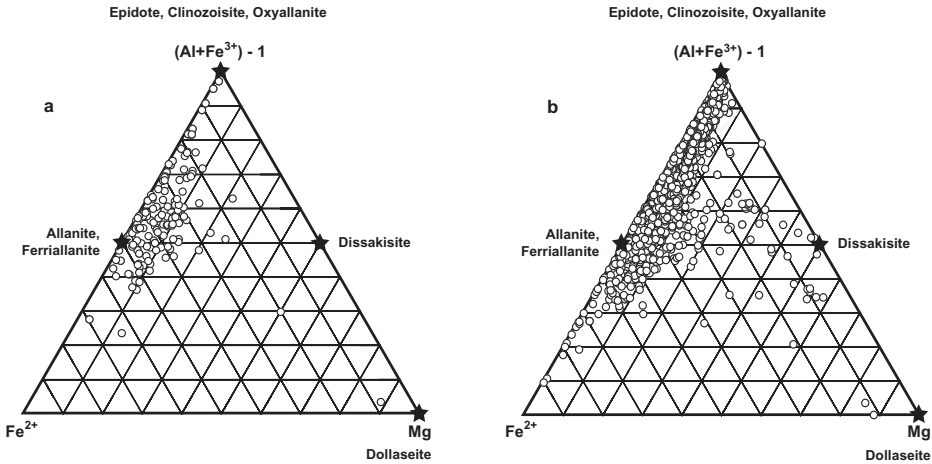

Figure 4. Extent of solid solution in the Fe^{2+}-Mg^{2+}-(Al+Fe^{3+}) subsystem. Asterisks show projections of endmember compositions into this space. **a)** analyses, where Fe^{2+} and Fe^{3+} have been directly analyzed (n = 215); **b)** analyses, for which Fe^{2+} and Fe^{3+} have been calculated (n = 1521). Early studies (which generally relied on gravimetric analysis for determination of Fe^{2+} and Fe^{3+}) did not focus on the Mg-rich part of the system, whereas modern ones (which rely on the electron microprobe, and thus calculate Fe^{2+}/Fe^{3+}) have shown a more substantial solution toward the Mg-endmembers. Figure ignores the possible presence of Fe^{2+} in the A sites.

and interatomic distances for ferriallanite-(Ce) should consult the paper of Kartashov et al. (2003), which lists values that have been corrected relative to those published in the original description (Kartashov et al. 2002). Ferriallanite-(Ce) has the largest unit cell of all the REE-rich epidote minerals (Table 2). Mössbauer spectroscopy indicates that Fe^{2+} is present in only the strongly distorted M(3) octahedral site (Kartashov et al. 2002; Holtstam et al. 2003). Although Fe^{3+} partitions between the other two octahedral sites, it is the dominant cation in M(1). This feature appears to be unique in the epidote-group minerals and is in contrast to epidote, where Fe^{3+} prefers the M(3) site (Dollase 1973; Nozik et al. 1978; Kvick et al. 1988; see also Franz and Liebscher 2004).

The chemical relationships among ferriallanite, allanite, epidote, and clinozoisite are illustrated in an REE vs. Al diagram, first proposed by Petrík et al. (1995). This diagram (Fig. 5) can be used to estimate the proportions of Fe^{3+} and Fe^{2+} in the solid solutions defined by these four endmembers. The diagram graphically represents substitution (1), relating epidote and allanite, and the exchange vector $Fe^{3+}Al_{-1}$, which connects clinozoisite to epidote and allanite to ferriallanite. The data in Figure 6 show that there are almost no analyses on the Al-rich side of the tie-line between clinozoisite and allanite; data in this area of the diagram would require REE substitution to be balanced by some other mechanism than Me^{2+} for Me^{3+}. In contrast, quite a few analyses plot on the Fe-rich side of the epidote-ferriallanite join, and some analyses are characterized by REE+Th > 1 (compare with Fig. 3). The diagrams further document that ferriallanite is an important component of many epidote-group minerals with $Fe^{3+}/Fe_{tot} < 0.5$.

At the Mongolian type locality, ferriallanite is of metasomatic origin and is associated with zircon, quartz, aegirine, magnetite, fayalite, fluorite, and the REE minerals kainosite-(Y), β-fergusonite-(Y), hingganite-(Ce), and allanite-(Ce). To date, there is only one other ferriallanite-(Ce) locality, the Bastnäs Fe-Cu-REE deposit in the Skinnskatteberg district, Västmanland, Sweden (Holtstam et al. 2003). There, ferriallanite-(Ce) is closely associated with cerite-(Ce), bastnäsite-(Ce), bastnäsite-(La), törnebohmite-(Ce), quartz, fluocerite-(Ce), and various sulfide minerals. Next to cerite-(Ce), ferriallanite-(Ce) is the most common REE mineral at this deposit, where it was discovered long before its true nature was established: it was first reported in 1781, described as "black hornblende" in 1804, and then recognized as a

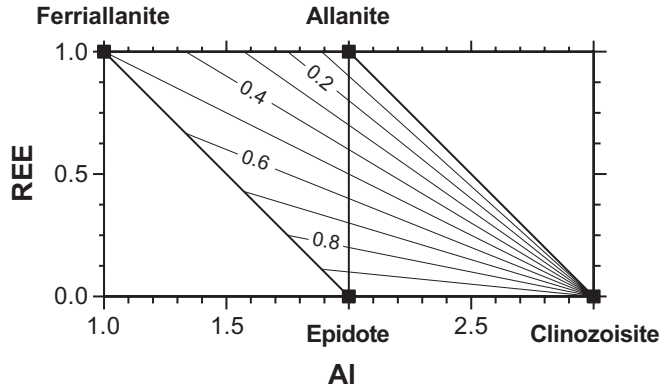

Figure 5. REE vs. Al (cations per formula unit) diagram showing the chemical relationships in the system allanite-ferriallanite-epidote-clinozoisite. Lines radiating from the clinozoisite endmember represent lines of constant Fe-oxidation state and are labeled for Fe^{3+}/Fe_{total}. This diagram, introduced by Petrík et al. (1995), can be used to estimate the proportions of Fe^{2+} and Fe^{3+} in compositions within this chemical system.

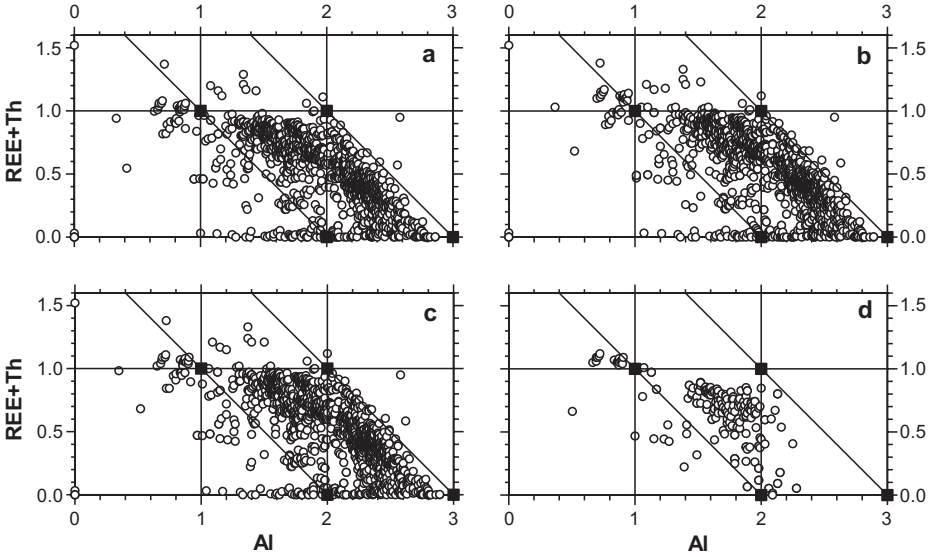

Figure 6. Allanite compositions from the database plotted in a diagram similar to the one shown in Figure 5 to estimate Fe^{3+}/Fe_{total} (Petrík et al. 1995). Full squares show projections of endmember compositions into this space (see Fig. 5). **a)** all ferric, with no estimate of Fe^{2+}/Fe^{3+}; **b)** all ferrous, with no estimate of Fe^{2+}/Fe^{3+}; **c)** all ferrous, with Fe^{2+}/Fe^{3+} estimated; **d)** data points represent analyses, where Fe^{2+} and Fe^{3+} have been analyzed (n = 215). Although the diagram was used for formula parameters calculated on the basis of 12.5 oxygens, and all iron as Fe^{2+} or as Fe^{3+}, the positions of points in a-c (n = 1521) are relatively insensitive to the formula calculation procedure. This is likely because both parameters total to relatively large fractions of the formula.

new Ce-bearing mineral named "cerine" in 1815 (see discussion and references in Holtstam et al. 2003). The samples from Bastnäs contain Mg and are richer in REE and F than the Mg-free specimens from Mongolia.

Oxyallanite

Oxidation of Fe^{2+} to Fe^{3+}, the release of H_2, and the concomitant replacement of OH^- by O^{2-} would produce an oxy-equivalent of allanite. The reaction

$$Fe^{2+} + OH^- \leftrightarrow Fe^{3+} + O^{2-} + 1/2\ H_2 \quad (7)$$

is formally equivalent to the oxy-reaction observed in other hydrous Fe^{2+}-bearing silicate minerals, e.g., mica and amphibole (Hogg and Meads 1975; Ferrow 1987; Popp et al. 1995a, b). In contrast to micas and amphiboles, the OH^- group, which loses a H atom, is not directly bonded to the Fe^{2+}, which is being oxidized; rather, the OH^- group is bonded to M(2) only, a site that is almost entirely filled by Al (Dollase 1973; Nozik et al. 1978; Kvick et al. 1988; Giuli et al. 1999; Franz and Liebscher 2004). Anhydrous oxyallanite $CaREEAl_2Fe^{3+}Si_3O_{11}O(O)$ is a theoretical endmember (Table 1), for which there is good experimental evidence: Dollase (1973) heated allanite from a pegmatite in Pacoima Canyon, California in air at different temperatures and run durations, and analyzed Fe^{3+} and Fe^{2+} of the run products with Mössbauer spectroscopy. Heating at $T < 400$°C did not noticeably change the value of $Fe^{2+}/(Fe^{2+}+Fe^{3+})$, even if samples were heated for several days. At $T > 400$°C, the Fe^{2+} contents decreased with increasing temperature, such that the sample was almost completely oxidized at 700°C (Fig. 7a). The degree of oxidation was apparently independent of duration of heating. Dollase (1973) further showed that heating in a reducing atmosphere could reverse the oxidation. The changes in

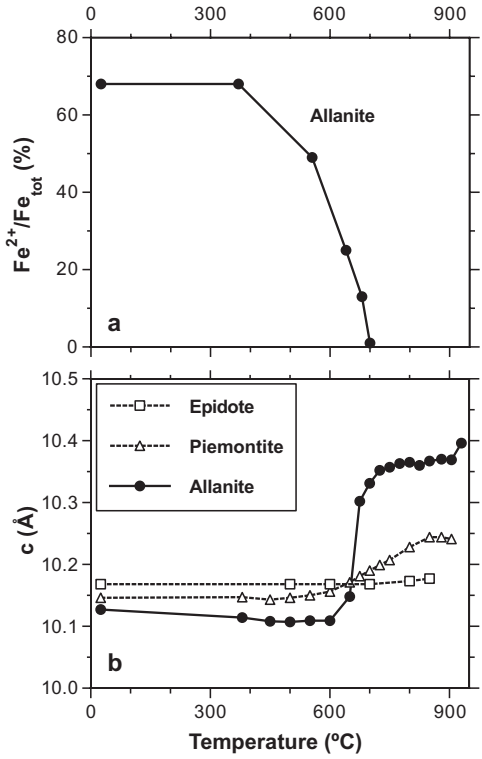

Figure 7. Effects of heating allanite, epidote and piemontite in air. **a)** $Fe^{2+}/(Fe^{2+}+Fe^{3+})$ vs. temperature for allanite from Pacoima Canyon (data from Dollase 1973); **b)** Unit-cell parameter *c* vs. temperature for allanite, epidote, and REE-rich piemontite (data from Bonazzi and Menchetti 1994).

unit-cell dimensions associated with the transformation of allanite into oxyallanite are small (Table 2). Kumskova and Khvostova (1964) and Khvostova (1962), who published weight-loss curves obtained from allanite dehydration experiments, reported similar observations.

Bonazzi and Menchetti (1994) heated single crystals of allanite from granite of the Rhodope Massif, Bulgaria in air for 48 hours at temperatures in the range of 380–900°C. These authors found that the oxidation-dehydrogenation of allanite begins at ~600°C and is essentially complete at about 700–725°C (Fig. 7b). Above 725°C, unit-cell parameters do not change significantly until ~905°C. At the latter temperature, there is a marked change in the unit-cell parameters, which Bonazzi and Menchetti (1994) ascribed to oxidation of Ce^{3+} to Ce^{4+}. This oxidation ends with the breakdown of the allanite structure, via the precipitation of CeO_2. Earlier studies also reported that cerianite is a breakdown product of allanite at high temperatures (see below).

Bonazzi and Menchetti (1994) also heated single crystals of REE-rich piemontite from Monte Brugiana in the Alpi Apuane, Italy. The piemontite behaved similarly to allanite upon heating, although the oxidation-dehydrogenation process

$$Mn^{2+} + OH^- \leftrightarrow Mn^{3+} + O^{2-} + 1/2\ H_2 \quad (8)$$

took place more gradually, i.e., over a larger *T* interval, and complete oxidation of Mn^{2+} did not occur until 850°C (Fig. 7b). In contrast, epidote, appeared to be unaffected by heat treatment.

The presence of an oxyallanite component in natural members of the epidote group is difficult to verify, because of analytical uncertainties and the general lack of direct

determination of H_2O contents. Based upon chemical analyses of natural samples, Grew et al. (1991) proposed that substitution (7) is important in numerous natural allanite, dissakisite and dollaseite compositions, for which analytical data for both Fe^{3+} and Fe^{2+} were available. As will be discussed, the oxidation-dehydrogenation process may be of considerable petrological importance.

Dollaseite

Dollaseite-(Ce) was first reported by Geijer (1927). He named it magnesium orthite, because it appeared to be the Mg-analogue of orthite. However, Peacor and Dunn (1988) showed that the specimen studied by Gejier (1927) was not the Mg-analogue of what is now termed allanite (i.e., dissakisite). These authors named it to honor Wayne Dollase, who refined the structures of epidote, allanite, and hancockite (Dollase 1971). Dollaseite-(Ce) contains Mg on both the M(3) and M(1) sites, and compensates for the resulting charge imbalance by the substitution of F for O(4), i.e., the O atom that is not coordinated to Si (Peacor and Dunn 1988). The substitution

$$Mg^{2+} + F^{-} \leftrightarrow Al^{3+} + O^{2-} \quad (9)$$

relates dollaseite, with the idealized formula $CaREEAlMg_2Si_3O_{11}F(OH)$, to dissakisite. The relationship between dollaseite and clinozoisite can be described by an overall substitution

$$REE^{3+} + 2\ Mg^{2+} + F^{-} \leftrightarrow Ca^{2+} + 2\ Al^{3+} + O^{2-} \quad (10)$$

(Burt 1989), which is a combination of (6) and (9).

The structure refinement of Peacor and Dunn (1988) showed that the dollaseite-(Ce) structure displays only minor shifts from the atomic positions of epidote or allanite. These refinement data are compatible with nearly complete ordering of Mg in M(1), Al in M(2), and Mg and Fe^{2+} in M(3) (Table 1). The unit cell is approximately the same size as that of allanite (Table 2).

Dollaseite-(Ce) is found in a skarn at the Östanmossa Mine in the Norberg district of Sweden, where it is associated with tremolite, norbergite, and calcite (Geijer 1927).

Khristovite

The second REE-rich species of the epidote group with two divalent cations in octahedral sites was discovered by Sokolova et al. (1991), and was subsequently named khristovite, in honor of Evgenia Valdimirovicha Khristova, a Russian geologist and specialist in Tien-shan geology (Pautov et al. 1993). As in the case of dollaseite-(Ce), a charge imbalance results from two divalent cations on the M sites, which is compensated for by replacing O(4) with F. In contrast to dollaseite-Ce, however, khristovite contains Mn^{2+} rather than Mg on the M(3) site (Table 1, Fig. 8), and thus has the idealized formula $CaREEMgAlMn^{2+}Si_3O_{11}F(OH)$. According to the structural refinement of Sokolova et al. (1991), the A(1) site in khristovite-(Ce) is not occupied exclusively and completely by Ca. Instead, 20% of the site is vacant, and 20% occupied by La. These data indicate that REE are not restricted to the A(2) sites in all epidote-group minerals (see also Cressey and Steel 1988).

Khristovite-(Ce) is found in a Mn-rich rock from the Tien-shan in Kirgizia, where it is associated with other Mn minerals, including rhodonite, tephroite, and rhodochrosite (Sokolova et al. 1991; Pautov et al. 1993). The unit cells of dollaseite-(Ce) and khristovite-(Ce) display almost identical volumes (Table 2), but the density of khristovite is greater (Table 3). Khristovite-(Ce) also exhibits higher indices of refraction than dollaseite-(Ce).

Androsite

Androsite is extremely rich in Mn and poor in Fe, and has the idealized formula $Mn^{2+}REEMn^{3+}AlMn^{2+}Si_3O_{11}O(OH)$ (Bonazzi et al. 1996). Its name is derived from the type

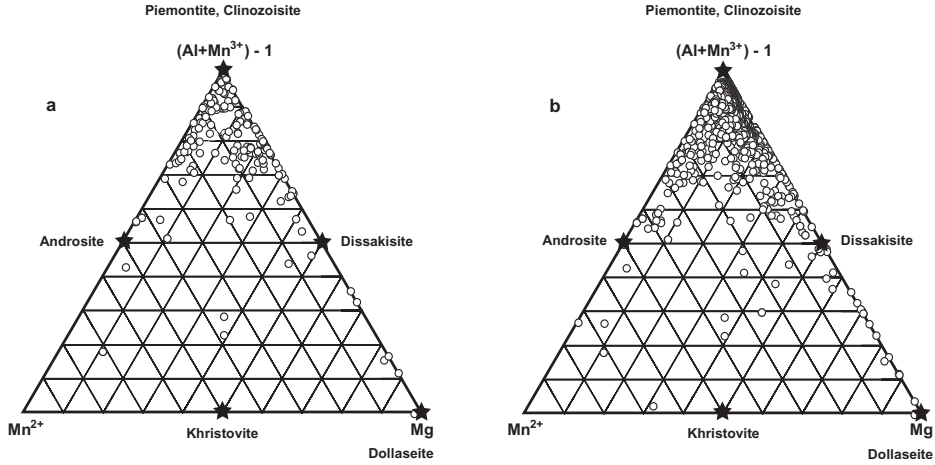

Figure 8. Extent of solid solution in the Mn^{2+}-Mg^{2+}-(Al+Mn^{3+}) subsystem. Asterisks show projections of endmember compositions into this space. **a)** analyses, where Fe^{2+} and Fe^{3+} have been directly analyzed (n = 215); **b)** analyses, for which Fe^{2+} and Fe^{3+} have not been analyzed (n = 1521). For the calculation of Mn^{2+}/Mn^{3+}, all Fe was first assumed to be Fe^{3+}; then, the analyses were normalized to 12.5 oxygens and 8 cations by adjusting Mn^{2+}/Mn^{3+}. Figure ignores the possible presence of Mn^{2+} in the A sites.

locality, the Cycladic Island of Andros in Greece. As seen in the structural formula, androsite contains Mn in three different sites, and in both the divalent and trivalent states (Table 1). Androsite is related to allanite by

$$Mn^{2+} \leftrightarrow Ca^{2+} \text{ on A(1)} \quad (11)$$

$$Mn^{3+} \leftrightarrow Al^{3+} \text{ on M(1)} \quad (12)$$

$$Mn^{2+} \leftrightarrow Fe^{2+} \text{ on M(3)} \quad (13)$$

The structure of androsite is virtually identical to that of allanite. In contrast to the epidote-piemontite solid solution, in which Mn^{3+} prefers the more distorted M(3) site (Dollase 1973; Ferraris et al. 1989), Mn^{3+} is accommodated in the M(1) site of androsite. The unit cell of androsite-(La) is smaller than those of most other REE-dominant epidote-group minerals (Table 2). Its calculated density is almost identical to that of ferriallanite (Table 3).

The described specimen from the type locality in Greece, a Mn-ore deposit, contains La as the predominant REE, and thus, is androsite-(La). The Mn-rich, Fe-poor composition is interpreted to reflect the unusual bulk composition of the host rock, in which androsite coexists with braunite, rhodonite, rhodochrosite, spessartine-rich garnet, and quartz.

Until the discovery of khristovite-(Ce), Mn was thought to be a common, but typically relatively minor component of REE-rich epidote-group minerals. Substantial MnO contents (5 to 7 wt%), however, have been reported for allanite (Hutton 1951a; Ovchinnikov and Tzimbalenko 1948; Kimura and Nagashima 1951; Hagesawa 1957, 1958; Pavelescu and Pavelescu 1972). For many of these specimens, described as manganoan allanite and manganorthite, the host rock is a granitic pegmatite. Deer et al. (1986) suggested that Mn^{2+} probably replaced Ca in these minerals, but speculated that, in some cases, Mn might also enter the octahedral sites. This conclusion is consistent with rare occurrences of REE-rich piemontite in Mn-deposits and other Mn-rich rock types (Williams 1893; Kramm 1979; Schreyer et al. 1986; see also Bonazzi and Menchetti 1994, 1995, 2004). These examples provide evidence for extensive solid solution between piemontite and allanite (Bonazzi et al. 1992; Bonazzi and

Menchetti 1994; Bermanec et al. 1994). The substitution is

$$REE^{3+} + Fe^{2+} \leftrightarrow Ca^{2+} + Mn^{3+} \quad (14)$$

and represents the Mn-equivalent of (1). Bonazzi et al. (1996) also reported an intermediate composition between piemontite and androsite-(La). The compositional relationships for REE-rich epidote in the Mn-Mg-Al system are shown in Figure 8, which ignores the possibility of Mn^{2+} in A sites. The substitution of Mn^{2+} for Ca in the A site (Eqn. 11) is not only important in androsite, but has also been proposed for other members of the epidote group (Bonazzi et al. 1992).

MINOR AND TRACE ELEMENTS IN ALLANITE

In addition to REE, allanite incorporates many other elements, which, depending on the geological environment, can become essential structural constituents present in weight percent quantities (Deer et al. 1986). The wide range of chemical components that can be incorporated into allanite documents that the structure is able to accept ions with widely different radii and charges. These ions are accommodated primarily in the A and M sites, but some have been interpreted to replace Si. Although some elemental abundances and element distributions within grains may reflect secondary processes, such as metamictization and weathering, most minor elements appear to have been incorporated during mineral growth, and thus testify to diverse environments of mineral formation.

The advent of new instrumental techniques designed specifically for the analysis of trace elements has led to a wealth of extensive data sets over the past few years. Most significant among these new instrumental techniques is *in situ* analysis by laser-ablation inductively-coupled plasma mass spectrometry (LA-ICP-MS), a trace element technique that has also been used for epidote-group minerals (e.g., Bea 1996; Hermann 2002; Holtstam et al. 2003; Spandler et al. 2003).

Substitutions in the A sites

Most minor substitutions in the A sites of allanite and other REE-rich epidote-group minerals are on the A(2) site, but rarely the A(1) site is also involved (Sokolova et al. 1991).

Thorium. This element is a commonly observed A-site constituent present in trace to minor amounts (e.g., Smith et al. 1957; Rao and Babu 1978; Rao et al. 1979; Gieré 1986; Janeczek and Eby 1993; Banno 1993; Barth et al. 1989, 1994; Liu et al. 1999; Wood and Ricketts 2000; Yang and Enami 2003; Oberli et al. 2004). Reported ThO_2 contents in allanite are often in the range of 2–3 wt% (Hagesawa 1959, 1960; Khvostova 1962; Ploshko and Bogdanova 1963; Kalinin et al. 1968; Oberli et al. 1981; Peterson and MacFarlane 1993; Buda and Nagy 1995; Bea 1996), and the maximum concentration reported so far is 4.9 wt%, reached at two different localities (Hagesawa 1960; Exley 1980). Two analyses presented by Oberli et al. (1981) show ThO_2 contents of 22.2 wt% and 37.3 wt%, and large amounts of UO_2 (5.5 wt%, 23.5 wt%) and P_2O_5 (2.28 wt%, 2.0 wt%), but the calculated formulae are not consistent with those of epidote-group minerals. The substitution mechanisms responsible for Th incorporation are speculative; proposals for the Mg-free system include (Gieré et al. 1999)

$$Th^{4+} + 2\ Fe^{2+} \leftrightarrow Ca^{2+} + 2\ Fe^{3+} \quad (15)$$

$$Th^{4+} + Fe^{2+} \leftrightarrow REE^{3+} + Fe^{3+} \quad (16)$$

$$Th^{4+} + Fe^{2+} \leftrightarrow REE^{3+} + Al^{3+} \quad (17)$$

All are accompanied by a change in Fe^{2+}/Fe^{3+}. Accommodation of Th might, however, also be achieved without involving Fe (or Mg or Mn^{2+}), for example,

$$Th^{4+} + Ca^{2+} \leftrightarrow 2\ REE^{3+} \quad (18)$$

(Gromet and Silver 1983; Chesner and Ettlinger 1989; Gieré et al. 1999; Wood and Ricketts 2000), which is an important substitution in other minerals as well (e.g., monazite group), and

$$3\ Th^{4+} + \square \leftrightarrow 4\ REE^{3+} \quad (19)$$

in which $\square$ = vacancy. With the exception of (15), these substitutions require REE-bearing compositions to effect charge balance.

Uranium. A parallel set of substitutions to those for Th could be formulated for U^{4+}, but U is typically present in much smaller concentrations than Th (Hickling et al. 1970; Smith et al. 1957; Sawka 1988; Sawka and Chappell 1988; Barth et al. 1989, 1994; Zakrzewski et al. 1992; Oberli et al. 2004). Allanite only rarely contains more U than Th; an example of this unusual feature is seen in the metasomatically formed crystals from the Mary Kathleen U-REE skarn in Queensland (Maas et al. 1987). The predominance of Th relative to U in REE-rich epidote-group minerals is clearly displayed in Figure 9, which contains all analyses from our dataset that list values for both U and Th, and which shows that U is typically present in the < 1000 ppm range. However, Janeczek and Eby (1993) measured up to 0.21 wt% UO_2 for allanite from pegmatites. Banno (1993) described allanite with even higher UO_2 contents (up to 0.36 wt%). The latter occurs in blueschists from the Sanbagawa belt of Japan, and is unusual as it appears to be one of only very few reported allanites with U/Th > 1 (see Figure 9). The maximum UO_2 content observed is 0.82 wt% in a crystal containing 1.09 wt% ThO_2 from the Cacciola granite in the central Gotthard massif, Switzerland (Oberli et al. 1981).

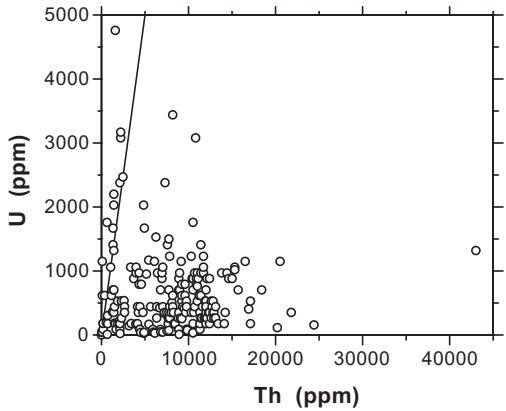

Figure 9. U vs. Th diagram showing analyses that contain both U and Th in detectable concentrations (n = 220). Of these analyses, only 16 plot above the line of slope 1 and thus contain U in excess of Th.

Strontium. This element has been observed as a minor or trace component of allanite at various localities (e.g., Ploshko and Bogdanova 1963; Bocquet 1975; Rao and Babu 1978). Papunen and Lindsjö (1972) found allanite with 0.87 wt% SrO from a skarn at Korsnäs, Finland. Exley (1980) described an allanite containing 1.5 wt% SrO from altered basalt on the island of Skye, but noted that the Sr content is mostly less than 1000 ppm. Sorensen (1991) reported 1.1–1.8 wt% SrO in zoned allanite from tectonic blocks of metasomatized garnet amphibolite from the Catalina Schist, southern California. Zdorik et al. (1965) observed 3.72 wt% for allanite from carbonatite. Allanite containing 4.28 wt% SrO has been described from a fenite associated with the Mount Bisson REE deposits, British Columbia (Halleran and Russell, 1996). REE-rich epidote that contains 2.2–4.0 wt% SrO is present in lawsonite blueschist from New Caledonia (Spandler et al. 2003), and allanite grains from a leucosyenite

in China contain an average of 1.65±0.34 wt% SrO, with values that range to 4.5 wt% (Jiang et al. 2003).

Lead. Bermanec et al. (1994) reported Pb-rich piemontite with total REE_2O_3 contents of 6.09 to 8.56 wt%, up to 10.4 wt% PbO, and ZnO from 0.6 to 0.75 wt%, as an accessory mineral associated with ardennite, gahnite, and franklinite (?) in mica schist from Nezilovo, Macedonia. This piemontite is characterized by a significant allanite component, a component of the Pb-epidote mineral hancockite, and minor Zn-substitution.

Alkali elements. Bermanec et al. (1994) determined up to 0.02 wt% K_2O and 0.12 to 0.24 wt% Na_2O for the aforementioned Pb- and REE-rich piemontite. Similarly, all analyses given by Yang and Enami (2003) reported between 0.14 and 0.21 wt% of Na_2O in dissakisite-(Ce) from China. These values are significantly larger than the 0.02 wt% detection limit of the electron microprobe used by these researchers. Furthermore, all compositions listed by Bea (1996) for allanites from granitoid rocks appear to contain small amounts of Na_2O (0.06 to 0.56 wt%; determined by electron microprobe). Alkali element substitution seems to be rather uncommon and limited (cf. Deer et al. 1986), because of the cation sizes and charge densities. However, Semenov et al. (1978) observed a Na_2O content of 1.36 wt% for allanite from a carbonatite complex in Tamil Nadu. Coulson (1997) reported an analysis of allanite with 3.28 wt% Na_2O (= 0.61 cations, based upon a 12.5 oxygen formula); this allanite was produced by alteration of eudialyte in a lujavrite (described by the author as eudialyte microsyenite) from the Igaliko complex in the Gardar province of South Greenland. Although the overall alteration process is described as Na-loss from the system, the original rock and the primary minerals are extremely sodic, which may account for this exceptional value for Na in allanite. Possible mechanisms for Na incorporation are (Yang and Enami 2003)

$$Na^{+} + Ti^{4+} \leftrightarrow Ca^{2+} + Fe^{3+} \quad (20)$$

$$Na^{+} + Fe^{3+} \leftrightarrow Ca^{2+} + Fe^{2+} \quad (21)$$

which could also be formulated analogously for Al instead of Fe^{3+}. Another possible substitution is

$$Na^{+} + REE^{3+} \leftrightarrow 2\ Ca^{2+} \quad (22)$$

which is common in minerals, such as the perovskite and apatite groups (e.g., Burt 1989; Rønsbo 1989; Mitchell 1996; Campbell et al. 1997).

Manganese and iron. Divalent Mn and Fe may also substitute for Ca. However, with the exception of androsite-(La) and some altered allanites, the substitutions are not significant (Bonazzi et al. 1992; Bonazzi and Menchetti 1995; Catlos et al. 2000; Poitrasson 2002).

Vacancies. Although it is possible that the A sites of some allanites may be partially vacant, the presence of vacancies is difficult to document due to the chemical complexity of the mineral, and especially the viscissitudes of the calculation of Fe^{2+}/Fe^{3+} from electron microprobe analyses. As discussed above and in this section, allanite typically contains several elements with multiple oxidation states as well as water. Furthermore, as pointed out by Catlos et al. (2000), allanite can contain minor amounts of many elements, not all of which may be detected without detailed wavelength scans by electron microprobe, prior to analysis. Therefore, the calculation of vacancies based on electron microprobe data can be associated with large uncertainties (see, for example, Ercit 2002). However, a small body of evidence exists to support the idea that vacancies may occur in the A sites of allanite and related minerals. In conjunction with microprobe data, the structural refinement of khristovite-(Ce) yielded considerable amounts of vacancies in the A sites (Sokolova et al. 1991), particularly in the A(1) site (20% vacant). Peterson and MacFarlane (1993) also inferred existence of vacancies in allanite from granite pegmatites and calcite veins in the Grenville Province,

Ontario, Canada. These authors observed that most of the studied allanites exhibited A-site vacancies, but to varying degrees. Moreover, they concluded that in addition to substitutions (1) and (2), an omission-type substitution:

$$3\ Ca^{2+} \leftrightarrow 2\ REE^{3+} + \square \tag{23}$$

was required to explain their data. However, the average formula (based on 12.5 oxygens and 8 cations) for the allanites studied by Peterson and MacFarlane (1993) is $A_{1.88}M_{3.06}T_{3.06}O_{11}O(OH)$, and thus shows excess charge on the M and T sites. This too is a common feature of "A-site-deficient" allanite (Sorensen 1991; Catlos et al. 2000). Although the M and T excess charges could be dismissed as being within the error of a microprobe determination, hundreds of analyses show them; they may hold a clue for explaining the A-site deficiencies.

Substitutions in the M sites

Titanium. This element is a minor constituent of REE-rich epidote-group minerals (Ploshko and Bogdanova 1963; Exley 1980; Hagesawa 1960, Deer et al. 1986; Gieré 1986; Rudashevskiy 1969; Grew et al. 1991; Banno 1993; Liu et al. 1999; Jiang et al. 2003; Yang and Enami 2003). TiO_2 contents of 1 to 2 wt% are often observed for allanite from volcanic and plutonic rocks (e.g., Ploshko and Bogdanova 1963; Ghent 1972; Duggan 1976; Brooks et al. 1981; Chesner and Ettlinger 1989; Catlos et al. 2000; Wood and Ricketts 2000; Jiang et al. 2003). Similarly, khristovite-(Ce) contains 1.5 to 1.8 wt% Ti (Pautov et al. 1993). Poitrasson (2002) reported TiO_2 contents that range from 1.44 to 4.67 wt% for variably altered allanite occurring in Paleozoic granitoid rocks on Corsica. Besides the 7.46 wt% TiO_2 observed by Khvostova (1962), the maximum TiO_2 content reported so far is 5.2 wt% for allanite from a fayalite-hedenbergite syenite (Krivdik et al. 1989). Titanium can be incorporated into epidote-group crystal structures via

$$Ti^{4+} + Fe^{2+} \leftrightarrow 2\ Fe^{3+} \tag{24}$$

and

$$Ti^{4+} + Fe^{2+} \leftrightarrow 2\ Al^{3+} \tag{25}$$

These substitutions may also involve Mg^{2+} and Mn^{2+}, as well as less abundant divalent cations. As is the case for incorporation of Ti in amphibole and mica structures, octahedral-site substitutions such as (24) will be strongly influenced by f_{O_2}. Alternatively, Ti can enter the allanite structure along with Na according to substitution (20).

Vanadium. As in REE-free epidote-group minerals (Shepel and Karpenko 1969; Franz and Liebscher 2004), V can be incorporated into REE-rich epidotes (Ovchinnikov and Tzimbalenko 1948; Papunen and Lindsjö 1972; Bocquet 1975; Rao and Babu 1978; Rao et al. 1979). In khristovite-(Ce), V_2O_3 ranges from 1.0 to 1.7 wt% (Pautov et al. 1993), and Pan and Fleet (1991) described allanite and REE-rich epidote with up to 9.07 wt% V_2O_3 from Hemlo in Ontario, Canada. Kato et al. (1994) reported core and rim analyses of a vanadian allanite from the Mn-Fe ore of the Odaki ore body, Kyurazawa Mine, Ashio, Tochigi Prefecture, Japan, with 9.58 and 8.83 wt% V_2O_3, respectively. Vanadium probably enters the M site of the allanite structure as V^{3+}, as in the case of mukhinite (Shepel and Karpenko 1969); an extremely oxidizing environment would probably be needed to stabilize V^{5+} in allanite.

Chromium. Typically, Cr is a minor constituent of the epidote-group minerals, but in some cases, it may be present in relatively large amounts (e.g., Papunen and Lindsjö 1972; Grapes 1981; Sorensen 1991; Grapes and Hoskin 2004; Franz and Liebscher 2004). For example, khristovite-(Ce) contains 1.3 to 2.1 wt% Cr_2O_3 (Pautov et al. 1993). Allanite with even greater amounts of Cr has been reported from the Outokumpu mining district in Finnish Karelia, where it occurs in mica- and spinel-rich layers of mica schist (Treolar and Charnley 1987). These authors concluded that the mica schist had become enriched in Cr that had

ultimately been derived from underlying ultramafic and volcanic rocks. The Cr-rich allanite from Outokumpu contains 3.63–5.40 wt% Cr_2O_3 (= 0.51–0.77 atoms per formula unit), exhibits $Mg/(Mg+Fe^{2+}) > 0.5$, and is thus a Cr-rich dissakisite (for the compositional limits of dissakisite, see Grew et al. 1991). The apparently coexisting spinel and biotite are Cr-rich. From the same area, Treolar (1987) reported epidote with > 15 wt% Cr_2O_3, i.e., close to the endmember tawmawite, $Ca_2CrAl_2Si_3O_{11}O(OH)$. Thus, there appears to be at least limited solid solution between tawmawite and dissakisite, via the substitution

$$REE^{3+} + Mg^{2+} \leftrightarrow Ca^{2+} + Cr^{3+} \quad (26)$$

Chromian dissakisite-(Ce) that contains 4.6 to 5.4 wt% Cr_2O_3 was described by Yang and Enami (2003). It is an inclusion in a clinopyroxene grain in garnet lherzolite from Zhimafang, eastern China. Yang and Enami (2003) concluded from microstructural relationships that chromian dissakisite-(Ce) had reacted with olivine to form clinopyroxene. In addition to Outokumpu and Zhimafang, two other localities have yielded Cr-rich allanite compositions. At the Orford Ni mine in Québec, Canada, allanite with 7.11 wt% Cr_2O_3 is associated with Cr-rich grossular (Tarassoff and Gault 1994), but this allanite analysis does not list MgO. Blueschists interbedded with serpentinite conglomerates in the Ise area of the Sanbagawa belt, Japan, contain aggregates of chromian phengite, sodic pyroxene, and Cr-rich spinel. Allanite from one such aggregate contains 7.49 wt% Cr_2O_3 and 0.03 to 0.09 wt% MgO (Banno 1993).

Substitutions in T sites

Many analyses of epidote-group minerals yield formulae with <3 Si atoms per formula unit (e.g., Deer et al. 1986). In our database of allanite and related minerals, about 480 analyses (i.e., ~1/3) show Si < 2.95, indicating that substitution of other components for Si is possible. However, extensive substitution for Si in the T sites is not observed in REE-poor epidote minerals. Neutron diffraction of epidote (Nozik et al. 1978; Kvick et al. 1988) and strontian piemontite (Ferraris et al. 1989) has not yielded evidence for substantial Al in tetrahedral coordination. On the other hand, Poitrasson (2002) presented electron microprobe data for altered allanite, which are characterized by overfilling of the M sites and by a Si deficiency of ≈0.15 atoms per formula unit. Based on these results, he suggested that some Al should be present in the T sites. A few studies indicate that, in some rare cases, Si may be partially replaced by P^{5+}, Ge^{4+}, or possibly Be^{2+}.

Phosphorus. This element is present in some REE-rich epidote group minerals, but typically at low concentrations (Hagesawa 1960; Mahood and Hildreth 1983; Grew et al. 1991; Petrík et al. 1995; Hermann 2002). Bea (1996) noted that allanite in granitic rocks nearly invariably contains some P (up to 0.2 wt% P_2O_5). Bocquet (1975) described a specimen with 0.36 wt% P_2O_5 from a hydrothermal allanite-albite-hematite vein, and similar concentrations have been reported for altered allanite occurring in leucosyenite in northern China (Jiang et al. 2003). In a pegmatite, Iimori et al. (1931) found an unusual specimen that contains 6.48 wt% P_2O_5, which corresponds to 0.54 P atoms per formula unit. Based on physical properties (including optical) and molar ratios of all chemical elements present, these authors concluded that the specimen resembles allanite, but provided no crystallographic data to corroborate their interpretation. The name proposed for this unusual composition was "nagatelite", after the Japanese locality where it was discovered.

Germanium. Typical Ge concentrations in epidote-group minerals range from 1 to 20 ppm (Bernstein 1985; Hermann 2002). However, what appears to be a Ge-rich allanite crystal has been described from a sphalerite ore deposit in Haute Garonne, French Pyrenees (Johan et al. 1983). This specimen contains 10.63 wt% GeO_2 in addition to 2.52 wt% Ga_2O_3, suggesting considerable replacement of Si^{4+} by the larger Ge^{4+} (26 pm vs. 39 pm; Shannon 1976) in the T sites, and of Al and Fe by Ga^{3+} in the M sites. Because the original analysis does not give quantitative data for the REE, however, the exact amount of these cations in each of the sites

cannot be calculated. It is of note that this Ge-rich specimen also contains Zn (see below), reflecting the well-known geochemical association of Ge and Zn in sphalerite deposits (Bernstein 1985).

Beryllium. In some pegmatites, allanite incorporates trace to minor amounts of Be (Deer et al. 1986; Hagesawa 1960). Kimura and Nagashima (1951) reported a BeO content of 1.35 wt% for an allanite from Japan. Another relatively fresh specimen from a pegmatite at Iisaka, Fukushima Prefecture, Japan, has been reported to contain 2.49 wt% BeO (Iimori 1939). The Be content of the latter crystal, which also contains 2.05 wt% MnO, is significantly greater than values from other localities (see additional references in, e.g., Iimori 1939; Quensel 1945; Hagesawa 1960; Grew 2002). The effective ionic radius of Be^{2+} in tetrahedral coordination is 27 pm, which is almost identical to that of Si^{4+} (26 pm; Shannon 1976). This close similarity between Si^{4+} and Be^{2+} suggests the latter could possibly be incorporated into the T sites of silicate minerals, including allanite. Iimori (1939) noted, however, that the ionic radius of Be^{2+} is similar to that of Al^{3+} and concluded that Be probably substitutes for Al in the octahedral sites. Iimori (1939) did not provide crystallographic data to corroborate his conclusion that the studied specimen was allanite. Another unusual specimen from a pegmatite at Skuleboda, western Sweden, contains 3.83 wt% BeO, but the analyzed separate is probably not pure. It contains nearly 9 wt% CO_2 and approximately 8 wt% H_2O; it is also isotropic (n = 1.663), and strongly altered (Quensel 1945).

The presence of Be in substantial quantities in allanite has never been confirmed by modern *in situ* analytical techniques. The existence of Be-rich allanite therefore remains unproven (for discussion, see Grew 2002). The few allanite crystals that have been analyzed by LA-ICP-MS did not contain detectable amounts of Be (e.g., Hermann 2002). Moreover, Lee and Bastron (1962, 1967) have documented that allanite did not incorporate Be (< 2 ppm; one out of 21 analyses contained 3 ppm), even though the studied crystals occur in a quartz-monzonite near to a Be mineralization.

Other substitutions

Halogens. In many cases, allanite displays halogen substitution for O^{2-}. Fluorine is typically more abundant than Cl (Rao et al. 1979; Mahood and Hildreth 1983). Chlorine contents of 0.95 wt% were reported for allanite from a skarn in the Hemlo area, Ontario (Pan and Fleet 1990), where one analysis shows Cl > F. Allanite from a granite and its endoskarn in the Tertiary igneous complex on Skye contains substantial amounts of F, with average values that range from 0.21 to 0.44 wt% (Smith et al. 2002). A similar range of F contents (0.11–0.49 wt%) was also described for ferriallanite-(Ce) from the Bastnäs deposit in Sweden (Holtstam et al. 2003). There, F increases with the Mg content. This relationship was not attributed to substitution (9), but rather to the "Fe-F avoidance" phenomenon, which has been observed in several minerals (e.g., Mason 1992). Fluorine contents up to 0.61 wt% are also typical for allanite in peraluminous granitoid intrusions along the Velence-Balaton Line in Hungary (Buda and Nagy 1995). Ivanov et al. (1981) found 0.9 wt% F in allanite from a tungsten deposit on the Chukchi Peninsula. The greatest F content reported for unaltered specimens is 1.10 wt%. It was measured in allanite that occurs at the contact between a microcline pegmatite and calc-granulites (Rao et al. 1979), corresponds to 0.33 F atoms per formula unit, and indicates the sample may be intermediate between allanite and dollaseite. Even larger F contents have been described for altered allanite: Jiang et al. (2003) observed average F contents of 1.7±1.1 wt% in allanite crystals that are intergrown with melanite garnet in leucosyenite. These allanite grains also contain 0.4±0.5 wt% P_2O_5.

Scandium. Dissakisite (3.8 wt% MgO) enriched in Sc was reported by Meyer (1911) from a granite pegmatite at Impilaks, Finland. This author observed Sc_2O_3 contents of 0.8 wt% and 1.0 wt% in relatively fresh and altered material, respectively.

Zinc. Considerable amounts of Zn may be present in REE-rich epidote-group minerals. Bermanec et al. (1994) reported ZnO contents of 0.6 to 0.75 wt%, values similar to the 0.72 wt% determined by Ovchinnikov and Tzimbalenko (1948). However, these values may not be accurate, because Johan et al. (1983) observed only 0.21 wt% ZnO in allanite from a Zn deposit. Ivanov et al. (1981) found 0.24 wt% ZnO in allanite from a tungsten deposit on the Chukchi Peninsula.

Gallium. One allanite sample from a sphalerite ore deposit in Haute Garonne, French Pyrenees has been reported to contain Ga (Johan et al. 1983; presence of REE verified, but REE not analyzed for). The specimen contains 2.52 wt% Ga_2O_3, in addition to 10.63 wt% GeO_2. Judging from the effective ionic radii of Ga^{3+} ($^{[VI]}r$ = 62 pm, $^{[IV]}r$ = 47 pm; Shannon 1976), it most likely replaces Al or Fe in the octahedrally coordinated M sites.

Zirconium. A trace element that is only rarely reported for REE-rich epidote minerals is Zr (Hagesawa 1960; Rao and Babu 1978; Rao et al. 1979; Coulson 1997). Hermann (2002) observed Zr at the 2 ppm level, and also lists a wide range of other trace element contents, determined by LA-ICP-MS for two allanite samples from subducted eclogites from the Dora Maira massif in the Western Alps. In blueschist and eclogite samples from New Caledonia, Spandler et al. (2003) found Zr contents that range from 1 to 16 ppm (LA-ICP-MS data). There are only a few localities where considerably larger concentrations have been reported. Gieré (1986) described metasomatically formed allanite-(Ce) from a skarn in the Bergell contact aureole, Italy, which contains an average of 0.51 wt% ZrO_2, and a maximum value of 0.58 wt%. This value is similar to that observed by Iimori (1939) for a Be-rich allanite from Fukushima Prefecture, Japan. Zirconium-rich allanite (0.76 wt%) has also been reported by Khvostova (1962), but the largest ZrO_2 content observed so far is 2 wt% (Bea 1996). This author states that allanite in granitic rocks typically contains relatively large amounts of ZrO_2. Because its ionic radius is similar to that of Ti^{4+}, Zr^{4+} most likely enters the M sites in epidote-group minerals, probably by exchange mechanisms that are analogous to substitutions (20), (24), and (25).

Tin. This element is a fairly common constituent of allanite, but SnO_2 concentrations are generally relatively small (<0.85 wt%; Kimura and Nagashima 1951; Ueda 1955; Hagesawa 1960; Khvostova 1962). The mechanism for Sn incorporation has been described as

$$Sn^{4+} + Fe^{2+} \leftrightarrow 2\ (Fe^{3+}, Al^{3+}) \qquad (27)$$

for epidote containing up to 2.84 wt% SnO_2 that occurs in a skarn (van Marcke de Lummen 1986).

Barium. Semenov et al. (1978) reported that allanite contains considerable amounts of Ba in syenite associated with carbonatite complexes in Tamil Nadu. They found concentrations up to 0.69 wt% BaO and noted that these allanites are also enriched in MnO and TiO_2. Sawka (1988) found up to 0.28 wt% BaO in allanite from the McMurray Meadows granodiorite, Sierra Nevada, California. Sawka's data suggest that BaO should be routinely analyzed in pluton-hosted allanite with the electron microprobe by using wavelength-dispersive techniques. Hermann (2002) found Ba in two allanites from eclogites, albeit in much smaller amounts (214 and 11 ppm Ba, LA-ICP-MS data). Similarly, Spandler et al. (2003) measured ~250 ppm Ba in allanite from a lawsonite blueschist (LA-ICP-MS data).

RARE EARTH CHARACTERISTICS

The compiled database with more than 1700 chemical analyses was used to explore the REE characteristics of allanite and related members of the epidote group. Most of the analyses were made by electron microprobe, and therefore, show scant data for REE heavier than Sm. Exley (1980), Gieré (1986), and Sorensen (1991) pointed out that interference corrections

become sizeable for REE heavier than Sm, and microprobe detection limits therefore rise for these elements. Accordingly, many of the chondrite-normalized REE patterns discussed in this section display data that were obtained in the last 20 years, mostly with analytical techniques that have low detection limits for REE (e.g., by LA-ICP-MS or instrumental neutron activation analysis [INAA]). These diagrams were specifically selected to discuss the characteristics of allanite across the entire lanthanide series. For the LREE, the available electron microprobe data confirm the trends discussed below.

The total REE content of allanite can exceed 1 atom per formula unit (see Fig. 3). In these cases, however, the total number of Me^{2+} cations in M sites is not always greater than 0.333, consistent with REE charge balance by substitutions (1), (2), (5), (6), or (14). Together, these two observations suggest that there must be additional mechanisms of REE incorporation into "excess REE" members of the epidote group. An example of this problem is presented by the ferriallanite-(Ce) analyses of Holtstam et al. (2003). To accommodate excess REE, the authors invoked the substitution

$$Ca + Si \leftrightarrow REE + {}^{IV}Al \qquad (28)$$

which would not affect the Me^{2+} content of the M sites. As mentioned above, accommodation of Al by the T sites is not very common, and therefore, the excess REE can probably in most cases be accommodated by substitutions, such as, (18), (19), (22), or (23).

The bulk of the REE data show that chondrite-normalized values of La range from about 10,000 to 200,000, whereas chondrite-normalized Sm values range from 4,000 (the lower values would represent an REE-rich epidote) to 60,000. All chondrite-normalized diagrams in this chapter were calculated with the chondrite data of Wakita et al. (1971). The data show that not only is allanite rich in LREE, but that it appears to be richest in La, Ce, Pr, and Nd, which have the largest ionic radii. The preference of allanite for LREE was described by Goldschmidt and Thomassen (1924) in their pioneering work on element distribution in minerals. Semenov (1958) attributed this preference to a crystal-chemical effect, arguing that the large cation site available in allanite preferentially accommodates the larger REE. Classifying allanite as a "complex mineral with a Ce tendency," this author noted that, in contrast to "selective minerals" (e.g., monazite, bastnäsite, and xenotime), "the REE composition maxima are subject to changes" in allanite. Semenov (1958) concluded that allanite's REE composition reflects the proportions of the lanthanides in the petrogenetic environment. Several investigators have, in fact, observed that the REE content of allanite depends on the bulk chemical composition of the host rocks. Lee and Bastron (1967), for example, described that the degree of REE fractionation varies with the CaO content of granitic rocks in the Mt. Wheeler area, Nevada. Similarly, Murata et al. (1957) and Fleischer (1965) have shown that the average relative enrichment of LREE in allanite varies with rock type, increasing from granitic pegmatite to granodiorite to carbonatite (Fig. 10). Kosterin et al. (1961) pointed out that allanite from granodiorite and diorite has the largest La/Nd and Ce/Nd ratios, those from syenites the lowest; allanite from granite and alaskite displays intermediate ratios.

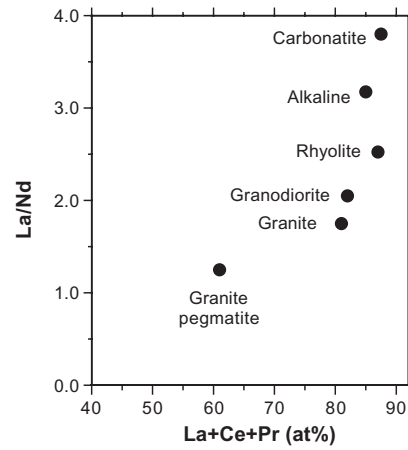

Figure 10. La/Nd vs. (La+Ce+Pr) showing *average* compositions (in at%) of allanites in different rock types. Modified after Fleischer (1965).

The REE characteristics of most allanites from igneous rocks are basically similar. As demonstrated by chondrite-normalized REE patterns, allanite strongly fractionates the LREE from the heavy REE (HREE), and typically exhibits a pronounced negative Eu anomaly. In rhyolitic volcanic rocks, allanite phenocrysts are characterized by chondrite-normalized La/Yb values between ~250 and 2340, in strong contrast to the La/Lu values of the glass matrix (Figs. 11-13; Table 4), which are two orders of magnitude lower. The great affinity of allanite for the LREE is also emphasized by the phenocryst/glass partition coefficients for individual elements (Mahood and Hildreth 1983; Brooks et al. 1981; Chesner and Ettlinger 1989). These coefficients are defined as $D(i) = X_i^{\text{Allanite}}/X_i^{\text{Glass}}$, where X_i is the weight fraction of a specific element *i* in each phase. The $D(i)$ values decrease by about two orders of magnitude across the lanthanide series, irrespective of the rhyolite type (Fig. 14); a rapid decrease in $D(i)$ with atomic number is observed even within the LREE group. There is a striking similarity in the $D(i)$ *trends* of the Sandy Braes obsidian (Northern Ireland) and the Bishop tuff (California). However, the *values* of $D(i)$ for any given REE are markedly higher (except

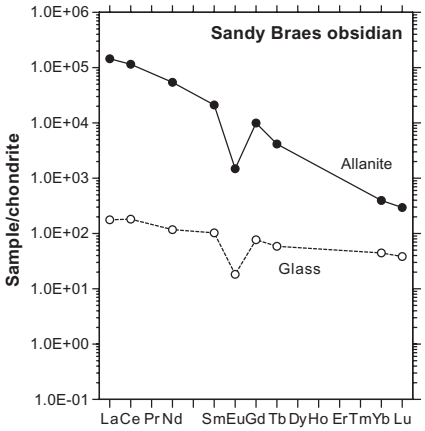

Figure 11. REE patterns for allanite phenocrysts and glass matrix in the Sandy Braes obsidian, Northern Ireland. Data from Brooks et al. (1981).

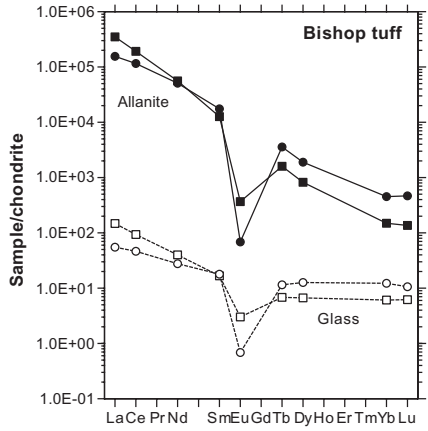

Figure 12. REE patterns for allanite phenocrysts and coexisting glass (corresponding open symbols) in the Bishop tuff, California. Data from Mahood and Hildreth (1983).

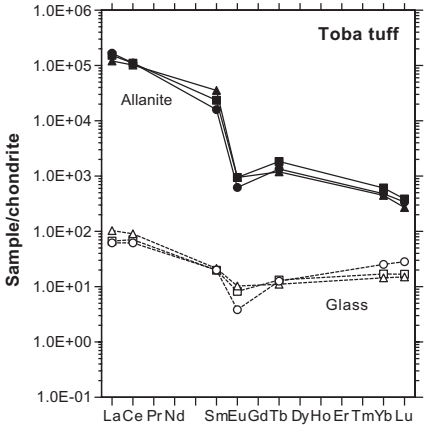

Figure 13. REE patterns for allanite phenocrysts and coexisting glass (corresponding open symbols) in the Toba tuff, Sumatra. Dot/open dot symbol = Youngest Toba tuff, other symbols = Middle Toba tuff. Data from Chesner and Ettlinger (1989).

Table 4. Chemical characteristics of allanite phenocrysts and their rhyolitic host rocks

Locality	SiO_2 in host rock (wt%)	Al_2O_3 in host rock (wt%)	CaO in host rock (wt%)	ASI #	Total REE in allanite (ppm) *	Total REE in glass (ppm) *	La/Yb in allanite	La/Yb in glass	Th in allanite (ppm)	Th in glass (ppm)	U in allanite (ppm)	U in glass (ppm)	Ref.
Sandy Braes obsidian, Northern Ireland	72.8	12.4	0.91	0.995	195490	355	366	4	7600	45.2	< 62	9.3	(1)
Bishop tuff, California	75.7	13.0	0.83	0.986	332235	168	2342	24	5544	13.2	47.6	3.4	(2)
Bishop tuff, California	77.4	12.3	0.45	0.990	194948	90	344	4	11914	20.4	119.0	7.0	(2)
Youngest Toba tuff, Sumatra					160594 **	89	348 **	2					(3)
Middle Toba tuff, Sumatra					140390 **	126	270 **	7					(3)
Middle Toba tuff, Sumatra					156962 **	97	249 **	4					(3)

References: (1) Brooks et al. 1981; (2) Mahood and Hildreth 1983; (3) Chesner and Ettlinger 1989

\# Aluminum saturation index: ASI = $Al_2O_3/(CaO+Na_2O+K_2O)$, in molar units

* minimum value (sum of all REE reported in original paper)

** calculated from partition coefficients and coexisting glass compositions (Table 4 and Table 3B in original paper, respectively)

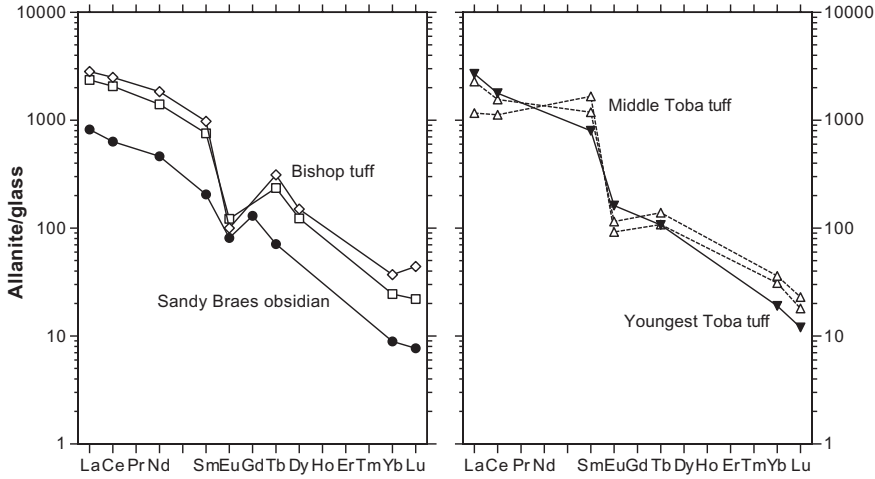

Figure 14. Variation of the allanite/glass partition coefficients for rhyolitic rocks across the lanthanide series. Data represent measured concentrations in allanite phenocrysts and coexisting glass (from Brooks et al. 1981; Mahood and Hildreth 1983; Chesner and Ettlinger 1989).

for Eu) for the Bishop tuff, which exhibits $D(i)$ values of similar magnitude to those observed for the Toba tuff (Fig. 14). Allanite was therefore more effective at fractionating REE from the melts of the Bishop and Toba tuffs. Because the total REE content of the tuff glasses is considerably lower than that of the Sandy Braes glass (Table 4), the total REE contents and chondrite-normalized patterns of the allanite phenocrysts are similar in all three rhyolites (Figs. 11-13). Differences in $D(i)$ values between the different rock types are also observed for other elements, for example Th and U. In the Bishop tuff, these elements have again been more effectively partitioned into allanite compared with the Sandy Braes obsidian, whose glass is richer in both elements (Fig. 15). In both rhyolites, however, allanite preferentially accommodated Th, documenting that it strongly fractionates Th from U during crystallization.

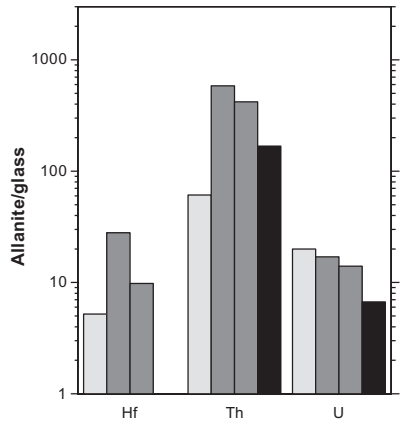

Figure 15. Allanite/glass partition coefficients for Hf, Th, and U. Data represent measured concentrations in allanite phenocrysts and coexisting glass. Symbols: light grey = experimental data for granodioritic melt (Hermann 2002); dark grey = data for rhyolitic Bishop tuff, California (Mahood and Hildreth 1983); black = data for Sandy Braes obsidian, Northern Ireland (Brooks et al. 1981).

The vast majority of published REE data are available for allanite from plutonic rocks, primarily different types of granite and granitic pegmatite. Most analyses of such allanites, however, only list the LREE (typically La-Sm). The few fairly recent datasets containing the entire lanthanide series (or a large part thereof) show REE characteristics that are broadly similar to those of allanite from rhyolite. These data have been used to construct chondrite-normalized REE patterns (Fourcade and Allègre 1981; Buda and Nagy 1995; Bea 1996;

Poitrasson 2002). Where available, the REE patterns of the host rocks have also been plotted. The diagrams, shown in Figures 16-21, reveal pronounced negative Eu anomalies for examples of allanite from plagiogranite, tonalite, granodiorite, and monzogranite. It seems likely that negative Eu anomalies also exist in allanite from granite (Fig. 22). The enrichment of LREE relative to HREE is variable, with chondrite-normalized La/Yb values ranging from ~50–300. Only the allanite hosted by the Urbalacone calc-alkaline granodiorite, Corsica (Poitrasson 2002) displays extremely fractionated patterns (La/Yb ≈ 900; Fig. 19).

The basic similarities observed for allanite are not universal within the population of REE-rich epidote minerals, as illustrated by Sorensen (1991) and by the REE-patterns of various endmembers of this group (Fig. 23). However, it is not clear what dictates the

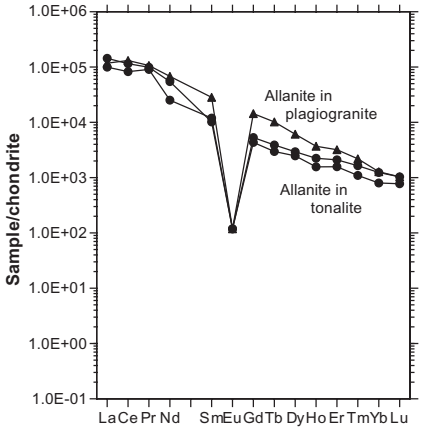

Figure 16. REE patterns for allanite in plagiogranite (Khabarny, Southern Urals) and tonalite (Sirostan). LA-ICP-MS data from Bea (1996).

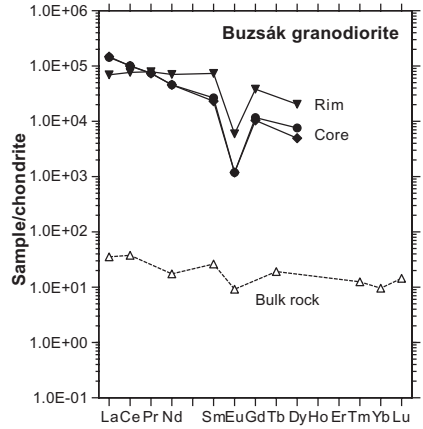

Figure 17. REE patterns for allanite and its host rock, Buzsák granodiorite, Hungary. Electron microprobe data from Buda and Nagy (1995).

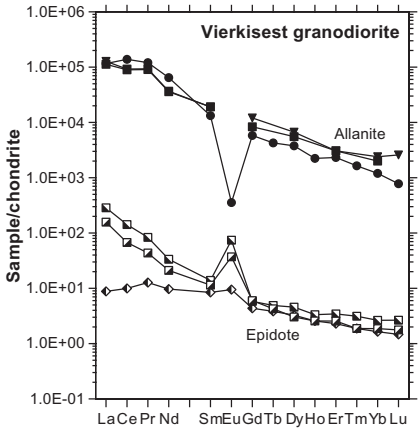

Figure 18. REE patterns for allanite and magmatic epidote in the Vierkisest granodiorite, Central Urals. LA-ICP-MS and electron microprobe data from Bea (1996).

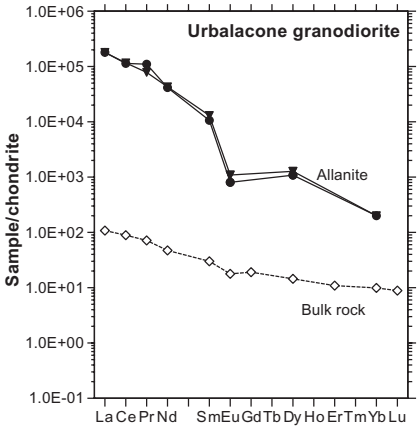

Figure 19. REE patterns for allanite and its host rock, Urbalacone granodiorite, Corsica. LA-ICP-MS and electron microprobe (allanite) and ICP-AES (bulk rock) data from Poitrasson (2002).

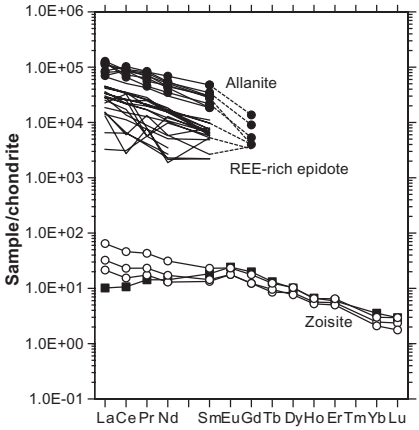

Figure 20. REE patterns for allanite and REE-rich epidote in the granodiorite complex of Central Sardinia (electron microprobe data from Carcangiu et al. 1997). Zoisite patterns for mineral separates from two amphibolite samples in the Tauern Window, Austria (X-ray fluorescence data from Brunsmann et al. 2000).

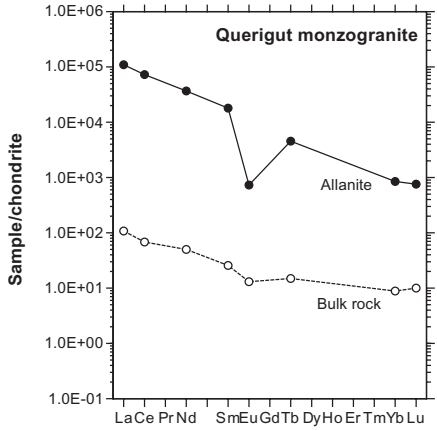

Figure 21. REE patterns for allanite and its host rock, Querigut monzogranite, French Pyrenees. INAA data from Fourcade and Allègre (1981).

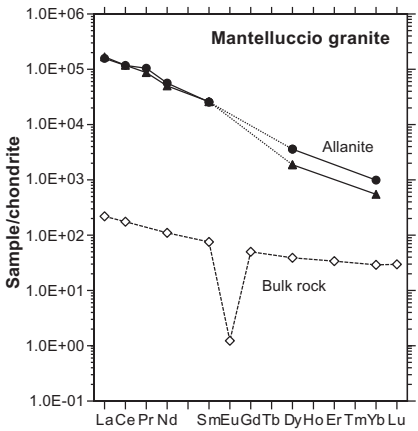

Figure 22. REE patterns for allanite and its host rock, Mantelluccio granite, Corsica. LA-ICP-MS and electron microprobe data from Poitrasson (2002).

Figure 23 (*on facing page*). Chondrite-normalized REE patterns for the near-endmember or type specimens of REE-rich epidote-group minerals. *Allanite-(La):* dots = electron microprobe data from Pan and Fleet (1991); diamonds = electron microprobe and SIMS data from Bonazzi et al. (1992). Note that the Bonazzi et al. (1992) data represent REE-rich piemontite (ΣREE < 0.5). *Dissakisite-(Ce):* dots = electron microprobe data from Grew et al. (1991); diamond = electron microprobe data from de Parseval et al. (1997); x = detection limit for Grew et al. (1991) data. *Ferriallanite-(Ce) :* dots = LA-ICP-MS data for sample #882234, from Holtstam et al. (2003); other symbols = electron microprobe data from Kartashov et al. (2002), diamond = data for crystal used for structure refinement. *Androsite-(La):* electron microprobe data from Bonazzi et al. (1996). *Khristovite-(Ce):* dots = electron microprobe data from Sokolova et al. (1991); diamond = electron microprobe data from Pautov et al. (1993). *Dollaseite-(Ce):* electron microprobe data from Peacor and Dunn (1988).

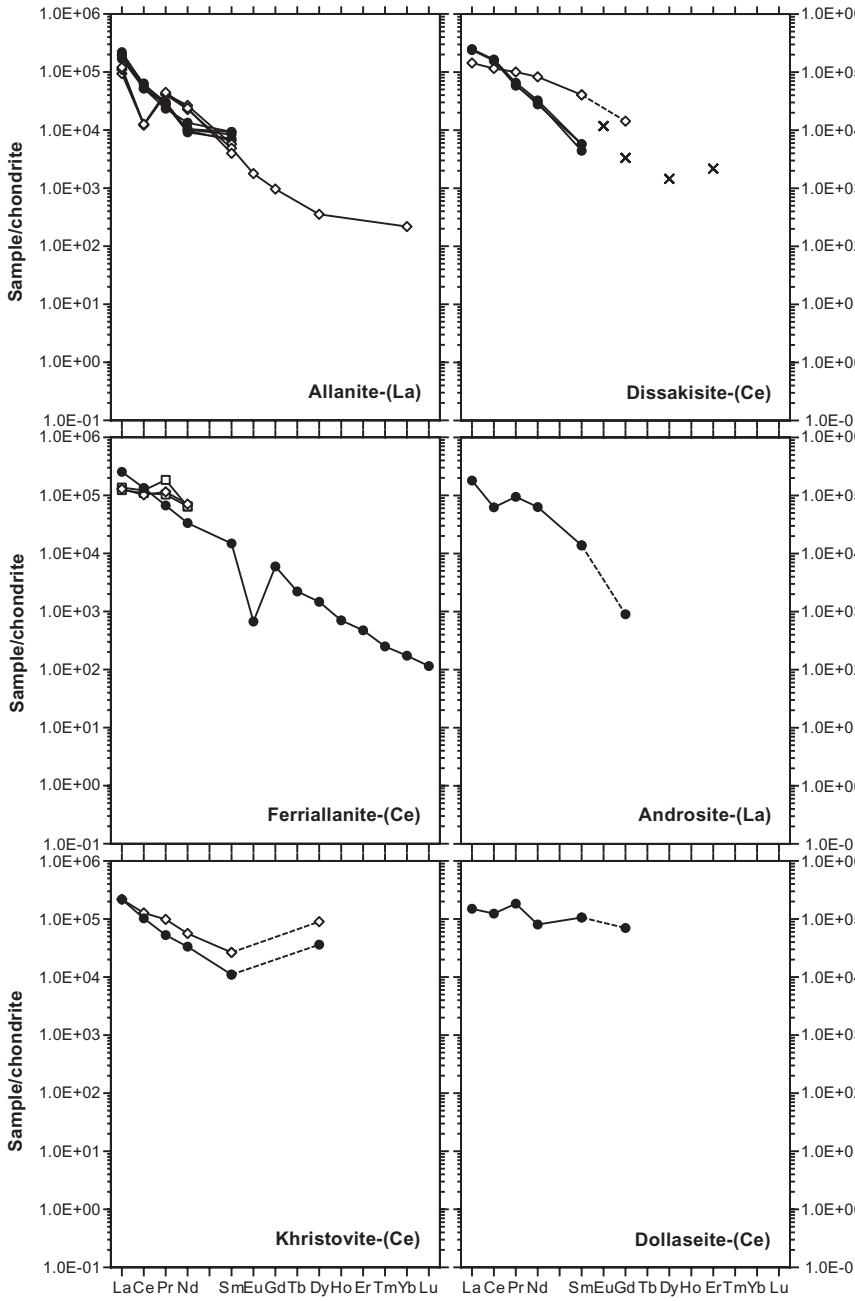

Figure 23. *caption on facing page*

extremely fractionated patterns of allanite-(La), ferriallanite-(Ce), and dissakisite-(Ce) versus the relatively flat one of dollaseite-(Ce). Zhirov et al. (1961), who studied pegmatites in north Karelia, offered a possible explanation for this disparity. They observed that if allanite is associated with monazite and xenotime, it is LREE-enriched, but that it is Y-dominant in the absence of phosphate minerals. These data suggest that the REE pattern of allanite is strongly influenced by the crystallization sequences of other REE minerals.

The effect of competitive crystallization of other REE-bearing minerals is not restricted to igneous rocks, but is also observed in metamorphic and metasomatic environments. An example of metamorphic allanite is shown in Figure 24: the two allanites, which occur in eclogites from Dora Maira, Western Alps, exhibit the most strongly fractionated REE patterns reported for allanite (chondrite-normalized La/Yb = 54,686 and 22,498), and they lack an Eu anomaly. Furthermore, the crossover of the allanite patterns with those of the respective bulk rocks implies that HREE-rich phases must be present. Such phases are indeed part of the assemblage and were identified as garnet and zircon, which both show typical HREE-enriched patterns (Hermann 2002). In their study of REE redistribution during high-pressure, low-temperature metamorphism of Fe-gabbros from Liguria (Italy), Tribuzio et al. (1996) also observed that allanite is strongly enriched in LREE and depleted in HREE, but that the chondrite-normalized REE patterns exhibit a peak at Nd (Fig. 25). As indicated in this diagram, the concentrations of Er and Yb are detectable in the eclogite host rock, but not in allanite. Tribuzio et al. (1996) showed that the HREE in the studied Ligurian eclogite primarily reside in garnet, as is the case for Dora Maira eclogite, and also that a significant portion of the bulk-rock REE have been incorporated in apatite. Spandler et al. (2003) published REE patterns of allanites from high-pressure metamorphic rocks in New Caledonia. These authors showed for allanites from lawsonite blueschist that the chondrite-normalized REE values are approximately 60,000 from La to Nd, and then decrease smoothly, without an Eu anomaly, to ~50 for Lu (Fig. 26). The other REE patterns reported by Spandler et al. (2003) are for REE-rich epidote and zoisite, rather than allanite (Fig. 27). The REE-rich epidotes, which occur in an epidote blueschist, display fairly flat, smooth patterns, with chondrite-normalized values ranging from ~1200 (La) to ~20 (Lu); those from a quartz-phengite schist are richer in LREE, with chondrite-normalized values ranging from ~10,000 (La) to ~2 (Lu). None of the metamorphic allanites, for which datasets spanning the entire lanthanide series are available, exhibits an Eu anomaly. These allanites, all from high-pressure rocks, are thus clearly distinct from the igneous allanites.

Another mechanism that may lead to changes in the REE patterns is fractional crystallization. Evidence for this mechanism exists in igneous allanite, which is often strongly zoned, as documented by numerous published backscattered electron (BSE) images (e.g., Pantó 1975; Buda and Nagy 1995; Petrík et al. 1995; Catlos et al. 2000; Poitrasson 2002; Oberli et al. 2004). Zoning is also responsible for the variable chondrite-normalized REE patterns shown for allanite from the Buszák granodiorite in Hungary (Fig. 17; Buda and Nagy 1995).

An example of distinct magmatic zoning in allanite has recently been described by Oberli et al. (2004), who studied allanite occurring as a relatively abundant (~0.9 vol%) phase in the tonalite of the Tertiary Bergell pluton in the eastern Central Alps. All crystals are optically zoned. They exhibit dark brown allanite cores, surrounded by a series of lightly colored zones, and an outermost rim of colorless REE-free epidote. A BSE image of part of a typical allanite grain (Fig. 28) shows that both the core and surrounding area consist of at least two individual sub-zones (labeled A and B, and C and D, respectively). The rim zones C and D are separated by a distinct straight boundary (dashed line in Fig. 28, top left), which traces an euhedral shape that is in marked contrast to the boundary between zones A and B in the core. The BSE image reveals that zone B can be further subdivided into at least two additional zones, B1 and B2 (Fig. 28, top right). The complex dentate, serrate and embayed boundaries observed in the core

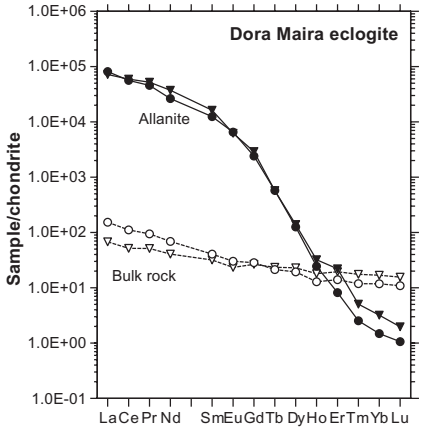

Figure 24. REE patterns for allanite and its phengite eclogite host rocks from Dora Maira, Western Alps. LA-ICP-MS (allanite) and solution ICP-MS (bulk rock) data from Hermann (2002).

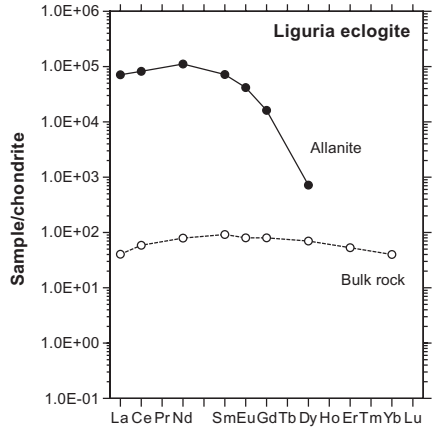

Figure 25. REE patterns for allanite and its eclogite host rock from Liguria, northwestern Italy. Ion microprobe (allanite; mean value) and solution ICP-MS (bulk rock) data from Tribuzio et al. (1996).

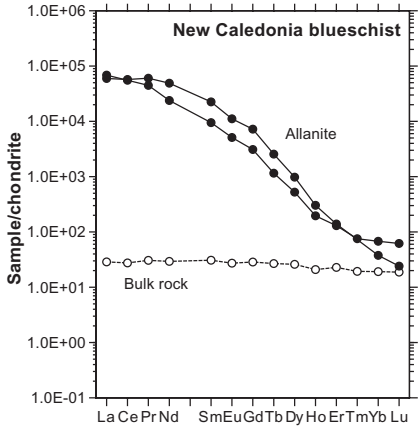

Figure 26. REE patterns for allanite and its lawsonite blueschist host rock from New Caledonia. LA-ICPS-MS data from Spandler et al. (2003).

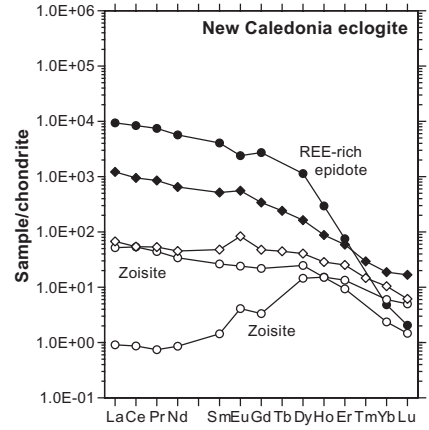

Figure 27. REE patterns for zoisite and REE-rich epidote in eclogite from New Caledonia. LA-ICPS-MS data from Spandler et al. (2003). Symbols: diamonds = garnet-bearing epidote blueschist; dots = quartz-phengite schist.

area possibly reflect various growth and corrosion stages during allanite crystallization from a melt. Similar observations can also be made in the element distribution maps of a neighboring area of the same crystal (Fig. 28, bottom; for color version of the element distribution maps, see back cover). To quantify the pronounced zoning, Oberli et al. (2004) have performed a series of electron microprobe analyses along various traverses. As shown in Figures 29-31, the core is characterized by high contents of Th and REE, and is also enriched in Ti and Mg relative to the rim. Figure 29 further shows estimated Fe^{3+}/Fe_{tot} values of around 0.4 for the core, in contrast to the essentially Fe^{2+}-free epidote rim. Density separates that proxy core to rim aliquots of the same sample used by Oberli et al. (2004) have been analyzed by ^{57}Fe

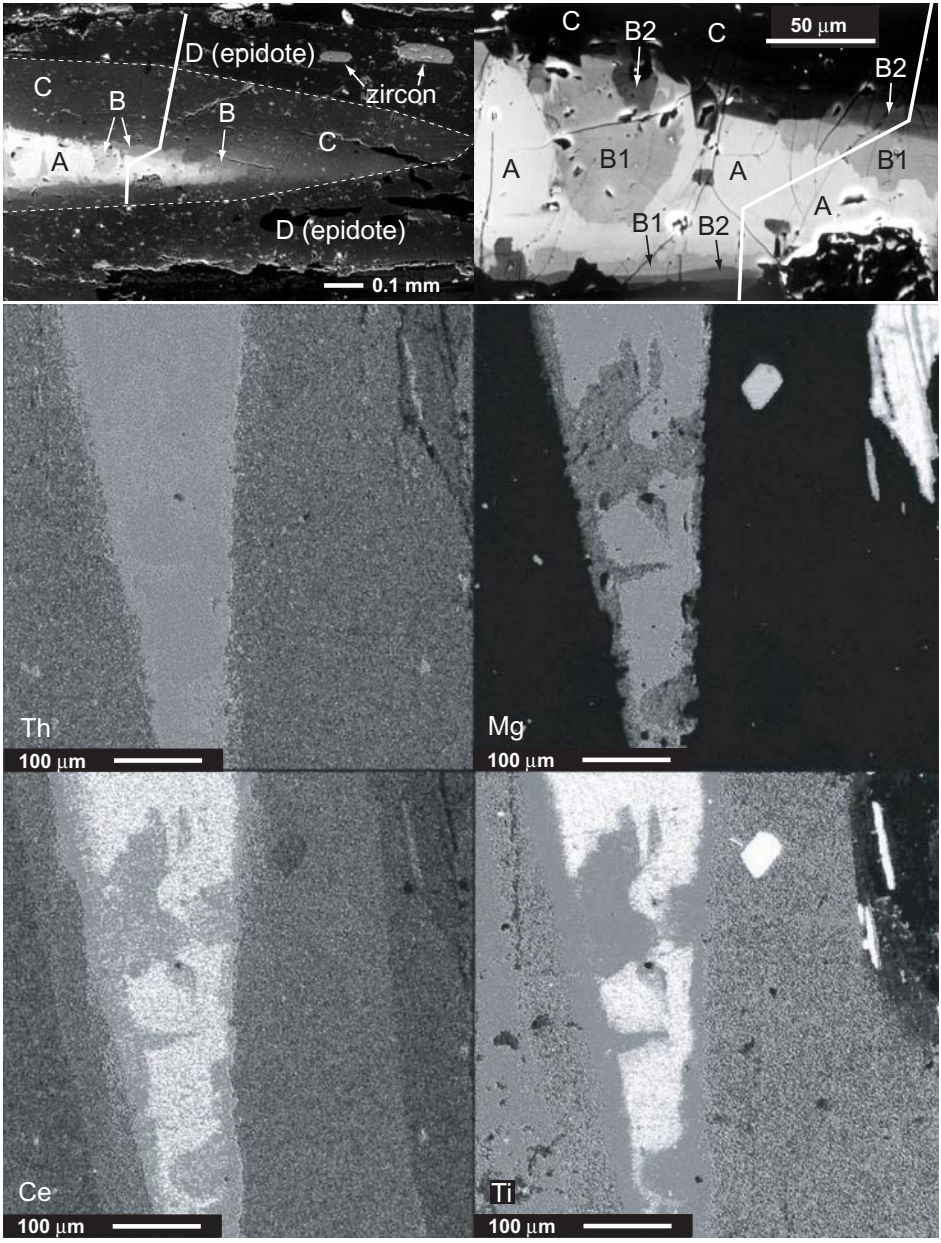

Figure 28. BSE images (top) of a part of an allanite crystal studied by Oberli et al. (2004). The allanite occurs in tonalite of the Bergell pluton, Central Alps. Solid line shows trace of electron microprobe traverse. The bright core (zones A and B) displays complex zoning (top left). A detail of the zoning in the core is shown in the top right BSE image. Dashed line marks the euhedral boundary between the allanite rim zone (C) and epidote (D). The X-ray maps (bottom) show the distribution of Th, Mg, Ce, and Ti in an area that is adjacent to the view seen in the BSE images (Gieré, unpublished data). For a color version of the element distribution maps, see back cover.

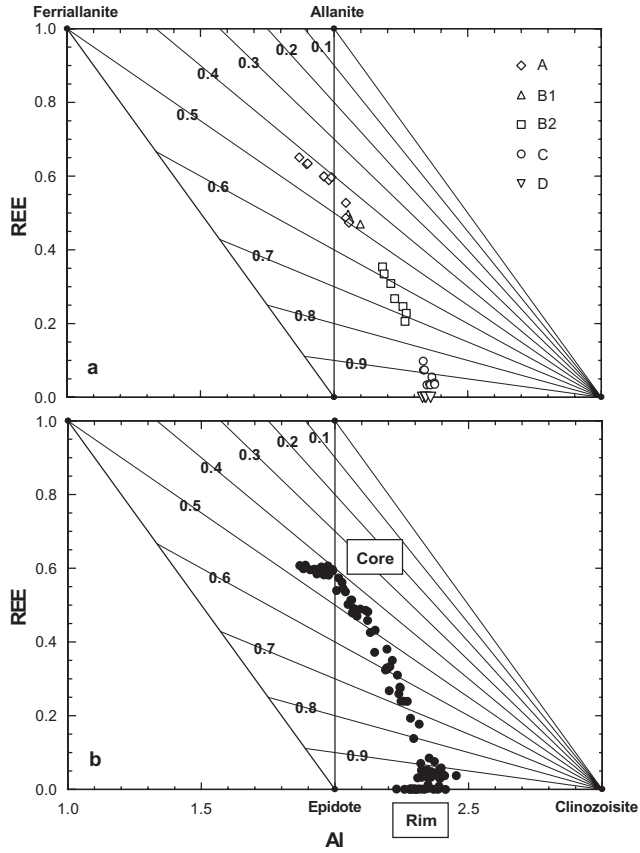

Figure 29. Variation of REE vs. Al in the Bergell allanite crystal shown in Figure 28. **a)** Data for zones A (allanite core) – D (epidote rim); from Oberli et al. (2004); **b)** Data for two traverses across the same crystal in the area shown in the lower part of Figure 28 (Gieré, unpublished electron microprobe data). Lines radiating from the clinozoisite endmember represent lines of constant Fe-oxidation state and are labeled for Fe^{3+}/Fe_{total}.

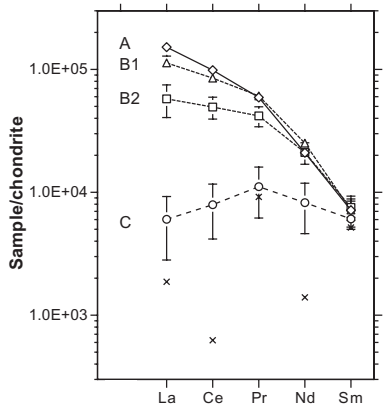

Figure 30. Chondrite-normalized REE patterns for the individual zones in allanite from the Bergell tonalite, changing from highly LREE enriched in the core (A) to nearly flat in the rim (C). Allanite data are averages for each zone shown in Figure 28, and are from Oberli et al. (2004). Electron microprobe detection limit shown by × symbol.

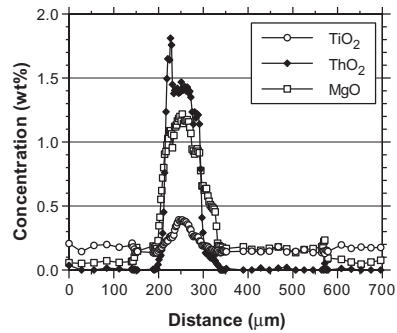

Figure 31. Concentration profile for TiO_2, ThO_2, and MgO across the zoned allanite crystal shown in Figure 28 (Gieré, unpublished electron microprobe data).

Mössbauer spectroscopy (Virgo, unpublished data), and the results confirmed the trend in Fe^{3+}/Fe_{tot} inferred from microprobe data (Gieré et al. 1999). The total REE_2O_3 content decreases dramatically from core (17.6 wt%) to rim (not detectable). This decrease in REE content is accompanied by strong fractionation effects (Fig. 30): Zone A exhibits a chondrite-normalized pattern that is typical for many igneous allanites (compare, for example, with Fig. 16, which shows the pattern of allanite from another tonalite). In comparison to zone A, the LREE enrichment is less pronounced in zone B, which is particularly evident for zone B2. The younger zone C is poor in REE and exhibits a nearly flat chondrite-normalized pattern. In zone D, the youngest part of the crystal, the REE contents are generally below electron microprobe detection limits (see also Fig. 30) and the composition corresponds to epidote (Fig. 29). The regular, correlated changes in major and trace element compositions are distinct from those resulting from hydrothermal overprint (e.g., Poitrasson 2002) and thus, suggest that the observed zonation in allanite is an expression of a magmatic crystallization sequence.

Allanite also exhibits pronounced zoning in many metamorphic and hydrothermal environments (e.g., Sorensen 1991; Catlos et al. 2000; Boundy et al. 2002; Poitrasson 2002; Spandler et al. 2003). Here, zoning is due primarily to release or consumption of REE during metamorphic reactions involving other REE-bearing minerals (see below) or to multiple interactions with hydrothermal fluids of variable REE contents (e.g., Smith et al. 2002; Exley 1980). In several cases, zoning ranges from allanite to zoisite or epidote.

The available REE data, obtained recently for epidote and zoisite by sensitive new techniques and thus spanning the entire lanthanide series, demonstrate that these minerals have chondrite-normalized REE patterns that are distinct from those of allanite and other REE-rich epidote-group minerals. Figure 18 shows chondrite-normalized REE patterns of magmatic epidotes from a granodiorite, which also contains allanite (Bea 1996); two epidotes have chondrite-normalized La/Yb values that are similar to those of allanite, but they exhibit a distinctly positive Eu anomaly. The third epidote pattern is nearly flat, demonstrating that significant variation in the REE fractionation of epidote is possible within a single rock. Two epidote patterns reported by Tribuzio et al. (1996) from an eclogite show yet another distinct shape: a maximum in the middle REE (MREE) with chondrite-normalized values of ~100, and La/Yb values between ~2 and ~8. These patterns are also in marked contrast to those of allanite from the same rock. Similar variability in REE patterns is found for zoisite as well: Brunsmann et al. (2000) described chondrite-normalized REE patterns with a slight LREE enrichment ($La/Yb \approx 10–20$) and others with a maximum for the MREE (Fig. 20; see also Frei et al. 2003). Enrichment in either MREE or HREE is displayed by zoisites from eclogites in New Caledonia (Fig. 27; Spandler et al. 2003).

GEOCHRONOLOGY

Allanite has been shown to be a useful phase for geochronological purposes (Mezger et al. 1989; von Blanckenburg 1992; Barth et al. 1989, 1994; Davis et al. 1994; see also Morrison 2004). The use of allanite as a geochronometer remains relatively restricted in comparison to zircon and monazite, primarily due to its tendency to incorporate common Pb during crystallization and alteration (e.g., Poitrasson 2002; Romer and Siegesmund 2003). Most U-Th-Pb dating studies of allanite have been performed by applying isotope dilution methods to multi-grain samples. To overcome some of the disadvantages of these methods, the use of secondary ion mass spectrometry (SIMS) for Th-Pb dating *in situ* (Catlos et al. 2000; Wing et al. 2003), and in particular the dating of individual growth zones of allanite (Oberli et al. 1999, 2004) has yielded promising results. In addition, U-series dating can be applied to young samples (Vazquez and Reid 2001, 2003).

Catlos et al. (2000) employed a planar solution to matrix corrections for SIMS analyses of allanite that improved the precision of this method to yield about ±10% age accuracy. Their calibration procedure used $^{208}Pb^*/Th^+$ versus ThO_2^+/Th^+ versus FeO^+/SiO^+. Although less accurate than U-Pb dating of monazite by ion microprobe, this procedure allows the examination of many types of geological problems for which monazite ages cannot be obtained—as discussed below, detrital monazite reacts in certain types of metamorphic rocks to form allanite, which can then be used in some metamorphic terrains to determine the age of this isograd. Catlos et al. (2000) used SIMS-based geochronology to determine ages of metamorphic allanite grains from garnet-zone pelitic rocks from the footwall of the Himalayan Main Central Thrust in Nepal. There, allanite inclusions in garnet cores are significantly older than monazite found as inclusions in garnet rims and the rock matrix. Monazite appears to record Tertiary tectonic events, whereas allanite formed in the Paleozoic era, perhaps during the Pan-African orogeny. Catlos et al. (2000) also examined an allanite grain from a famous allanite mineral locality, the Pacoima Canyon pegmatite in California. This pegmatite is renowned for cm-long, gemmy, purple crystals of zircon that appear to coexist with equally large, black, apparently non-metamict allanite grains. A well-determined, U-Pb age of 1191 ± 4 Ma (e.g., Barth et al. 1994) for the zircon is significantly older than the Catlos et al. (2000) Th-Pb SIMS age of allanite (1006 ± 37 Ma). The latter authors attributed the difference to Pb loss from allanite during slow cooling.

In contrast to the predominant practice of dating accessory minerals exclusively by the U-Pb method, Oberli et al. (1999, 2004) presented an approach that makes full use of both U-Pb and Th-Pb isotope systematics. In order to investigate the potential of combined Th-U-Pb isotope and $^{230}Th/^{238}U$ disequilibrium systematics for tracing magmatic crystallization and melt evolution, these authors applied conventional high-resolution single-crystal thermal ionization mass spectrometry (TIMS) techniques to a suite of accessory minerals, including allanite. Because allanite is typically characterized by high Th/U, the observed (apparent) $^{206}Pb/^{238}U$ ages can be considerably enhanced by excess ^{206}Pb derived from ^{230}Th, an intermediate daughter nuclide of the ^{238}U decay series incorporated in excess of its secular equilibrium ratio. In relatively young rocks, high-resolution $^{206}Pb/^{238}U$ data require correction for radioactive disequilibrium. Such corrections are commonly based on the assumption that Th/U of the melt, from which the minerals grew, can be approximated by Th/U of the host rock. In addition, the crystallizing melt is assumed to have remained close to radioactive equilibrium. These assumptions, however, do not necessarily hold if there has been fractional crystallization of Th- or U-enriched phases (Oberli et al. 2004). If fractionation occurs at time scales similar to or shorter than the half-life of ^{230}Th (75,380 yr), it will also cause $^{230}Th/^{238}U$ in the residual melt to deviate from secular equilibrium.

In view of these difficulties, ^{235}U-^{207}Pb dating would be a viable alternative to the use of the ^{238}U-^{206}Pb system, but the presence of even a moderate common Pb component in young allanite results in imprecise ^{235}U-^{207}Pb ages. On the other hand, Th-Pb dating is not affected by these problems, and thus is the method of choice for precise and accurate dating of allanite or other Th-rich minerals, because there are no long-lived intermediate daughter nuclides in the ^{232}Th-^{208}Pb decay system, and the effect of common Pb is mitigated by relatively high Th concentrations (e.g., Barth et al. 1989, 1994).

Oberli et al. (2004) studied zircon, titanite and fragments of chemically characterized growth zones of allanite in a tonalite sample from the feeder zone of the Tertiary Bergell pluton, eastern Central Alps. The isotopic data obtained for these crystals and crystal fragments document crystallization and melt evolution during at least 5 m.y. Zircon ages range from 33.0 to 32.0 Ma. Crystallization of zircon was followed by the formation of zoned allanite between 32.0 and 28.0 Ma, and the crystallization of magmatic epidote possibly as late as 26 Ma. Trace and major element patterns in the zoned allanite closely mirror melt evolution;

they are characterized by a progressive increase of U concentration and sharp decrease of Th and LREE during grain formation (Figs. 28-32). These zoning patterns reflect the early crystallization of phases low in U and document the dominating control of Th by allanite precipitation. Preservation of substantial amounts of excess ^{206}Pb derived from initial excess ^{230}Th in all analyzed allanite grains indicates that their isotopic systems have not been reset by loss of radiogenic Pb during prolonged residence at magmatic conditions and regional-metamorphic cooling, and that the measured sequence of $^{208}Pb/^{232}Th$ dates translates into a real age sequence. Based on these results, Oberli et al. (2004) suggested closure temperatures ≥700°C for magmatic allanite, consistent with the estimates of von Blanckenburg (1992).

The observed $^{230}Th/^{238}U$ disequilibrium relationships reveal a smooth, initially steep decrease of $(Th/U)_{magma}$ from values of 2.9 at 32.0 Ma to less than 0.1 at 28.0 Ma in equilibrium with sequential allanite zoning (Fig. 33). Comparison of calculated $(Th/U)_{magma}$ with $(Th/U)_{bulk\ rock}$, measured at 0.79, requires fractional crystallization of allanite at an early stage. Removal of allanite, and thus Th, from the melt took place until ~31.5 Ma, which provides an upper time limit for emplacement of the studied magma batch. Because zircon and much of allanite crystallization predate emplacement, ages determined on refractory minerals from deep-seated plutons should not be equated with their emplacement ages.

A different approach at unraveling the history of magmatic evolution with the aid of zoned allanite has been taken by Vazquez and Reid (2001, 2003). These authors used electron and ion microprobe techniques for *in situ* analysis of compositional and isotopic zoning in volcanic allanite occurring in the 75,000 year-old Youngest Toba tuff, Indonesia. Core-to-rim zoning in most crystals shows decreases in both their LREE and MgO contents, and increases of MREE, FeO and ThO_2. By coupling the observed chemical zoning with *in situ* ^{238}U-^{230}Th age determinations and other features, such as resorbed boundaries, Vazquez and Reid (2001, 2003) concluded that single allanite crystals from the Toba tuff record a complex differentiation history of fractionation and episodic mixing during protracted residence (up to 150,000 yr) in a large rhyolitic magma chamber.

Similar chemical zoning was also described for allanite in a granodiorite from Southern California (Gromet and Silver 1983). The increase in Th concentration from core to rim observed at this locality as well as in allanite from the Toba tuffs (Vazquez and Reid 2001, 2003) is in marked contrast to the pronounced decrease observed in allanite from the Bergell Tonalite (see Figs. 31, 32).

Romer and Siegesmund (2003) studied texturally and chemically heterogeneous allanite from the Riesenferner Pluton, Austria, and found that samples from two rocks scatter in the concordia diagram, defining discordias from 31.8 ± 0.4 Ma and 32.2 ± 0.4 Ma to ~540 Ma. These authors were able to show that the apparent inheritance is not due to the presence of inclusions of older allanite or other minerals (e.g., zircon, monazite, xenotime), but results from incorporation of radiogenic Pb originating from a precursor phase. The inheritance is thus chemical rather than physical. Because crystallization of allanite requires the availability of REE and Th, it will preferentially occur where REE- and Th-rich precursor minerals have been dissolved in the melt. Romer and Siegesmund (2003) concluded that monazite, originating from assimilated Paleozoic rocks, was the precursor and gave rise to the localized enrichment of REE and Th. They further suggested that similar chemical inheritance might also be observed in metamorphic rocks, where allanite can form at the expense of monazite (see below).

RADIATION DAMAGE AND THERMAL ANNEALING

Natural radioactivity is a process in which an atomic nucleus spontaneously disintegrates (or decays). Radioactive decay is accompanied by emission of α-, β-, or γ-radiation. A stream

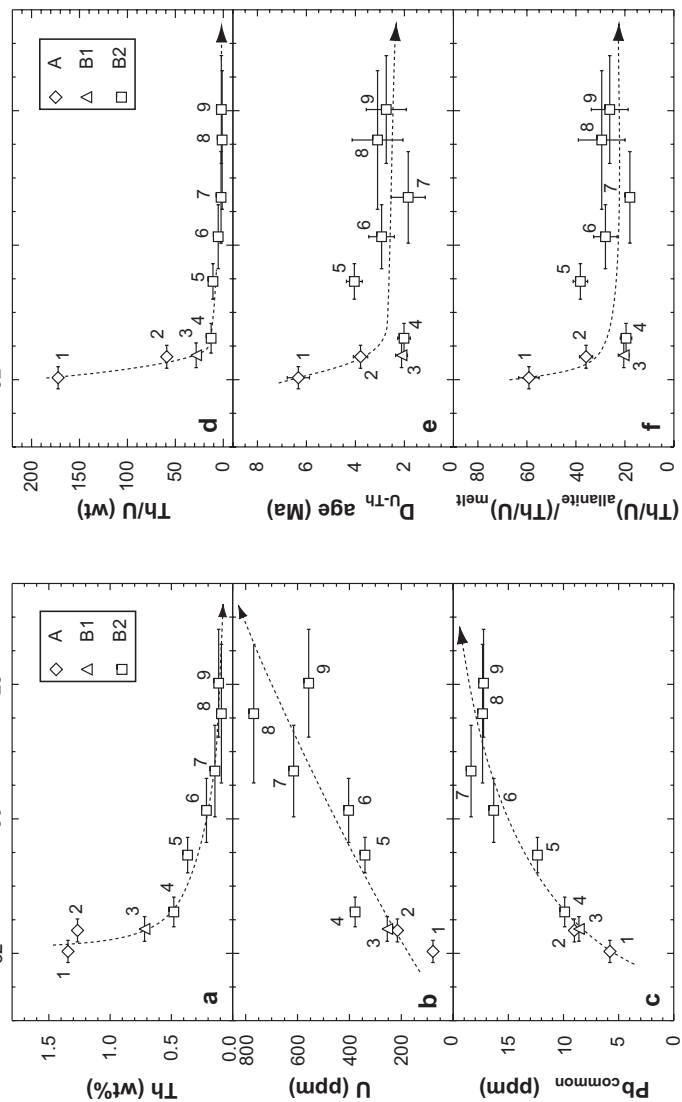

Figure 32. Plot of **a)** Th, **b)** U and **c)** Pb concentrations, and of **d)** Th/U vs. $^{208}Pb/^{232}Th$ age for density-separated allanite fragments from the Bergell tonalite (data symbols and names as shown in Figs. 28-30). The results define an extended crystallization interval of 4 m.y. The marked decrease of Th and increase of U and Pb concentrations with decreasing age are interpreted to mirror incompatible element concentration in an evolving melt. **e)** Difference between $^{206}Pb/^{238}U$ and $^{208}Pb/^{232}Th$ age. Positive age differences of 2-6 Ma between the U-Pb and Th-Pb ages for all analyses are proof for preservation of excess ^{230}Th-derived radiogenic ^{206}Pb, which excludes major resetting of the U-Th-Pb isotopic system in allanite after crystallization. **f)** Allanite/melt fractionation coefficient for Th/U. Diagrams modified after Oberli et al. (2004).

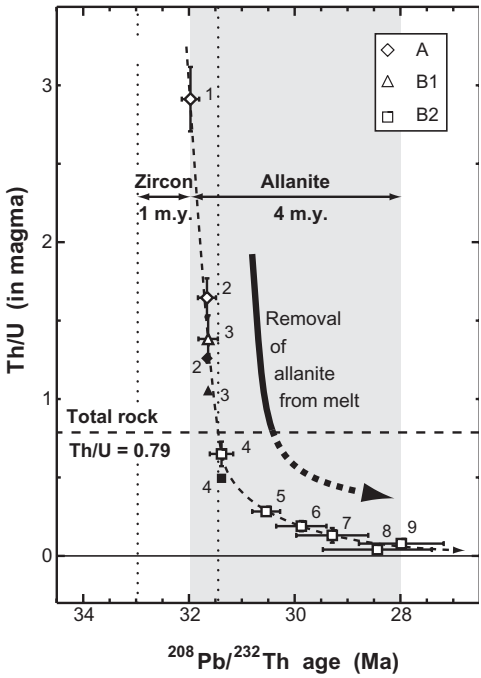

Figure 33. Evolution of Th/U in the magma versus time calculated from the allanite data shown in Figure 32d-f. Open and solid symbols (shown only when not overlapped) denote data points uncorrected and corrected for disequilibrium in $(^{230}Th/^{238}U)_{magma}$, respectively. Diagram modified after Oberli et al. (2004). Data symbols and names as shown in Figures 28-30.

of α-particles (^{4}He nuclei) is α-radiation; β-radiation consists of β-particles (electrons or positrons); and γ-radiation is made up of high-energy electromagnetic waves. Both α- and β-decay cause significant radiation damage in radionuclide-containing minerals, primarily via collisions between the nuclear particles and the neighboring atoms in the host. Most of the damage is produced by recoil nuclei, which collide with and displace neighboring atoms in the crystal structure, thus leading to amorphization.

Radiation damage in minerals results essentially from the α-decay of U and Th. When α-particles are ejected from a parent nucleus, the resulting product nucleus experiences recoil. Because an α-particle has a small mass (4 g/mol) and a high energy (~4.5–5.5 MeV), most of the energy is deposited by ionization. The radiation damage occurs primarily near the end of the path (10–20 μm) and causes approximately 100–200 atomic displacements, mostly Frenkel defects. The recoil nuclei, on the other hand, are much heavier (206–234 g/mol) and have a lower energy (~70–100 keV) than the α-particles. Most of their energy is lost via collisions, which cause approximately 1000–2000 atomic displacements along a track of 10–20 nm length (recoil track). These processes cause physical and chemical changes in materials (for recent reviews, see Ewing et al. 1995; Weber et al. 1998).

In many crystalline substances, collisions resulting from α-decay may transform a periodic, crystalline substance into an aperiodic, amorphous (metamict) material. High-resolution transmission electron microscope (TEM) imaging of crystalline, slightly damaged, and metamict materials, shows that the crystalline-to-metamict transition takes place in various stages (e.g., Ewing et al. 1987). The principal long-term effects of this structural transformation are a volume increase and density decrease. The expansion, which is strongly dependent on the structure type of the material, can lead to the development of two types of microfractures: 1) internal fractures, generated by differential volume expansion between zones of different actinide content; and 2) external fractures, or the development of cracks

in neighboring minerals. Microfracturing increases the surface area of a metamict grain and creates pathways that permit fluids to more easily interact with the mineral. The amorphous form of a mineral may be metastable and therefore is often more susceptible to leaching and/or dissolution (e.g., Mitchell 1973; Geisler and Schleicher 2000; Geisler et al. 2001; Lumpkin 2001; Lumpkin et al. 2004).

Metamict allanite

Studies of optical properties, water content, density, and crystallinity of allanite specimens with various levels of radiation damage have shown that increasing amorphization leads to optical and other physical isotropy, a decrease in mean refractive index and density, and a progressive hydration.

Crystalline allanite shows pleochroism, and has three principal refractive indices (α, β, γ), which vary between 1.690 and 1.891 (Table 3). In contrast, fully amorphous allanite is isotropic and thus has only one refractive index (n). The mean refractive index of allanite decreases with decreasing density (ρ), as was first noted by Zenzén (1916). By examining a series of allanite samples with specific gravities between 4.15 and 2.68 and mean refractive indices of 1.78 to 1.53, Zenzén (1916) discovered that isotropic allanite displays $\rho < 3.50$ g/cm^3 and $n < 1.70$. This effect was also observed by Khvostova (1962), who, like Zenzén (1916), attributed it to increasing metamictization. Frondel (1964), on the other hand, showed that heating metamict or partially metamict allanite increased the indices of refraction, due to the restoration of the allanite structure (i.e., annealing, see below). Tempel (1938) showed that the mean refractive index of allanite decreases with increasing water contents.

Radiation damage in minerals is commonly accompanied by hydration (e.g., Mitchell 1973). Partially or fully metamict allanite specimens may contain substantial amounts of water, and therefore exhibit low microprobe-determined oxide totals (e.g., Khvostova 1962; Deer et al. 1986). Low oxide totals in metamict parts of allanite have, in fact, often been used to infer the presence of substantial amounts of H_2O in the mineral (e.g., Campbell and Ethier 1984; Buda and Nagy 1995). Large H_2O contents are associated with low densities (Tempel 1938). The density of metamict allanite may be as low as 2.68 g/cm^3 (Zenzén 1916), and such allanites are often strongly altered (see below).

In their pioneering studies of metamictization of radioactive minerals, including allanite, Ueda and Korekawa (1954) and Ueda (1957) examined a series of allanites with density varying between 3.65 and 4.08 g/cm^3. They observed that, as the density of allanite decreases, its X-ray diffraction (XRD) peaks decrease in both sharpness and intensity, shift towards lower 2θ angles (i.e., show larger d-spacings), and finally fade away. The least dense allanite specimens yield XRD patterns with a single smooth hump that is produced by diffuse scattering of X-rays by aperiodic material. Ueda (1957) further discussed how the unit-cell dimensions of allanite, as calculated from the XRD patterns, increase with the degree of metamictization. The total volume expansion associated with metamictization of minerals can, in certain cases, form radial cracks in surrounding minerals or host phases, particularly the more brittle ones (e.g., Lumpkin 2001). This typical metamictization feature has been reported for: (1) quartz and feldspar around allanite in veins within granulite (Fig. 1 in Hugo 1961), and in pegmatites from Texas (Ehlmann et al. 1964, their Fig. 3) and North Carolina (Fig. 4 in Mitchell 1973); (2) fluorite that hosts allanite inclusions in a hydrothermal vein at the Buffalo fluorite mine, South Africa (Watson and Snyman 1975); and (3) clinopyroxene around dissakisite-(Ce) with a ThO_2 content of 1.7–2.1 wt% (Yang and Enami 2003, their Fig. 2).

Many investigations of radiation damage in minerals have been carried out with a TEM. This instrument can be used to observe: 1) α-recoil damage in high-resolution bright-field images showing discontinuous lattice fringes and localized amorphous material; and 2) the presence of amorphous domains in selected area electron diffraction (SAED) images on the basis of diffuse haloes, which result from diffuse electron scattering. Moreover, the chemical

composition of the same area that has been imaged by TEM can be determined by energy-dispersive X-ray analytical techniques. Janeczek and Eby (1993) studied three samples of allanite that exhibited different degrees of metamictization as a result of different radionuclide content and age. But even within individual crushed allanite grains, variable amounts of α-recoil damage were observed by TEM, documenting that the radionuclides are not homogeneously distributed. Two of the samples examined by Janeczek and Eby (1993) exhibit the full range of amorphization, from minor radiation damage to complete metamictization, as documented by SAED images. Two parameters that are important for the characterization of radiation damage in minerals, however, have not yet been determined for allanite: the first is the *initial amorphization dose*, i.e., the dose at which a decrease in the total Bragg diffraction intensity is first observed; the second parameter is the *critical amorphization dose*, i.e., the dose where the total Bragg intensity goes to zero. These two parameters could be determined fairly easily for allanite crystals of known age and with pronounced radionuclide zoning (particularly Th).

Annealing of metamict allanite

Thermal annealing of metamict minerals is typically carried out to restore their original crystal structures for phase identification and to determine thermal stability. Ueda (1957) studied the effect of heating on partially metamict allanites. After heat treatment at 400°C and 800°C in vacuum, the XRD peaks were sharper and more intense, and shifted towards higher 2θ angles, consistent with increased crystallinity and unit-cell contraction. Thermal annealing was also investigated by Lima de Faria (1964) for several metamict allanite specimens. During heating at 700°C, this author observed recrystallization of metamict allanite both in air and in a N_2 atmosphere, but the experiments in air produced a slightly different allanite structure. This effect was attributed to oxidation, and indeed probably produced oxyallanite (see Fig. 7). After heating metamict allanite at 1000°C, Lima de Faria (1964) noted new phases, including: magnetite; a phase similar to lessingite†, $(REE,Ca)_5(SiO_4)_3(OH,F)$; and, under oxidizing conditions, cerianite (CeO_2), which was the main phase after heat treatment in air. Some allanite crystals started melting at 1000°C and had melted completely at 1300°C. Kumskova and Khvostova (1964) observed restoration of the allanite structure at 800°C, but only for slightly metamict specimens. Heating of more extensively damaged samples at the same temperature only partially restored the allanite structure, but additionally generated CeO_2 (see also Khvostova 1962; Ehlmann et al. 1964). Similar results were obtained by Vance and Routcliffe (1976), who heated severely damaged allanite specimens in air. These authors also observed CeO_2 formation at temperatures < 1000°C. This result led Vance and Routcliffe (1976) to conclude that the samples examined by Lima de Faria (1964) were not sufficiently damaged for CeO_2 precipitation to occur below 1000°C. At 1200°C, Vance and Routcliffe (1976) observed complete decomposition of allanite, yielding crystalline polyphase mixtures of lessingite + hematite + cerianite in air, and lessingite + magnetite + cerianite in vacuum. Neither Lima de Faria (1964) nor Vance and Routcliffe (1976) discussed the fate of Al upon decomposition of allanite. Mitchell (1966), on the other hand, discovered the presence of anorthite as an additional phase in the breakdown assemblage consisting of magnetite, cerianite, and an apatite-structured silicate. These crystalline polyphase assemblages were formed upon heating of metamict allanite specimens in air at temperatures above 800°C. Similarly, Janeczek and Eby (1993) observed that allanite decomposed above 850°C to an assemblage that included anorthite, hematite and a britholite-like phase (related to lessingite), which was predominant in the mixture of breakdown phases. Janeczek and Eby (1993), however, did not observe formation of CeO_2 during their annealing experiments, which were performed in an Ar atmosphere, thus preventing oxidation of Ce^{3+}.

† The name lessingite has a questionable status, and its IMA-approved synonym is britholite, $(REE,Ca)_5(SiO_4,PO_4)_3(OH,F)$ (de Fourestier 1999). However, in this chapter we are following the terminology used in the original publications referred to.

Thermal annealing experiments can additionally provide information on both the mechanisms and kinetics of recrystallization. For allanite, these aspects of recrystallization were investigated by Janeczek and Eby (1993), Paulmann and Bismayer (2001a), and Paulmann et al. (2000) in progressive and isothermal annealing experiments. *Progressive annealing* experiments showed that the onset of recrystallization took place at 200 to 300°C. At higher temperatures, changes in XRD peak intensities testify to a two-stage annealing mechanism for some partially metamict allanites: the first stage, with pronounced changes in crystallinity occurs between 500 and 600°C; the second stage occurs between 700 and 800°C, and is followed by the breakdown of the allanite structure at about 850°C (Fig. 34). These changes are reflected by associated variations of density (Fig. 34b) and unit-cell parameters (Figs. 34c-e). The response to thermal annealing of the *a*- and *b*-parameters is anisotropic: the unit-cell contraction was more pronounced along *b* than *a* between 500 and 700°C, but the opposite was found above 700°C (Fig. 34c,d). The annealing path of allanites with different degrees of metamictization is similar if they are not fully amorphous. Janeczek and Eby (1993) found that the rate of recrystallization depends on the amount of α-recoil damage: heavily damaged samples anneal faster. These authors also concluded that the activation energy of allanite at 600°C is sufficient to induce heterogeneous recrystallization of amorphous material adjacent to crystalline areas, but not high enough to initiate homogeneous nucleation within larger volumes of amorphous material. *Isothermal annealing* at fixed temperatures between 400 and 700°C indicated a two-stage mechanism. This mechanism consists of a short initial period of rapid recrystallization, followed by a longer time period during which only slight changes in crystallinity are observed. The annealing behavior of allanite is thus similar to that of other partially metamict minerals, such as zircon (Weber 1990) and titanite (Lumpkin et al. 1991). Anisotropic contraction of the *a*- and *b*-parameters of the unit cell is also observed during isothermal annealing, whereby the decrease of *a* is faster than that of *b* at 400 and 500°C (Paulmann and Bismayer 2001b).

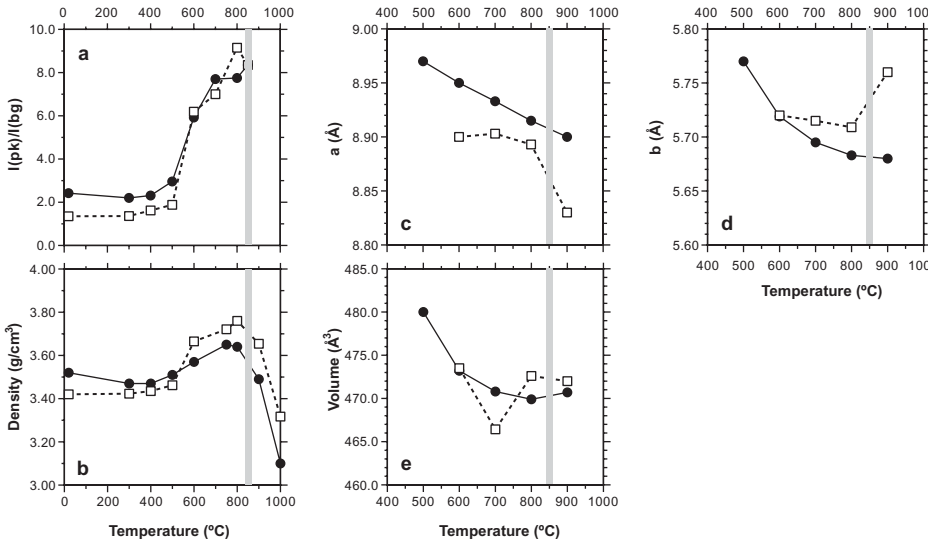

Figure 34. Annealing characteristics of two partially metamict allanite samples as a function of temperature (*T*). **a)** XRD-intensity ratio of the (311) peak to background vs. *T*; **b)** Density vs. *T*; **c)** Unit-cell parameter *a* vs. *T*; **d)** Unit-cell parameter *b* vs. *T*; and **e)** Unit-cell volume vs. *T*. The plots were generated using data from Janeczek and Eby (1993) and show the behavior of their most metamict (open squares) and their least metamict (solid dots) samples. Vertical gray bar shows temperature where allanite starts to decompose.

Annealing of fission tracks

The annealing characteristics of fission tracks in allanite have been studied by Saini et al. (1975). These authors heated allanite specimens from an Indian pegmatite at 800°C to erase fossil fission tracks, irradiated them with thermal neutrons, and then etched the specimens. The annealing experiments were carried out at 640°C to 730°C, and it was found that all fission tracks faded at 720°C if the specimens were heated for one hour. Extrapolation of Arrhenius plots to geological time periods indicates that allanite will lose all fission tracks in 1 m.y. at 380°C, or in 1000 m.y. at 320°C. The authors concluded that allanite is suitable for dating of thermal geological events by fission track dating techniques.

PHASE RELATIONS

Allanite in igneous systems

Much of the interest in igneous epidote has centered on whether there is a threshold pressure (*P*) required for epidote to crystallize in silicic systems (e.g., Zen and Hammarstrom 1984, 1986; Moench 1986; Tulloch 1986; Vyhnal et al. 1991). The cores of epidotes in calc-alkaline granitoids (including pegmatites), dacitic dikes, and volcanic tuffs are commonly REE-rich solid solutions of ferriallanite, allanite, clinozoisite, and epidote (e.g., Gromet and Silver 1983; Chesner and Ettlinger 1989; Dawes and Evans 1991; Buda and Nagy 1995; Petrík et al. 1995; Bea 1996; Oberli et al. 2004). As discussed above, the total REE content in allanite commonly decreases from core to rim, and the rim is often a REE-poor epidote. Such relationships between allanite and epidote have been long recognized: Fersman (1931), for example, concluded that allanite crystallization in granitic systems takes place above ≈600°C (his "stage épimagmatique"), is followed by the formation of epidote rims on allanite, and finally by crystallization of separate epidote grains. It has further been shown (Petrík et al. 1995; Oberli et al. 2004) that the decrease in REE from core to rim in allanite is accompanied by an increase in Fe^{3+}/Fe_{tot}. Moreover, an analogous relationship exists between Th and Fe^{3+}/Fe_{tot} as well as between Ti and Fe^{3+}/Fe_{tot} (see, e.g., Figs. 28, 31). The relationship between oxidation state of Fe and REE content have in two cases also been confirmed by Mössbauer spectroscopy (Petrík et al. 1995; Gieré et al. 1999).

One possibility that explains these chemical relationships between REE, Th, Ti, and Fe^{3+}/Fe_{tot} is that ferriallananite-allanite-epidote-clinozoisite solid solutions only crystallize in silicic melts as a result of elevated REE, Th and Ti abundances (Gromet and Silver 1983; Sawka et al. 1984). Chesner and Ettlinger (1989), however, concluded in their study of allanite phenocrysts in the Toba tuffs that high concentrations of REE in the melt are not necessary for allanite crystallization to occur. Instead, these authors suggested that temperature is a critical factor for allanite crystallization, because Toba tuffs that erupted below 800°C contain allanite regardless of bulk-rock composition, whereas those that erupted above 800°C contain none. Chesner and Ettlinger (1989) concluded that magmatic allanite can exist only within a restricted temperature range in calc-alkaline volcanic rocks. Moreover, if the oxidation state of Fe in natural allanite is controlled by the oxy-reaction (Eqn. 7), then the stability of allanite in magmatic environments may more closely reflect the relationship between *T* and f_{H_2}, rather than *P* and the REE content of the melt (Gieré et al. 1999). Although Fe is present primarily as Fe^{3+} in clinozoisite-epidote solid solutions in metamorphic rocks, the situation may be different in magmatic, REE-free epidotes, as evidenced by the f_{O_2}-dependent supersolidus stability curve for epidote over a range of oxygen fugacities (Schmidt and Thompson 1996).

Chesner and Ettlinger (1989) have shown petrographic evidence suggesting that allanite is a liquidus phase in the Toba tuffs. They also stated that allanite is a fractionating phase since it is present in the tuffs with a content of SiO_2 that ranges from 68 to 76 wt%. Allanite

fractionation caused the LREE to behave compatibly in the magma; the HREE, on the other hand, are incompatible in the Toba magmas. Similar observations have also been reported for the Bishop tuff (Michael 1983; Cameron 1984), and document the importance of allanite crystallization in controlling the behavior of REE in granitic magmas. As discussed by Oberli et al. (2004), allanite also has a considerable impact on the evolution of Th and U concentrations in the melt, from which it crystallizes (see Fig. 33). Their data were obtained from allanite that exhibited a sharp decrease in Th content, and an increase in U content from core to rim (see Figs. 31, 32). Such a core-to-rim decrease in Th, however, is not observed in all magmatic allanites, as demonstrated by zoned phenocrysts in the Toba tuffs (Vazquez and Reid 2001, 2003) and in a granodiorite from the eastern Peninsular Ranges batholith, southern California (Gromet and Silver 1983), which both show an opposite trend. Gromet and Silver (1983) explained this increase in Th from core to rim by allanite growth via substitution of other components to replace the less available (depleted) REE, e.g., substitution (18).

In his study of the residence of REE, Th and U, Bea (1996) observed that allanite is, after monazite, the most important LREE carrier in granitoid rocks. He found that primary allanite occurs in all granite types, except the most peraluminous, P-rich varieties, and that it is particularly abundant in rocks that contain magmatic epidote. The fraction of LREE that reside in allanite depends on the bulk-rock Al_2O_3 concentration relative to the contents of Na_2O, K_2O, and CaO (see also Broska et al. 2000): in metaluminous granite, the LREE fraction that resides in allanite is 50–60 wt%, whereas this value is 20–45 wt% in peralkaline granite, in which LREE-fluorocarbonates or aeschynite may be dominant. The respective fractions of Th are 15–42 wt% (metaluminous) and 10–15 wt% (peralkaline). The maximum fraction of U residing in allanite (23 wt%) was observed for a metaluminous granodiorite.

Petrík et al. (1995) and Broska et al. (2000) too noted that allanite is a typical accessory mineral in metaluminous granitoids, where it is often associated with magnetite. However, Broska et al. (2000) reported that allanite can also occur in peraluminous granitoids. They found the mineral in a peraluminous biotite granodiorite and a tonalite from the western Carpathians. In these rocks, allanite occurs together with apatite in polymineralic inclusions within monazite, which is the characteristic LREE phase in peraluminous granites. Further present in the inclusions are albite, potassium feldspar, white mica, and biotite, which probably represent crystallized melt trapped by monazite. The petrographic observations point to early crystallization of allanite, which was subsequently enclosed by monazite. The included assemblage of allanite+apatite indicates that crystallization of monazite began specifically at those locations with high activities of REE and P. Broska et al. (2000) suggested that the replacement of allanite by monazite was due to a decrease in Ca concentration, which resulted from plagioclase crystallization. Based on the monazite saturation equation of Montel (1993), Broska et al. (2002) calculated that the crystallization temperature of allanite must have been higher than ~850°C and 790°C for the two samples they examined. Their study suggests that Ca-rich granitoid melts may precipitate allanite, but that early crystallization of plagioclase lowers the Ca concentration in the melt and induces formation of monazite, which becomes the dominant LREE mineral in these rocks.

Allanite in metamorphic systems

Allanite is found in pelitic (e.g., Sakai et al. 1984; Wing et al. 2003) and mafic rocks (e.g., Banno 1993; Sorensen and Grossman 1989; Hermann 2002), as well as in granitic gneisses (e.g., Liu et al. 1999) and in carbonate rocks (Boundy et al. 2002) in Buchan, Barrovian, contact, collisional, ultrahigh-pressure collisional and subduction-zone metamorphic settings. Much of it probably forms by greenschist-facies metamorphic reactions that consume detrital or igneous monazite. Smith and Barreiro (1990) first suggested that metamorphic allanite breaks down to form monazite via prograde reactions at temperatures >525°C. Monazite as a breakdown product of allanite has also been described in amphibolite-facies metasedimentary

rocks from the Monte Giove area in Italy (Gieré et al. 1998). These observations have led to an extended discussion of allanite-forming and allanite-consuming reactions in various metamorphic systems.

In both Buchan and Barrovian terrains of northern New England, Wing et al. (2003) determined that detrital monazite breaks down and euhedral metamorphic allanite forms in pelitic rocks by means of the reaction

$$\underset{(Monazite)}{3\ REEPO_4} + \underset{(Muscovite)}{3\ KAl_2AlSi_3O_{10}(OH)_2} + \underset{(Ankerite)}{8\ Ca(Fe,Mg)(CO_3)_2} + \underset{(Siderite)}{4\ (Fe,Mg)CO_3} + \underset{(Quartz)}{9\ SiO_2} + 2\ H_2O \leftrightarrow$$

$$\underset{(Allanite)}{3\ CaREEAl_2FeSi_3O_{11}O(OH)} + \underset{(Biotite)}{3\ K(Fe,Mg)_3AlSi_3O_{10}(OH)_2} + \underset{(Apatite)}{Ca_5(PO_4)_3(OH)} + 20\ CO_2 \quad (29)$$

In the contact aureole of the Onawa pluton in south-central Maine, in which pelitic rocks lack biotite, ankerite, and siderite, and contain chlorite, plagioclase, and calcite, Wing et al. (2003) proposed a different allanite-forming reaction:

$$\underset{(Monazite)}{15\ REEPO_4} + \underset{(Chlorite)}{3\ Fe_5Al_2Si_3O_{10}(OH)_8} + \underset{(Plagioclase)}{12\ CaAl_2Si_2O_8} + \underset{(Calcite)}{28\ CaCO_3} + \underset{(Quartz)}{12\ SiO_2} \leftrightarrow$$

$$\underset{(Allanite)}{15\ CaREEAl_2FeSi_3O_{11}O(OH)} + \underset{(Apatite)}{5\ Ca_5(PO_4)_3(OH)} + 2\ H_2O + 28\ CO_2 \quad (30)$$

Wing et al. (2003) also showed that allanite and biotite isograds coincide in the studied area in New England. Here, Ferry (1984, 1988) concluded that biotite-producing reactions had been driven by aqueous fluid infiltration. Reaction (29) requires the addition of H_2O, and both (29) and (30) are decarbonation reactions. Wing et al. (2003) therefore suggested that the reactions that produce the allanite isograd in the pelites were driven by aqueous fluid infiltration. These allanite-forming reactions are similar to those responsible for monazite breakdown during amphibolite-facies metamorphism of granitic rocks in the eastern Alps and in orthogneisses from the west Carpathians (Finger et al. 1998; Broska and Siman 1998). The latter authors proposed the reaction

$$\underset{(Monazite)}{3\ REEPO_4} + \underset{(Annite)}{KFe_3AlSi_3O_{10}(OH,F)_2} + \underset{(Plagioclase)}{4\ CaAl_2Si_2O_8} + \underset{(Quartz)}{3\ SiO_2} + \underset{(Fluid)}{4\ Ca^{2+}} + 2\ H^+ \leftrightarrow$$

$$\underset{(Apatite)}{Ca_5(PO_4)_3(OH,F)} + \underset{(Allanite)}{3\ CaREEAl_2FeSi_3O_{11}O(OH,F)} + \underset{(Muscovite)}{KAl_2AlSi_3O_{10}(OH)_2} \quad (31)$$

They suggested that the reaction occurred in "a gel form," with apatite nucleating on monazite rims via subsolidus retrogression of granite during Alpine metamorphism. Finger et al. (1998) reported that igneous monazite grains in granite from the Tauern Window, central eastern Alps, had been partly replaced by apatite-allanite-epidote coronae during amphibolite-facies Alpine metamorphism. The replacement textures are annular: a core of magmatically zoned monazite is successively surrounded by rings of apatite + thorite, allanite, and epidote. These authors concluded that a metamorphic fluid was required to create the coronae, the kinetics of the reaction were controlled primarily by diffusion, and that a balanced reaction to explain the entire association was difficult to write. However, they noted that plagioclase, biotite, and muscovite could all have been involved in such a reaction.

Aluminosilicate minerals and metamorphic monazite appear at roughly the same pressure-temperature conditions in pelitic rocks. Wing et al. (2003) reported that in all three types of terrains they studied (Buchan, Barrovian, and contact aureole settings), monazite is formed via breakdown of metamorphic allanite at conditions that are recorded by the first appearance of either andalusite, kyanite, or staurolite, along with apatite, muscovite, biotite, plagioclase, and quartz. These authors constructed an allanite-to-monazite reaction that conserves REE in

allanite and monazite:

$$\underset{(Allanite)}{3\ CaREEAl_2FeSi_3O_{11}O(OH)} + \underset{(Apatite)}{Ca_5(PO_4)_3(OH)} + \underset{(Muscovite)}{KAl_2AlSi_3O_{10}(OH)_2} + \underset{(Andalusite/\ Kyanite)}{4\ Al_2SiO_5} + \underset{(Quartz)}{3\ SiO_2} \leftrightarrow$$

$$\underset{(Monazite)}{3\ REEPO_4} + \underset{(Biotite)}{KFe_3AlSi_3O_{10}(OH)_2} + \underset{(Plagioclase)}{8\ CaAl_2Si_2O_8} + 2\ H_2O \qquad (32)$$

Wing et al. (2003) noted that either cordierite or staurolite could play the same role as andalusite or kyanite in a monazite-forming reaction. In addition, the appearance of new monazite in rocks that both contain and lack aluminosilicate minerals marks similar pressure-temperature conditions for both the monazite and aluminosilicate isograds. Thus, the sequence

detrital or igneous monazite → metamorphic allanite → metamorphic monazite

should be expected during prograde greenschist- to amphibolite-facies metamorphism of pelitic rocks.

In contrast to these observations in rocks of low- and medium-pressure facies series, metasedimentary rocks of the high-pressure/low-temperature Sanbagawa subduction complex and granitic gneiss from the Dabie Shan ultrahigh-pressure metamorphic terrane are reported to preserve igneous or detrital cores of allanite through blueschist- and epidote-amphibolite-facies events, respectively. Sakai et al. (1984) discussed the contrasting optical properties and compositions of allanite core-epidote rim grains from Sanbagawa mica schists. These authors concluded that REE had become locally mobile as allanite broke down in metamorphic fluids, and that these REE had been deposited as REE-rich epidote rims upon allanite grains elsewhere in the fluid-flow system. The authors noted that this was a self-limiting process, because once REE-rich metasomatic epidote armored allanite, REE could not be released any more by the allanite grain. Liu et al. (1999) described dark grains of allanite surrounded by epidote within four samples of granitic gneiss from Dabie Shan. On the basis of core and rim analyses of these grains, they concluded that the allanite had little zoning, and therefore it was of igneous origin. Because the allanite was igneous, they also concluded that the studied Dabie Shan gneiss could not have undergone metamorphism at ultrahigh-pressure conditions. However, two of the four analyses of epidote rims contain weight percent quantities of total REE and thus, suggest a Sanbagawa-like, fluid-buffered origin for the REE-rich rims. Without BSE images, it is not possible to assess whether the allanite grain cores are of igneous origin. It is difficult to argue about the origin of composite grains of allanite, REE-rich-epidote, and epidote in these terranes, if the textures are not adequately documented and in the absence of Th-Pb SIMS geochronology.

The fate of metamorphic allanite or monazite at the amphibolite- to granulite-facies transition has been studied by Bingen et al. (1996), albeit more for the purpose of understanding the redistribution of LREE, medium-heavy REE (M-HREE), Th, and U in accessory mineral assemblages than as a possible indicator of metamorphic conditions. These authors examined accessory minerals in orthogneiss through the transition from the amphibolite to the granulite facies in southwestern Norway. They proposed three reactions that required the contribution of components from both rock-forming and accessory minerals. At the clinopyroxene-in isograd, the proposed schematic reaction is

$$\underset{(in\ hornblende,\ titanite)}{3\ (M\text{-}HREE)_2O_3} + \underset{(in\ allanite)}{3\ LREE_2O_3} + \underset{(Apatite)}{2\ Ca_5(PO_4)_3(F,OH)} + \underset{(Quartz)}{6\ SiO_2} \leftrightarrow$$

$$\underset{(Monazite)}{6\ LREEPO_4} + \underset{(in\ apatite)}{2\ Ca_2(M\text{-}HREE)_3(SiO_4)_3(F,OH)} + \underset{(in\ plagioclase)}{6\ CaO} \qquad (33)$$

This type of reaction would initiate the breakdown of either igneous or metamorphic

allanite, to produce some metamorphic monazite, along with lessingite-rich apatite. At the orthopyroxene-in isograd, apatite becomes further enriched in LREE and Th, either due to the partial breakdown of monazite according to:

$$\underset{(Monazite)}{3\ LREEPO_4} + \underset{(Quartz)}{3\ SiO_2} + \underset{(in\ plagioclase)}{7\ CaO} + \underset{(in\ fluid)}{(F_2, H_2O)} \leftrightarrow \underset{(Apatite)}{Ca_5(PO_4)_3(F,OH)} + \underset{(in\ apatite)}{Ca_2LREE_3(SiO_4)_3(F,OH)} \quad (34)$$

or the final disappearance of allanite:

$$\underset{(in\ allanite)}{3\ LREE_2O_3} + \underset{(Quartz)}{6\ SiO_2} + \underset{(in\ plagioclase)}{4\ CaO} + \underset{(in\ fluid)}{(F_2, H_2O)} \leftrightarrow \underset{(in\ apatite)}{2\ Ca_2LREE_3(SiO_4)_3(F,OH)} \quad (35)$$

Bingen et al. (1996) proposed that the breakdown of allanite in orthogneiss would most likely yield an increased component of lessingite in apatite, rather than the wholesale transformation of apatite + allanite into monazite.

Allanite has been reported in metacarbonate rocks from the Lindås nappe in the Caledonides of western Norway (Boundy et al. 2002). These rocks are found in the Bergen Arc system, and are associated there with the transition between eclogite and granulite facies. The allanite-bearing marble layers consist of calcite, calcian strontianite, clinopyroxene, epidote/allanite, titanite, garnet, barite, and celestine. They occur along eclogite-facies shear zones, and some are interlayered with eclogite on the scale of centimeters. In the marble layers, the epidote-allanite crystals are up to 0.5 cm in size and display oscillatory zoning, but lack systematic core-to-rim trends of REE-zoning. Titanite grains appear to be unzoned in REE. The temperature of marble formation is estimated at ~600°C, based on C-isotopes and a calcsilicate rock that contains garnet + omphacite (580-600°C). In these rocks allanite is interpreted to have crystallized from an H_2O-rich fluid that moved along the shear zones under eclogite-facies conditions in the lowermost continental crust. Thus, the REE contents of the allanite are tentatively interpreted to reflect fluid compositions. (See below for other examples of fluid-sourced REE in allanite from both metamorphic and metasomatic systems.)

Allanite is the principal residence site for LREE and Th in metabasites (i.e, blueschist, garnet amphibolite, and eclogite) and metasedimentary rocks from high-pressure/low-temperature terrains (e.g., Sorensen and Grossman 1989, 1993; Sorensen 1991; Tribuzio et al. 1996; Hermann 2002; Spandler et al. 2003). Such allanite is typically complexly zoned, but not in ways characteristic of igneous crystallization (for example, compare the BSE images of Dawes and Evans 1991 to those of Sorensen 1991). REE patterns of zoned allanite grains in garnet amphibolite from the Catalina Schist and the Gee Point locality of the Shuksan Schist (Sorensen and Grossman 1989, 1993; Sorensen 1991) display features that indicate differences in both LREE abundance and fractionation from zone to zone that cannot be readily modeled by igneous crystallization. Although some of the allanite samples studied from the Catalina Schist occur in rocks that appear to be migmatitic, several rocks from this locality and none of the Shuksan examples show evidence for anatexis. For these reasons, Sorensen (1991) interpreted the allanite zoning to have been acquired during subsolidus metasomatic reactions. Both pelitic and mafic rock samples from New Caledonia show zoning features similar to those seen at Catalina and Gee Point (compare the SEM images of Sorensen 1991 to Spandler et al. 2003).

Mass-balance arguments have been used to determine the residence sites of REE in mafic and pelitic rocks from subduction complexes. This method can be problematic for allanite. For example, such small amounts of allanite are required to house all of the LREE that it is difficult to verify that a mode agrees with a mass fraction estimate. Furthermore, allanite in these rocks is generally strongly zoned in LREE, which means it can be difficult to calculate

an average bulk composition for the mineral (Sorensen 1991). Nevertheless, Sorensen and Grossman (1989), Tribuzio et al. (1996), Hermann (2002), and Spandler et al. (2003) all used a mass balance approach to address the issue of the residence of LREE and Th in subducted rocks, and they concluded that allanite of metamorphic origin performed this role (see Figs. 35, 36). These figures emphasize the importance of allanite as an LREE host and, at the same time, demonstrate that the HREE mainly reside in other minerals (e.g., zircon, garnet).

In addition to examining eclogites from the Dora Maira massif in the Western Alps, Hermann (2002) conducted piston-cylinder synthesis experiments on a model crustal composition (granodioritic) doped with trace elements to address the allanite stability. He found that accessory allanite forms at the expense of zoisite above 700°C and 2 GPa. Allanite is stabilized by the presence of LREE and exists up to 1050°C and at least 4.5 GPa. The mineral is thus expected as a residual phase in subducted crust in the region of liquid extraction. Because allanite contained essentially all of the REE in his experimental composition, and its disappearance is caused by dissolution in the coexisting hydrous granodioritic melt (see

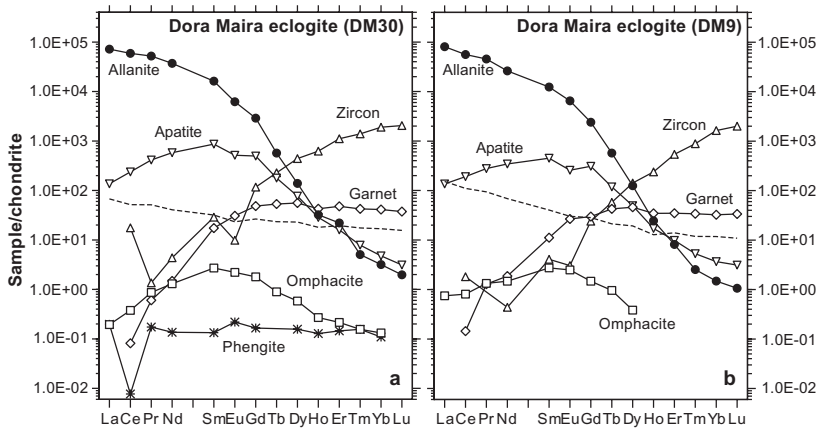

Figure 35. REE patterns for various minerals in phengite eclogite from Dora Maira, Western Alps. **a)** sample DM30; **b)** sample DM9. REE were not detected in phengite from sample DM9. Dashed line represents bulk-rock composition of the eclogite samples. LA-ICP-MS (minerals) and solution ICP-MS (bulk rock) data from Hermann (2002).

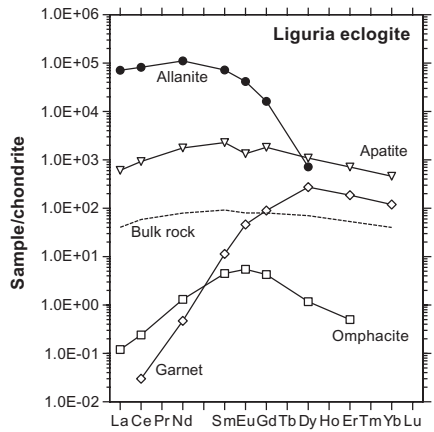

Figure 36. REE patterns for various minerals in eclogite from Liguria, northwestern Italy. Dashed line represents bulk-rock composition. Ion microprobe (allanite) and solution ICP-MS (bulk rock) data from Tribuzio et al. (1996).

also Broska et al. 1999), Hermann (2002) concluded that LREE cannot be significantly transported by hydrous fluids in subduction zones. This conclusion, however, is not consistent with the measured REE contents of some hydrothermal fluids (Banks et al. 1994) or the evidence of REE mobility in crustal fluids (e.g., Gieré 1996). Hermann (2002) further concluded that the REE characteristics of arc lavas must be derived from portions of the mantle wedge that had been contaminated by granitic melts. Unfortunately, some of his model experiments for extracting partitioning data have unusual melt and allanite compositions (compare Fig. 37 with Figs. 11-13, 17-20), so it is not clear how applicable the D(i) values obtained from these materials are to the questions he poses.

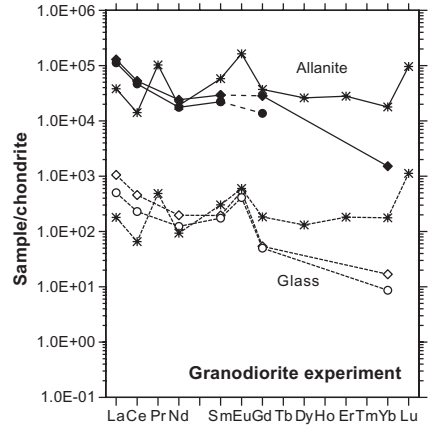

Figure 37. REE patterns for allanite and coexisting granodioritic glass. Experimental data from Hermann (2002). Symbols: dots and diamonds for experiments at 1000°C, 4.5 GPa and 1000°C, 3.5 GPa, respectively; asterisks for experiment 900°C, 2 GPa (these data are in contrast to all other granodiorite data, see Figs. 17-20).

Allanite in metasomatic systems

Metasomatically formed allanite has been reported from many geological environments (Söhnge 1945; Bocquet 1975; Watson and Snyman 1975; Exley 1980; Campbell and Ethier 1984; Moore and McStay 1990; Pan and Fleet 1990; Sorensen 1991; Ward et al. 1992; Zakrzewski et al. 1992; Gieré 1986, 1996; Smith et al. 2002; Weiss 2002; Weiss and Parodi 2002). Pantó (1975) described secondary allanite formed by the decomposition of feldspar. Similarly, Ward et al. (1992) observed that pervasive hydrothermal alteration of the Dartmoor granite (SW England) had led to mobilization of the REE from feldspar and biotite (with associated accessory monazite, xenotime, apatite and zircon), but noted that the REE were accommodated *in situ* by secondary minerals, including allanite and epidote. Allanite has also been described as a breakdown product of eudialyte in microsyenite of the Gardar province, South Greenland (Coulson 1997). There, eudialyte reacted with hydrothermal fluids to produce various assemblages via, for example, the reaction

$$\text{eudialite} + \text{fluid} \rightarrow \text{allanite} + \text{nepheline} \qquad (36)$$

The breakdown products form pseudomorphs after eudialite.

Banks et al. (1994) directly determined the distribution coefficients of LREE between allanite in quartz veins and REE-rich hydrothermal solutions (Table 5). These fluids originated from the Capitan pluton, New Mexico, and were subsequently trapped in fluid inclusions. The distribution coefficients can be used to estimate the concentration of REE in fluids in similar geological settings. In the Bergell contact aureole, allanite occurs in an exoskarn formed during the intrusion of the Bergell pluton at conditions similar to those in the Capitan pluton (Gieré 1986). Using the distribution coefficients of Banks et al. (1994), Gieré (1996) estimated total LREE (La-Sm) contents of 65–115 ppm in the fluid, with Ce as most abundant REE (30-55 ppm) for the Bergell aureole. The respective total concentrations of REE at the Capitan Pluton are 185 ppm. Both these LREE values, the *analyzed* REE content of fluids extracted from the Capitan fluid inclusions and the *calculated* REE content of the Bergell fluids, are very large compared to other hydrothermal fluids. To our knowledge, higher REE concentrations in fluids have only been reported from other fluid inclusions at the Capitan pluton (ΣREE = 1290 ppm; Banks et al. 1994). The REE patterns of allanite and inferred metasomatic fluids

Table 5. REE concentrations in hydrothermal fluid and calculated allanite/fluid partition coefficients for some LREE. Data derived from fluid inclusions and allanite in quartz veins from the Capitan pluton, New Mexico (Banks et al. 1994).

	REE concentration (ppm)		**Allanite/fluid partition coefficients**	
	Fluid	Std Dev	Upper value	Lower value
La	72.1	5.3	1559	1154
Ce	84.0	6.1	1633	1116
Pr	6.3	0.4	844	743
Nd	19.3	1.8	957	647
Sm	3.4	0.4	682	540

in the Bergell skarn (Fig. 38) emphasize the strong partition of REE into allanite at the conditions of contact metasomatism. Perhaps allanite could be used as a monitor of REE contents in metasomatic fluids.

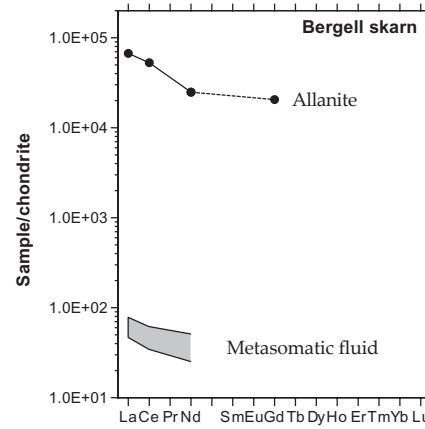

Figure 38. Chondrite-normalized REE patterns for allanite and coexisting metasomatic fluid in the Bergell contact aureole. Allanite data (electron microprobe) from Gieré (1986); data for fluid calculated from the REE partition coefficients between allanite and fluid trapped in fluid inclusions (Banks et al. 1994).

Fluid f_{O_2} may exert controls upon the development of metasomatic allanite. Smith et al. (2002) described the formation and alteration of allanite in skarn within the Beinn an Dubhaich granite aureole on the Island of Skye. There, allanite-(Ce) is present both as an igneous phase in the granite and as a metasomatic phase in the associated endoskarn. The metasomatic allanite exhibits distinct zoning. It occurs either as large single crystals, or as skeletal intergrowths with amphibole pseudomorphs of pyroxene. The skarn developed from highly saline, magmatic brines, which interacted with carbonate country rocks and led to the formation of hedenbergite (endoskarn) and diopside (exoskarn) at temperatures between 600 and 700°C. Allanite and amphibole (hastingsite) formed subsequently, when hedenbergite reacted with anorthite and REE-bearing, F-rich aqueous fluids during cooling from 600 to 540°C. The data of Smith et al. (2002) indicate that metasomatic allanite contains a significant component of ferriallanite and epidote, which indicates that oxidation accompanied the allanite-forming process. In contrast to its metasomatic counterpart, allanite in the granite is present either as unaltered, euhedral crystals or altered, sub- to euhedral grains associated with a fine-grained REE-rich phase. The altered allanite is poorer in Fe, REE, and Th, which suggests it formed via an interaction between early-crystallized allanite and either residual-magmatic or early-hydrothermal fluids. Smith et al. (2002) concluded, however, that the fluids from which the endoskarn allanite precipitated acquired their elevated REE contents mainly through partitioning from the melt, and only to a lesser extent through leaching from primary igneous allanite.

Alteration of allanite

Both hydrothermal and magmatic allanite commonly react with fluids and are transformed into a variety of alteration products. These alteration processes take place under hydrothermal and low-temperature to surficial conditions. Moreover, it has long been known that metamict allanite is in general strongly altered. This observation was initially made by Zenzén (1916) for specimens with $\rho < 3.1$ g/cm^3, which were all isotropic, i.e., metamict.

From his study of allanite in granitic pegmatites from the Precambrian basement of eastern Egypt, Gindy (1961) concluded that the original composition of allanite strongly influences its susceptibility to hydrothermal alteration. He noted that generally more radioactive crystals are more strongly altered than less radioactive ones, which suggests that the degree of metamictization plays a role in the alteration of allanite. Gindy (1961) further observed that the more altered parts of allanite are less radioactive than the unaltered ones. He interpreted this feature to be evidence for leaching of radioactive elements during alteration. Leaching of Th and LREE during the alteration of allanite was also observed by Morin (1977) for allanite in granitic rocks from Ontario, Canada.

Such observations can be quantified by using SEM, electron microprobe, and LA-ICP-MS. For example, Poitrasson (2002) examined the alteration of magmatically zoned allanite from both a granodiorite and a fayalite-bearing granite from Corsica. In BSE images, he observed that altered areas within individual allanite crystals typically appeared patchy, exhibited irregular limits, and had lower mean atomic numbers than unaltered portions. Alteration appeared to proceed from fractures penetrating the crystals, showing that fractures are preferential fluid paths. Moreover, some of the strongly altered areas displayed large numbers of small, irregular fractures, which are similar to those seen in heavily radiation-damaged areas of other minerals (e.g., Gieré et al. 2000; Lumpkin 2001). With a combination of electron microprobe and LA-ICP-MS data, Poitrasson (2002) showed that altered areas are generally characterized by lesser LREE contents, larger concentrations of common Pb and HREE (Fig. 39), and low analytical totals. The latter points to the incorporation of water into the altered areas of allanite. The behavior of Th and Ti was opposite in the samples from the two different host rocks. This study has documented that substantial leaching of A-site cations can take place during the alteration of allanite prior to its decomposition and transformation into other phases.

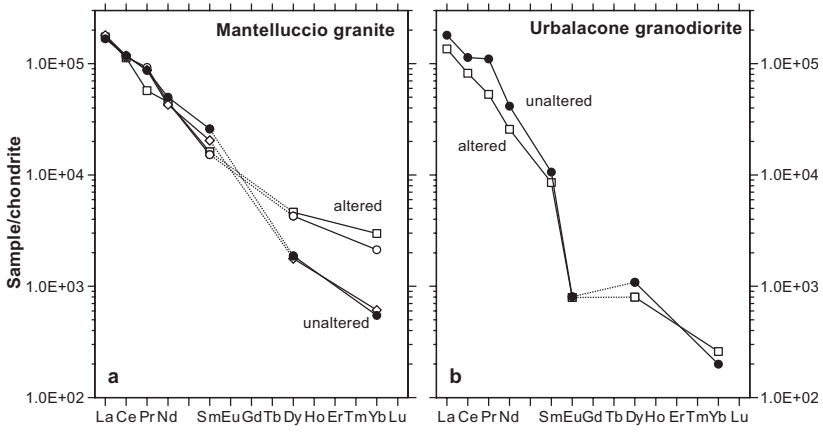

Figure 39. REE patterns for fresh and altered allanite in the **a)** Mantelluccio granite, Corsica, and **b)** Urbalacone granodiorite, Corsica. LA-ICP-MS and electron microprobe data from Poitrasson (2002).

The incorporation of water into allanite has long been recognized as an important early step of the weathering process (Meyer 1911). An indirect observation of this feature is seen in microprobe analyses of altered allanites. Low analytical totals, as well as reduced occupancy of the A, but not the M sites, have been reported for altered areas within allanite crystals in a quartz monzonite from Antarctica (Ghent 1972). Indeed, low analytical totals and reduced REE contents appear to be typical of altered allanite in various geological environments, as indicated also by other studies (e.g., Khvostova 1962; Pan and Fleet 1990; Jiang et al. 2003; Smith et al. 2002). Petrík et al. (1995) attributed the patchy appearance of allanite-(Ce) in various granitoids to interaction with late- to post-magmatic fluids. Their data indicated that this interaction led to an oxidation of allanite and a partial escape of REE.

Allanite commonly decomposes or transforms into other phases during its alteration (e.g., Gieré 1996). It is typically replaced by REE fluorocarbonate minerals, most commonly by bastnäsite ($REECO_3F$), and more rarely by synchisite ($CaREE(CO_3)_2F$; e.g., Sverdrup et al. 1959; Adams and Young 1961; Mineyev et al. 1962, 1973; Ehlmann et al. 1964; Perhac and Heinrich 1964; Mitchell 1966; Sakurai et al. 1969; Černý and Černá 1972; Mitchell and Redline 1980; Littlejohn 1981a, 1981b; Rimsaite 1984; Caruso and Simmons 1985; Lira and Ripley 1990; Pan et al. 1994; Buda and Nagy 1995). The bastnäsitization of allanite can be described schematically by the reaction

$$\text{allanite} + \text{fluid} \leftrightarrow \text{bastnäsite} + \text{clay minerals} + \text{thorite} \pm \text{fluorite} \pm \text{magnetite} \qquad (37)$$

in which the term "clay minerals" represents kaolinite, montmorillonite, or illite-series micas. The formation of thorite as a reaction product is due to the elevated Th contents commonly observed in allanite.

Less common is the replacement of allanite by phosphate phases during hydrothermal or epigene alteration. Mitchell and Redline (1980) described weathering of allanite into a mixture of bastnäsite, monazite, CeO_2, clay minerals, and Fe-oxyhydroxides in a Virginia granite pegmatite. Similarly, intense weathering of allanite in another Virginia pegmatite resulted in an assemblage consisting primarily of monazite and CeO_2 (Meintzer and Mitchell 1988). The overall decomposition of allanite under surficial weathering (i.e., epigene) conditions can be described schematically as

$$\text{allanite} + \text{fluid} \leftrightarrow \text{cerianite} + \text{monazite} + \text{clay minerals} + \text{goethite} \qquad (38)$$

where Th is trapped in both monazite and CeO_2 (Meintzer and Mitchell 1988). The formation of phosphates through allanite decomposition has also been described in a hydrothermal environment (Wood and Ricketts 2000). These authors studied the response of allanite-(Ce) to attack by low-salinity (<1.4 wt% NaCl equivalent), fluoride- and phosphate-bearing fluids in the Casto granite pluton, Idaho. These hydrothermal fluids interacted with igneous allanite-(Ce) at fairly low temperatures (100 to 200°C) to produce moderately altered crystals characterized by enrichment in Th, and depletion of La and Ce along fractures and rims. Substantial amounts of P were also observed along both fractures and rims. The most highly altered allanite grains exhibit substantial corrosion effects and are replaced by three phases: Y-bearing fluorite; a phosphate mineral rich in REE and Th, most likely monazite; and minor amounts of a Th-rich phase, probably thorianite. Neglecting the small amounts of the Th phase, Wood and Ricketts (2000) expressed the observed allanite replacement by the schematic overall alteration reaction

$$\text{allanite} + 2\,F^- + 5\,H^+ + 5\,H_2O + H_2PO_4^- \leftrightarrow \text{fluorite} + \text{monazite} + Fe^{2+} + 3\,H_4SiO_4^0 + 2\,Al(OH)_3^0, \qquad (39)$$

and suggested that Fe and Al may eventually be fixed in Fe-rich phases and clays, chlorite or white mica, respectively. These authors have not observed cerianite as replacement product of allanite, probably because the redox potential under the hydrothermal conditions in the

Casto pluton was lower than in the epigene environment of the Virginia pegmatites. REE fluorocarbonates are also absent in the breakdown products of the Casto allanites, probably as a result of high phosphate activity or low carbonate and fluoride activities in the hydrothermal fluid.

Several other alteration products of allanite have also been reported (see compilation of Meintzer and Mitchell 1988), including unspecified phases or amorphous material (Morin 1977); epidote (Carcangiu et al. 1997); lanthanite, $REE_2(CO_3)_3 \cdot 8H_2O$ (Saebø 1961); and britholite (Smith et al. 2002).

Many studies of allanite alteration document that REE and Th are removed almost completely during allanite replacement. However, the presence of breakdown products such as monazite, thorianite, thorite, cerianite, and REE fluorocarbonates indicates that REE and Th were captured again locally before they were transported any significant distance by hydrothermal or surficial fluids (e.g., Rimsaite 1982). Moreover, alteration of allanite involves in many cases fluids that are enriched in fluoride, which is known to form strong complexes with both REE (Wood 1990) and Th (Langmuir and Herman 1980). The activities of phosphate, carbonate and fluoride in the fluid, together with the activity of Ca^{2+}, are essential factors in determining whether allanite will be transformed into bastnäsite or monazite.

OUTLOOK

Many directions for future research are suggested by the current state of knowledge of allanite and related minerals, and by recent technological improvements of microanalysis of trace elements, in particular the REE. Existing studies have documented a large number of the most critical variables for understanding the substitutions of various elements into the allanite structure. However, the residence sites and compositional limits of three petrogenetically significant elements, namely P, Be, and V, are at present poorly understood. The V-richer allanite minerals could add to the conclusion that is suggested by Mn and Fe behavior, namely: f_{O_2} and T, rather than variations in P and element concentrations appear to be the most critical variables for determining transition metal and REE ratios in the epidote-group minerals (see Bonazzi and Menchetti 2004).

In particular, the characterization of allanite and REE-rich epidote minerals for their full complement of trace elements will likely be greatly enhanced as SIMS and LA-ICP-MS technology becomes more widely available. Many compositional parameters discussed in this chapter are poorly understood simply because they cannot readily be analyzed by the electron microprobe. High-contrast BSE imaging is also needed to conduct a first-rate study of these minerals, because it is so common for allanite and REE-rich epidote minerals to be zoned and altered.

The ratio Fe^{3+}/Fe_{tot} in allanite can be changed via the oxidation-dehydrogenation reaction (Eqn. 7), as demonstrated by Dollase (1973) and Bonazzi and Menchetti (1994). Both of these experimental studies, however, were carried out under metastable conditions. The Fe^{3+}/Fe^{2+} and H contents, therefore, need to be accurately measured for epidote-group minerals equilibrated within their stability fields, so that a thermodynamic model applicable to natural magmatic samples can be formulated. Such experimental data would be invaluable for a better understanding of igneous rocks, in particular rocks that contain coexisting amphibole, mica, and ferriallananite-allanite-epidote-clinozoisite solid solutions. In examples such as the Bergell tonalite, where detailed chronological data for allanite are available (Oberli et al. 2004), one can hope to additionally gain insight into how some petrologically important parameters of the tonalitic melt (e.g., T, P, f_{H_2O}) changed with time. Allanite, therefore, could become a powerful geothermobarometer as well as a hygrometer and chronometer for calc-alkaline systems.

In addition to such experiments, we suggest that the following topics be studied in the future.

1. Radiation damage: We anticipate that both the initial and the critical amorphization doses of allanite could be easily determined, because allanite is commonly zoned with respect to Th, and different zones thus would have received different α doses. Moreover, such studies would help in understanding the relationship between metamictization, hydration and release of REE, Th and Pb to fluids during alteration. Examples of such studies are given for other minerals by Lumpkin (2001) and Lumpkin et al. (2004).
2. Incorporation of Eu: the presence or absence of distinct Eu anomalies, both positive and negative, for different REE-rich epidote-group minerals in different environments has so far not been much discussed. This is in part because low values of Eu have been difficult to measure *in situ*. The use of either SIMS or LA-ICP-MS for microanalytical studies of Eu-incorporation into REE-rich epidote and allanite could reveal the behavior of this element in different petrogenetic environments.
3. Experiments are needed to determine the partition coefficients between allanite and various fluids at different pressures and temperatures. We anticipate that the composition of allanite could be used as a tool for monitoring REE compositions of fluids, once such data are available.
4. Thorium zoning in igneous allanite: it is not clear why some allanites display core-to-rim decreases in Th content (e.g., Oberli et al. 2004), whereas others show the opposite zoning (e.g., Vazquez and Reid 2001, 2003; Gromet and Silver 1983). Since allanite exerts such an important control on the behavior of Th in some igneous rocks, it would be desirable to study this feature in more detail and in various types of igneous rocks (e.g., with/without monazite).

ACKNOWLEDGMENTS

The authors would like to thank the reviewers of this manuscript, Jean Morrison (University of Southern California) and Jörg Hermann (Australian National University), for their helpful comments and constructive critcism. We are particularly grateful to Wayne Dollase (University of California, Los Angeles) and Felix Oberli (ETH Zürich), who both provided very thorough (unofficial) reviews of the manuscript. The present chapter also benefited from valuable suggestions by the volume editors Axel Liebscher and Gerhard Franz, and by Gregory Lumpkin (University of Cambridge). We further would like to thank Dr. James Beard (Virginia Museum of Natural History, Martinsburg, Virginia) for kindly permitting us to use his extensive, unpublished dataset for allanite from the Appalachians in the figures, and Dr. Jeffrey N. Grossman, USGS, for his assistance in data management. R.G. is grateful to the Purdue University Libraries for crucial help during various stages of this study, and to Dr. Alex Gluhovski for his translations of some Russian papers.

REFERENCES

Adams JW, Young EJ (1961) Accessory bastnäsite in the Pikes Peak granite, Colorado. U.S. Geol Survey Prof Paper 424-C:292-294

Anthony JW, Bideaux RA, Bladh KW, Nichols MC (1995) Handbook of Mineralogy. Vol. III, Silica, Silicates, Part 1. Mineral Data Publishing, Tuscon, Arizona

Banks DA, Yardley BWD, Campbell AR, Jarvis KE (1994) REE composition of an aqueous magmatic fluid: a fluid inclusion study from the Capitan Pluton, New Mexico. Chem Geol 113:259-272

Banno Y (1993) Chromian sodic pyroxene, phengite and allanite from the Sanbagawa blueschists in the eastern Kii Peninsula, central Japan. Mineral J 16/6:306-317
Barth S, Oberli F, Meier M (1989) U-Th-Pb systematics in morphologically characterized zircon and allanite: a high-resolution isotopic study of the Alpine Rensen pluton (northern Italy). Earth Planet Sci Lett 95: 235-254
Barth S, Oberli F, Meier M (1994) Th-Pb versus U-Pb isotope systematics in allanite from co-genetic rhyolite and granodiorite: implications for geochronology. Earth Planet Sci Lett 124:149-159
Bayliss P, Levinson AA (1988) A system of nomenclature for rare earth mineral species: revision and extension. Am Mineral 73:422-423
Bea F (1996) Residence of REE, Y, Th and U in granites and crustal protoliths; implications for the chemistry of crustal melts. J Petrology 37:521-552
Bermanec V, Armbruster T, Oberhänsli R, Zebec V (1994) Crystal chemistry of Pb- and REE-rich piemontite from Nezilovo, Macedonia. Schweizerische Mineralogische und Petrographische Mitteilungen 74:321-328
Bernstein LR (1985) Germanium geochemistry and mineralogy. Geochim Cosmochim Acta 49:2409-2422
Bingen B, Demaiffe D, Hertogen J (1996) Redistribution of rare earth elements, thorium, and uranium over accessory minerals in the course of amphibolite to granulite facies metamorphism: the role of apatite and monazite in orthogneisses from southwestern Norway. Geochim Cosmochim Acta 60:1341-1354
*Black P (1970) A note on the occurrence of allanite in hornfelses at Paritu, Coromandel County. New Zealand J Geology Geophys 13/2:343-345
Bocquet J (1975) Sur une allanite filonienne, à Bramans en Maurienne (Alpes occidentals, Savoie). Bulletin de la Société française de Minéralogie et de cristallographie 98:171-174
Bonazzi P, Garbarino C, Menchetti S (1992) Crystal chemistry of piemontites: REE-bearing piemontite from Monte Brugiana, Alpi Apuane, Italy. Eur J Mineral 4:23-33
Bonazzi P, Menchetti S (1994) Structural variations induced by heat treatment in allanite and REE-bearing piemontite. Am Mineral 79:1176-1184
Bonazzi P, Menchetti S (1995) Monoclinic members of the epidote group: Effects of the Al = Fe^{3+} = Fe^{2+} substitution and of the entry of REE^{3}. Mineral Petrol 53:133-153
Bonazzi P, Menchetti S (2004) Manganese in monoclinic members of the epidote group: piemontite and related minerals. Rev Mineral Geochem 56:495-552
Bonazzi P, Menchetti S, Reinecke T (1996) Solid solution between piemontite and androsite-(La), a new mineral of the epidote group from Andros Island, Greece. Am Mineral 81:735-742
Boundy TM, Donohue CL, Essene EJ, Mezger K, Austrheim H (2002) Discovery of eclogite-facies carbonate rocks from the Lindås Nappe, Caledonides, Western Norway. J Metamorph Geol 20:649-667
Brandon AD, Creaser RA, Chacko T (1996) Constraints on rates of granitic magma transport from epidote dissolution kinetics. Science 271:1845-1848
Braun M (1997) REE-Ungleichgewichte in Gesteinen der Lebendun Serie am Monte Giove (Val Formazza, Novara, Italien). Ph.D. thesis, University of Basel, Basel, Switzerland
Brooks CK, Henderson P, Rønsbo JG (1981) Rare-earth partition between allanite and glass in the obsidian of Sandy Braes, Northern Ireland. Mineral Mag 44:157-160
Broska I, Chekmir AS, Határ J (1999) Allanite solubility and the role of accessory mineral paragenesis in the Carpathian granite petrology. Geologica Carpathica 50:90-91
Broska I, Petrík I, Williams CT (2000) Coexisting monazite and allanite in peraluminous granitoids of the Tribec Mountains, Western Carpathians. Am Mineral 85:22-32
Broska I, Siman P (1998) The breakdown of monazite in the West-Capathian Veporic orthogneisses and Tatric granites. Geologica Carpathica 49:161-167
Brunsmann A, Franz G, Erzinger J, Landwehr D (2000) Zoisite- and clinozoisite-segregations in metabasites (Tauern Window, Austria) as evidence for high-pressure fluid-rock interaction. J Metamorph Geol 18: 1-21
Buda G, Nagy G (1995) Some REE-bearing accessory minerals in two rock types of Variscan granitoids, Hungary. Geologica Carpathica 46:67-78
Burt DM (1989) Compositional and phase relations among rare earth element minerals. Rev Mineral 21:259-307
Cameron KL (1984) The Bishop Tuff revisited: New rare earth element data consistent with crystal fractionation. Science 224:1338-1340
Campbell FA, Ethier VG (1984) Composition of allanite in the footwall of the Sullivan orebody, British Columbia. Can Mineral 22:507-511
Campbell L, Henderson P, Wall F, Nielsen TFD (1997) Rare earth chemistry of perovskite group minerals from the Gardiner Complex, East Greenland. Mineral Mag 61:197-212

Cappelli B, Franceschelli M., Memmi I (1993) LREE zoning in allanite-(Ce) from low-temperature metamorphics, Alpi Apuane, Italy. Terra: rivista di scienze ambientali e territoriali 5:414-415
Carcangiu G, Palomba M, Tamanini M (1997) REE-bearing minerals in the albitites of central Sardinia, Italy. Mineral Mag 61:271-283
Caruso L, Simmons G (1985) Uranium and microcracks in a 1000-meter core, Redstone, New Hampshire. Contrib Mineral Petrol 90:1-17
Catlos EJ, Sorensen SS, Harrison TM (2000) Th-Pb ion-microprobe dating of allanite. Am Mineral 85:633-648
Cech F, Vrána S, Povondra P (1972) A non-metamict allanite from Zambia. Neues Jahrbuch für Mineralogie, Abhandlungen 116(2):208-223
Černý P, Černá I (1972) Bastnaesite after allanite from rock lake, Ontario. Can Mineral 11:541-543
Chesner CA, Ettlinger AD (1989) Composition of volcanic allanite from the Toba Tuffs, Sumatra, Indonesia. Am Mineral 74:750-758
Coulson IM (1997) Post-magmatic alteration in eudialyte from the North Qoroq center, South Greenland. Mineral Mag 61:99-109
Cressey G, Steel AT (1988) An EXAFS Study of Gd, Er and Lu Site Location in the Epidote Structure. Phys Chem Min 15:304-312
*Dahlquist JA (2001) Low-pressure emplacement of epidote-bearing metaluminous granitoids in the Sierra de Chepes (Famatinian Orogen, Argentina) and relationships with the magma source. Revista Geologica de Chile 28 2:147-161
Davis DW, Schandl ES, Wasteneys HA (1994) U-Pb dating of minerals in alteration halos of Superior Province massive sulfide deposits: syngenesis versus metamorphism. Contrib Mineral Petrol 115:427-437
Dawes RL, Evans BW (1991) Mineralogy and geothermobarometry of magmatic epidote-bearing dikes, Front Range, Colorado. Geol Soc Am Bull 103:1017-1031
Dayvault RD, Krabacher JE, Hardy LC, Colby RJ (1986) Radiological characterization of the Lowman, Idaho, uranium mill tailings remedial action site, GJ-53, UNC Technical Services, Inc, prepared for the U.S. Department of Energy UMTRA Site Characterization Project, Grand Junction, Colorado, 29 p
Deer WA, Howie RA, Zussman J (1986) Rock-forming minerals, vol. 1B: Disilicates and ringsilicates (2nd edition). Longman, Harlow, United Kingdom
Demange M, Elsass P (1973) Présence d'allanite dans le gisement stratiforme cuprifère de Talate n'Ouaman (Maroc). Comptes rendus hébdomadaires des Séances de l'Académie des Sciences, Sciences naturelles 277D:1969-1972
de Fourestier J (1999) Glossary of mineral synonyms. Canadian Mineralogist Special Publication 2. Mineralogical Association of Canada, Ottawa
de Parseval P, Fontan F, Aigouy T (1997) Composition chimique des minéraux de terres rares de Trimouns (Ariège, France). Comptes rendusde l'Académie des Sciences, Paris. Série IIa: Sciences de la Terre et des Plantes 324:625-630
*Ding K, Zhang P, Li Z (1994) First discovery of Nd-rich allanite in xinjiang and its characteristics (in Chinese, English abstract and analysis). Scientia Geologica Sinica 29 1:95-104
Dollase WA (1971) Refinement of the crystal structures of epidote, allanite and hancockite. Am Mineral 56: 447-464
Dollase WA (1973) Mössbauer spectra and iron distribution in the epidote-group minerals. Z Kristallogr 138: 41-63
Duggan MB (1976) Primary allanite in vitrophyric rhyolites from the Tweed Shield Volcano, north-eastern New South Wales. Mineral Mag 40:652-653
Ehlmann AJ, Walper JL, Williams J (1964) A new, Baringer Hill-type, rare-earth pegmatite from the Central Mineral Region, Texas. Econ Geol 59:1348-1360
Enami M, Zang Q (1988) Magnesian staurolite in garnet-corundum rocks and eclogite from the Donghai district, Jiangsu province, east China. Am Mineral 73:48-56
Ercit TS (2002) The mess that is "allanite". Can Mineral 40:1411-1419
Ewing RC, Weber WJ, Clinard FW (1995) Radiation effects in nuclear waste forms for high-level radioactive waste. Prog Nucl Energy 29(2):63-127
Ewing RC, Chakoumakos BC, Lumpkin GR, Murakami T (1987) The metamict state. Mater Res Bull 12: 58-66
Exley RA (1980) Microprobe studies of REE-rich accessory minerals: implications for Skye granite petrogenesis and REE mobility in hydrothermal systems. Earth Planet Sci Lett 48:97-110
Ferraris G, Ivaldi G, Fuess H, Gregson D (1989) Manganese/iron distribution in a strontian piemontite by neutron diffraction. Z Kristallogr 187:145-151
Ferry JM (1984) A biotite isograd in south-central Maine, USA: mineral reactions, fluid transfer and heat transfer. J Petrol 25:871-893

Ferry JM (1988) Infiltration-driven metamorphism in northern New England, USA. J Petrol 29:1121-1159
Ferry JM (2000) Patterns of mineral occurrence in metamorphic rocks. Am Mineral 85:1573-1588
Ferrow E (1987) Mössbauer and X-ray studies on the oxidation of annite and ferriannite. Phys Chem Min 14: 270-275
Fersman AE (1931) Les pegmatites. – leur importance scientifique et pratique. Tomes I-III: Les pegmatites granitiques. Académie des Sciences de l'U.R.S.S, Leningrad, 675 p
Finger F, Broska I, Roberts MP, Schermaier A (1998) Replacement of primary monazite by apatitle-allanite-epidote coronas in an amphibolite facies granite gneiss from the eastern Alps. Am Mineral 83:248-258
Fleischer M (1965) Some aspects of the geochemistry of yttrium and the lanthanides. Geochim Cosmochim Acta 29:755-772
Fourcade S, Allègre CJ (1981) Trace Elements Behavior in Granite Genesis: A Case Study. The Calc-Alkaline Plutonic Association from the Querigut Complex (Pyrénées, France). Contrib Mineral Petrol 76:177-195
Franz G, Liebscher A (2004) Physical and chemical properties of the epidote minerals–an introduction. Rev Mineral Geochem 56:1-82
Frei D, Liebscher A, Wittenberg A, Shaw CSJ (2003) Crystal chemical controls on rare earth element partitioning between epidote-group minerals and melts: an experimental and theoretical study. Contrib Mineral Petrol 146:192-204
Frondel JW (1964) Variation of some rare earths in allanite. Am Mineral 49:1159-1177
Frye K (1981) Encyclopedia of Earth Sciences, Volume IVB: The Encyclopedia of Mineralogy. Hutchinson Ross, Stroudsburg, Pennsylvania
Geijer P (1927) Some mineral associations from the Norberg District. Sveriges Geologiska Undersokning. Avhandlingar och uppsatser series C 343 (Arsbok 20, 1926, No.4):1-32
Geisler T, Schleicher, H (2000) Improved U-Th-total Pb dating of zircons by electron microprobe using a simple new background modeling procedure and Ca as a chemical indicator of fluid-induced U-Th-Pb discordance in zircon. Chem Geol 163:269-285
Geisler T, Ulonska M, Schleicher H, Pidgeon RT, van Bronswijk W (2001) Leaching and differential recrystallization of metamict zircon under experimental hydrothermal conditions. Contrib Mineral Petrol 141:53-65
Ghent ED (1972) Electron Microprobe Study of Allanite from the Mt. Falconer Quartz Monzonite Pluton, Lower Taylor Valley, South Victoria Land, Antarctica. Can Mineral 11:526-530
Gieré R (1986) Zirconolite, allanite and hoegbomite in a marble skarn from the Bergell contact aureole: implications for mobility of Ti, Zr and REE. Contrib Mineral Petrol 93:459-470
Gieré R (1996) Formation of Rare Earth minerals in hydrothermal systems. *In:* Rare Earth Minerals: Chemistry, Origin and Ore Deposits. Jones AP, Williams CT, Wall F (eds) Mineralogical Society Series, Chapman & Hall, p 105-150
Gieré R, Williams CT, Braun M, Graeser S (1998) Complex Zonation Patterns in Monazite-(Nd) and Monazite-(Ce). International Mineralogical Association, 17th General Meeting, Toronto, Abstract Volume, p. A84
Gieré R, Virgo D, Popp R.K (1999) Oxidation state of iron and incorporation of REE in igneous allanite. Journal of Conference Abstracts 4: p. 721
Gieré R, Swope RJ, Buck EC, Guggenheim R, Mathys D, Reusser E (2000) Growth and alteration of uranium-rich microlite. *In:* Scientific Basis for Nuclear Waste Management XXIII. Smith R.W, Shoesmith D.W (eds) Materials Research Society, Symposium Proceedings 608:519-524
Gindy AR (1961) Allanite from Wadi el Gemal area, eastern desert of Egypt, and its radioactivity. Am Mineral 46:985-993
Giuli G, Bonazzi P, Menchetti S (1999) Al-Fe disorder in synthetic epidotes: a single-crystal X-ray diffraction study. Am Mineral 84:933-936
Goldschmidt VM, Thomassen L (1924) Geochemische Verteilungsgesetze der Elemente. III. Röntgenspektrographische Untersuchungen über die Verteilung der Seltenen Erdmetalle in Mineralen. Videnskapsselskapets Skrifter I. Mathematisk-Naturvidenskabelig Klasse 5:1-58
Grapes RH (1981) Chromian epidote and zoisite in kyanite amphibolite, Southern Alps, New Zealand. Am Mineral 66:974-975
Grapes RH, Hoskin PWO (2004) Epidote group minerals in low–medium pressure metamorphic terranes. Rev Mineral Geochem 56:301-345
Grew ES (2002) Mineralogy, petrology and geochemistry of beryllium: an introduction and list of beryllium minerals. Rev Mineral Geochem 50:1-76
Grew ES, Essene EJ, Peacor DR, Su S-C, Asami M (1991) Dissakisite-(Ce), a new member of the epidote group and the Mg analogue of allanite-(Ce), from Antarctica. Am Mineral 76:1990-1997
Gromet LP, Silver LT (1983) Rare earth element distributions among minerals in a grandiorite and their petrogenetic implications. Geochim Cosmochim Acta 47:925-939

Hagesawa S (1957) Chemical studies of allanites and their associated minerals from the pegmatites in the northern part of the Abukuma Massif. The Science Reports of Tohoku University, third series (Mineralogy, Petrology, Economic Geology) 5:345-371

Hagesawa S (1958) Chemical studies of allanites from the new localities in Fukushima and Kagawa Prefectures. Scientific Reports of Tohoku University, third series (Mineralogy, Petrology, Economic Geology) 6:39-56

Hagesawa S (1959) Allanites from the pegmatites of several localities in southwestern Japan. The Science Reports of Tohoku University, third series (Mineralogy, Petrology, Economic Geology) 6:209-226

Hagesawa S (1960) Chemical composition of allanite. The Science Reports of Tohoku University, third series (Mineralogy, Petrology, Economic Geology) 6(3):331-387

Halleran AAD, Russell JK (1996) REE-bearing alkaline pegmatites and associated light REE-enriched fenites at Mount Bisson, British Columbia. Econ Geol 91:451-459

Hanson RA, Pearce DW (1941) Colorado cerite. Am Mineral 26:110-120

*Hata S (1939) Studies on allanite from the Abukuma granite region. Scientific Papers of the Institute of physical and chemical Research, Tokyo 36:301-311

Hawkins BW (1975) Mary Kathleen uranium deposit. *In:* Economic geology of Australia and Papua New Guinea. Australasian Institute of Mining and Metallurgy, Monograph Series 5-8: 398-402. Parkville, Vic

Heinrich EW, Wells RG (1980) The diversity of rare-earth mineral deposits and their geological domains. The Rare earths in modern science and technology 2:511-516

Hermann J (2002) Allanite: thorium and light rare earth element carrier in subducted crust. Chem Geol 192: 289-306

Hickling NL, Phair G, Moore R, Rose Jr HJ (1970) Boulder Creek batholith, Colorado. Part I: allanite and its bearing upon age patterns. Geol Soc Am Bull 81:1973-1994

Hogg CS, Meads RE (1975) A Mössbauer study of the thermal decomposition of biotites. Mineral Mag 40: 79-88

Holtstam D, Andersson UB, Mansfeld J (2003) Ferriallanite-(Ce) from the Basntnäs deposit, Västmanland, Sweden. Can Mineral 41:1233-1240

Hugo PJ (1961) The allanite deposits on Vrede, Gordonia district, Cape Province. Republiek van Suid-Afrika, Departement van Mynwese, Geologiese Opname Bulletin 37:1-65

Hutton CO (1951a) Allanite from Yosemite National Park, Tuolumne Co, California. Am Mineral 36:233-248

Hutton CO (1951b) Allanite from Wilmot Pass, Fjordland, New Zealand. Amer J Sci 249:208-214

Iimori T (1939) A Beryllium-bearing variety of allanite. Scientific Papers of the Institute of physical and chemical Research, Tokyo 36:53-55

Iimori T, Yoshimora J, Hata S (1931) A new radioactive mineral found in Japan. Scientific Papers of the Institute of physical and chemical Research, Tokyo 15:83-88

Ivanov OP, Vorob'ev YuK, Efremenko LYa, Knyazeva DN (1981) Acicular allanite from the Itulin deposit veins. Zapiski Vsesoiuznogo mineralogicheskogo obshchestva 110:361-366 (in Russian)

Izett GA, Wilcox RE (1968) Perrierite, chevkinite, and allanite in Upper Cenozoic ash beds in the Western United States. Am Mineral 53:1558-1567

Janeczek J, Eby RK (1993) Annealing of radiation damage in allanite and gadolinite. Phys Chem Min 19: 343-356

Jiang N, Sun S, Chu X, Mizuta T, Ishiyama D (2003) Mobilization and enrichment of high-field strength elements during late- and post-magmatic processes in the Shuiquangou syenitic complex, Northern China. Chem Geol 200:117-128

Johan Z, Oudin E, Picot P (1983) Analogues germanifères et gallifères des silicates et oxydes dans les gisements de zinc des Pyrénées centrales, France; argutite et carboirite, deux nouvelles espèces minerals. Tschermaks Mineralogische und Petrographische Mitteilungen 31:97-119

Kalinin YeP, Yushkin, N.P, Goldin, B.A (1968) The influence of chemical composition on hardness of crystals of allanite. Zapiski vsesoyuznogo mineralogicheskogo Obshchestva 97:647-652 (in Russian)

Kartashov PM, Ferraris G, Ivaldi G, Sokolova E, McCammon CA (2002) Ferriallanite-(Ce), $CaCeFe^{3+}AlFe^{2+}(SiO_4)(Si_2O_7)O(OH)$, a new member of the epidote group: Description, X-Ray and Mössbauer study. Can Mineral 40:1641-1648

Kartashov PM, Ferraris G, Ivaldi G, Sokolova E, McCammon CA (2003) Ferriallanite-(Ce), $CaCeFe^{3+}AlFe^{2+}(SiO_4)(Si_2O_7)O(OH)$, a new member of the epidote group: Description, X-Ray and Mössbauer study: Errata. Can Mineral 41:829-830

Kato A, Shimizu M, Okada Y, Komuro Y, Takeda K (1994) Vanadium-bearing spessartine and allanite in the manganese-iron ore from the Odaki Orebody of the Kyurazawa Mine, Ashio town, Tochigi Prefecture, Japan. Bulletin National Science Museum, Tokyo, Series C 20 1:1-12

Khvostova VA (1962) Mineralogy of Orthite. Institut mineralogii, geokhimii i kristallokhimii redkikh elementov Akademii nauk SSSR, Trudy 11:119 p (in Russian)

Khvostova VA (1963) On the isomorphism of epidote and orthite. Doklady Academy of Sciences U.S.S.R, Earth Sciences Section 141:1307-1309
Khvostova VA, Bykova AV (1961) Accessory orthite of southern Yakutia. Institut mineralogii, geokhimii I kristallokhimii redkikh elementov. Akademii nauk SSSR, Trudy 7:130-137 (in Russian)
Kimura K, Nagashima K (1951) Chemical investigations of Japanese minerals containing rarer elements. XLII Journal of the Chemical Society of Japan, Pure Chemistry Sections 72:52-54 (in Japanese)
Kosterin AV, Kizyura VE, Zuev VN (1961) Ratios of rare earth elements in allanites from some igneous rocks of northern Kirgiziya. Geochemistry 5:481-484
Kramm U (1979) Kanonaite-rich viridines from the Venn-Stavelot Massif, Belgian Ardennes. Contrib Mineral Petrol 69:387-395
Krivdik SG, Tkachuk VI, Maximchuk IG, Michnik TL (1989) Accessory orthite from alkaline rocks and carbonatites of the Ukrainian Shield. Mineralogicheskii zhurnal 11(1):34-42 (in Russian)
Kumskova NM, Khvostova VA (1964) X-ray study of the epidote-allanite group of minerals. Geochem Int 4: 676-686
Kvick KA, Pluth JJ, Richardson JW Sr, Smith JV (1988) The ferric iron distribution and hydrogen bonding in epidote: a neutron diffraction study at 15 K. Acta Crystallogr Sec B Struc Sci 44:351-355
Langmuir D, Herman JS (1980) The mobility of thorium in natural waters at low temperatures. Geochim Cosmochim Acta 44:1753-1766
Lee DE, Bastron H (1962) Allanite from the Mt. Wheeler area, White Pine County, Nevada. Am Mineral 47: 1327-1331
Lee DE, Bastron H (1967) Fractionation of rare-earth elements in allanite and monazite as related to geology of the Mt. Wheeler mine area, Nevada. Geochim Cosmochim Acta 31:339-356
Levinson AA (1966) A system of nomenclature for rare-earth minerals. Am Mineral 51:152-158
Lima de Faria J (1964) Identification of metamict minerals by X-ray powder photographs. Junta de Investigaçoes do Ultramar; Estudos, Ensaios e Documentos, No. 112, Lisbon, Portugal, 74 p
Lira R, Ripley EM (1990) Fluid inclusion studies of the Rodeo de Los Molles REE and Th deposit, Las Chacras Batholith, Central Argentina. Geochim Cosmochim Acta 54:663-671
Littlejohn AL (1981a) Alteration products of accessory allanite in radioactive granites from the Canadian Shield. Curr Res Geol Sur Canada 81-1B:95-104
Littlejohn AL (1981b) Alteration products of accessory allanite in radioactive granites from the Canadian Shield: Reply. Curr Res Geol Sur Canada 81-1C:93-94
Liu X, Dong S, Xue H, Zhou J (1999) Significance of allanite-(Ce) in granitic gneisses from the ultrahigh-pressure metamorphic terrane, Dabie Shan, central China. Mineral Mag 63/4:579-586
Lumpkin GR (2001) Alpha-decay damage and aqueous durability of actinite host phases in natural systems. J Nucl Mat289:136-166
Lumpkin GR, Eby RK, Ewing RC (1991) Alpha-recoil damage in titanite ($CaTiSiO_5$) direct observation and annealing study using high-resolution transmission electron microscopy. J Mater Res 6:560-564
Lumpkin GR, Smith KL, Gieré R, Williams CT (2004) The geochemical behaviour of host phases for actinides and fission products in crystalline ceramic nuclear waste forms. *In:* Energy, Waste, and the Environment – a geochemical approach. Gieré R, Stille P (eds) Geological Society Special Publications, London (in press)
Maas R, McCulloch MT, Campbell IH (1987) Sm-Nd isotope systematics in uranium-rare earth element mineralization at the Mary Kathleen Uranium Mine, Queensland. Econ Geol 82:1805-1826
Mahood G, Hildreth W (1983) Large partition coefficients for trace elements in high-silica rhyolites. Geochim Cosmochim Acta 47:11-30
*Marble JP (1940) Allanite from the Barringer Hill, Llano County, Texas. Am Mineral 25:168-173
*Marble JP (1943) Possible age of allanite from Whiteface mountain, Essex Co., New York. Amer J Sci 241: 32-42
Mariano AN (1989) Economic geology of rare earth elements. Rev Mineral 21:309-337
Mason RA (1992) Models of order and iron-fluorine avoidance in biotite. Can Mineral 30:343-354
Meintzer RE, Mitchell RS (1988) The epigene alteration of allanite. Can Mineral 26:945-955
Mezger K, Hanson GN, Bohlen SR (1989) U-Pb systematics of garnet: dating the growth of garnet in the late Archean Pikwitonei granulite domain at Cauchon and Natawahunan Lakes, Manitoba, Canada. Contrib Mineral Petrol 101:136-148
Meyer RJ (1911) Über einen skandiumreichen Orthit aus Finnland und den Vorgang seiner Verwitterung. Sitzungsberichte der königlichen preussischen Akademie der Wissenschaften, Berlin 105:379-384 (in German)
Michael PJ (1983) Chemical differentiation of the Bishop Tuff and other high-silica magmas through crystallization processes. Geology 11:31-34

*Michael PJ (1984) Chemical differentiation of the Cordillera Paine granite (southern Chile) by in situ fractional crystallization. Contrib Mineral Petrol 87:179-195

Mineyev DA, Makarochkin BA, Zhabin AG (1962) On the behavior of lanthanides during alteration of rare earth minerals. Geochemistry 7:684-693

Mineyev DA, Rozanov KI, Smirnova NV, Matrosova TI (1973) Bastnaesitization products of accessory orthite. Doklady Akademia Nauk SSSR, Earth Science Sections 210:149-152

Mitchell RS (1966) Virginia metamict minerals: allanite. Southeastern Geology 7:183-195

Mitchell RS (1973) Metamict minerals: a review. Mineral Record 4:177-182

Mitchell RH (1996) Perovskite: a revised classification scheme for an important rare earth element host in alkaline rocks. *In:* Rare Earth Minerals: Chemistry, Origin and Ore Deposits. Jones AP, Williams CT, Wall F (eds) Mineralogical Society Series, Chapman & Hall, London, p 41-76

Mitchell RS, Redline GE (1980) Minerals of a weathered allanite pegmatite, Amherst County, Virginia. Rocks & Minerals 55:245-249

Moench RH (1986) Comment on "Implications of magmatic epidote-bearing plutons on crustal evolution in the accreted terranes of northwestern North America" and "Magmatic epidote and its petrologic significance." Geology 14:187-188

Möller P (1989) Rare earth mineral deposits and their industrial importance. *In:* Lanthanides, Tantalum and Niobium. Möller P, Černý P, Saupé F (eds) Special Pub Soc Geology Appl Mineral Dep 7:171-188

Montel J-M (1993) A model for monazite/melt equilibrium and application to the generation of granitic magmas. Chem Geol 110:127-146

Moore JM, McStay JH (1990) The formation of allanite-(Ce) in calcic granofelses, Namaqualand, South Africa. Can Mineral 28:77-86

Morin JA (1977) Allanite in granitic rocks of the Kenora-Vermilion Bay area, Northwestern Ontario. Can Mineral 15:297-302

Morrison J (2004) Stable and radiogenic isotope systematics in epidote group minerals. Rev Mineral Geochem 56:607-628

Murata KJ, Rose HJ Jr, Carron MK, Glass JJ (1957) Systematic variation of REE in cerium-earth minerals. Geochim Cosmochim Acta 11:141-161

*Nagasaki A, Enami M (1998) Sr-bearing zoisite and epidote in ultra-high pressure (UHP) metamorphic rocks from the Su-Lu province, eastern China: An important Sr reservoir under UHP conditions. Am Mineral 83:240-247

Nesse WD (2004) Introduction to optical mineralogy. Oxford University Press, 3rd edition. New York, London

Neumann H, Nilssen B (1962) Lombaardite, a rare earth silicate, identical with, or very closely related to allanite. Norsk Geologisk Tidsskrift 42:277-286

Nozik YK, Kanepit VN, Fykin LY, Makarov YS (1978) A neutron diffraction study of the structure of epidote. Geochem Int 15:66-69

Oberli F, Sommerauer J, Steiger RH (1981) U-(Th)-Pb systematics and mineralogy of single crystals and concentrates of accessory minerals from the Cacciola granite, central Gotthard massif, Switzerland. Schweizerische Mineralogische und Petrographische Mitteilungen 61:323-348

Oberli F, Meier M, Berger A, Rosenberg C, Gieré R (1999) U-Th-Pb isotope systematics in zoned allanite: a test for geochronological significance. Journal of Conference Abstracts 4: p. 722

Oberli F, Meier M, Berger A, Rosenberg C, Gieré R (2004) U-Th-Pb and $^{230}Th/^{238}U$ disequilibrium isotope systematics: precise accessory mineral chronology and melt evolution tracing in the Alpine Bergell intrusion. Geochim Cosmochim Acta (in press)

O'Driscoll M (1988) Rare earths – enter the dragon. Industrial Minerals 254:21-55

Olson JC, Shawe DR, Pray LC, Sharp WN (1954) Rare earth mineral deposits of the Mountain Pass District, San Bernardino County, California. US Geol Sur Prof Paper 261:1-75

Ovchinnikov LN, Tzimbalenko MN (1948) Mangan-orthite from Vishnevy Mountains. Doklady Acad. Sci, USSR 63:191-194 (in Russian)

Pan Y (1997) Zircon- and monazite-forming metamorphic reactions at Manitouwadge, Ontario. Can Mineral 35:105-118

Pan Y, Fleet ME (1990) Halogen-bearing allanite from the White River gold occurrence, Hemlo area, Ontario. Can Mineral 28:67-75

Pan Y, Fleet ME (1991) Vanadian allanite-(La) and vanadian allanite-(Ce) from the Hemlo gold deposit, Ontario, Canada. Mineral Mag 55:497-507

Pan Y, Fleet ME, Barnett RL (1994) Rare earth mineralogy and geochemistry of the Mattagami Lake volcanogenic massive sulfide deposit, Québec. Can Mineral 32:133-147

Pantó G (1975) Trace minerals of the granitic rocks of the Valence and Mecsek Mountains. Acta Geologica Academiae Scientiarum Hungaricae 19:59-93

Papunen H, Lindsjö O (1972) Apatite, monazite and allanite; three rare earth minerals from Korsnäs, Finland. Bull Geol Soc Finland 44:123-129

Paulmann C, Bismayer U (2001a) Thermal recrystallization of metamict allanite: a synchrotron radiation study. Eur J Mineral Beihefte 13:137

Paulmann C, Bismayer U (2001b) Anisotropic recrystallization effects in metamict allanite on isothermal annealing. *In:* Gehrke R, Krell U, Schneider JR (eds) HASYLAB Annual Report 2001 I: 435-436 (*www-hasylab.desy.de/science/annual_reports/2001_report/index.html*)

Paulmann C, Schmidt H, Kurtz R, Bismayer U (2000) Thermal recrystallization of metamict allanite on progressive and isothermal annealing. *In:* Dix, W, Kracht, T, Krell, U, Materlik, G, Schneider, J.R (eds) HASYLAB Annual Report 2000 I: 625-626 (*www-hasylab.desy.de/science/annual_reports/2000_report/index.html*)

Pautov LA, Khorov PV, Ignatenko KI, Sokolova EV, Nadezhina TN (1993) Khristovite-(Ce) – (Ca,RE E)REE(Mg,Fe)AlMnSi_3O_{11}(OH)(F,O) A new mineral in the epidote group. Zapiski Vserossiskogo mineralogicheskogo obshchestva, 122(3), 103-111 (in Russian). English abstract available in: Jambor JL, Puziewicz J, Roberts AC (1995) New mineral names. Am Mineral 80:404-409

Pavelescu L, Pavelescu M (1972) Study of some allanites and monazites from the South Carpathians (Romania). Tschermaks Mineralogische und Petrographische Mitteilungen 17:208-214

Peacor DR, Dunn PJ (1988) Dollaseite-(Ce) (magnesium orthite redefined) Structure refinement and implications for F + M^{2+} substitutions in epidote-group minerals. Am Mineral 73:838-842

Perhac RM, Heinrich EWM (1964) Fluorite-bastnäsite deposits of the Gallinas Mountains, New Mexico and bastnäsite paragenesis. Econ Geol 59:226-239

Peterson RC, MacFarlane DB (1993) The rare-earth-element chemistry of allanite from the Grenville Province. Can Mineral 31:159-166

Petrík I, Broska I, Lipka J, Siman P (1995) Granitoid Allanite-(Ce) Substitution Relations, Redox Conditions and REE Distributions (on an Example of I-Type Granitoids, Western Carpathians, Slovakia). Geologica Carpathica 46:79-94

Ploshko VV, Bogdanova VI (1963) Isomorphous substitutions in minerals of the epidote group from the northern Caucasus. Geochemistry 1:61-71

Poitrasson F (2002) *In situ* investigations of allanite hydrothermal alteration: examples from calc-alkaline and anorogenic granites of Corsica (southeast France). Contrib Mineral Petrol 142:485-500

Popp RK, Virgo D, Hoering TC, Yoder HS Jr, Phillips MW (1995a) An experimental study of phase equilibria and iron oxy-component in kaersutitic amphibole: Implications for f_{H2} and a_{H2O} in the upper mantle. Am Mineral 80:543-548

Popp RK, Virgo D, Phillips MW (1995b) H-deficiency in kaersutitic amphibole: Experimental verification. Am Mineral 80:1347-1350

Pudovkina ZV, Pyatenko IA (1963) Crystal structure of non-metamict orthite. Doklady Akad. Nauk SSSR 153: 695-698 (in Russian)

Quensel P (1945) Berylliumorthit (muromontite) från Skuleboda fältspatbrott. Arkiv för Kemi, Mineralogi och Geologi 18A (22):1-17 (in Swedish)

Rao AT, Babu VRRM (1978) Allanite in charnockites from Air Port Hill, Visakhapatnam, Andra Pradesh, India. Am Mineral 63:330-331

Rao AT, Rao A, Rao PP (1979) Fluorian allanite from calc-granulite and pegmatite contacts at Garividi, Andhra Pradesh, India. Mineral Mag 43:312

Rimsaite J (1982) The leaching of radionuclides and other ions during alteration and replacement of accessory minerals in radioactive rocks. Geol Sur Canada Paper 81-1B:253-266

Rimsaite J (1984) Selected mineral associations in radioactive and REE occurrences in the Baie-Johan-Beetz area, Québec: a progress report. Geol Sur Canada Paper 84-1A:129-145

Romer RL, Siegesmund S (2003) Why allanite may swindle about its true age. Contrib Mineral Petrol 146: 297-307

Rønsbo JG (1989) Coupled substitutions involving REEs and Na and Si in apatites in alkaline rocks from the Ilimaussaq intrusion, South Greenland, the petrological implications. Am Mineral 74:896-901

Rouse RC, Peacor DR (1993) The crystal structure of dissakisite-(Ce), the Mg analogue of allanite-(Ce). Can Mineral 31:153-157

Rudashevskiy NS (1969) Epidote-allanite from metasomatites of southern Siberia. Zapiski Vserossiskogo mineralogicheskogo obshchestva 98(6):739-749 (in Russian)

Saebø PC (1961) Contributions to the mineralogy of Norway. No. 11. On lanthanite in Norway. Norsk Geologisk Tidsskrift 41:311-317

Saini HS, Lal N, Nagpaul KK (1975) Annealing studies of fission tracks in allanite. Contrib Mineral Petrol 52:143-145

Sakai C, Higashino T, Enami M (1984) REE-bearing epidote from Sanbagawa pelitic schists, central Shikoku, Japan. Geochem J 18:45-53
Sakurai K, Wakita H, Kato A, Nagashima K (1969) Chemical studies of minerals containing rarer elements from the Far East. LXIII. Bastnäsite from Karasugawa, Fukushima Prefecture, Japan. Bull Chem Soc Japan 42:2725-2728
Sargent KA (1964) Allanite in metamorphic rocks, Horn Area, Bighorn Mountains, Wyoming. Geol Soc Am Spec Paper 76:143
Sawka WN (1988) REE and trace element variations in accessory minerals and hornblende from the strongly zoned McMurry Meadows Pluton, California. Trans R Soc Edinburgh: Earth Sci 79:157-168
Sawka WN, Chappell BW (1988) Fractionation of uranium, thorium and rare earth elements in a vertically zoned granodiorite: Implictions for heat production distributions in the Sierra Nevada batholith, California, U.S.A. Geochim Cosmochim Acta 52:1131-1143
Sawka WN, Chappell BW, Norrish K (1984) Light-rare-earth-element zoning in sphene and allanite during granitoid fractionation. Geology 12:131-134
Schmidt MW, Thompson AB (1996) Epidote in calc-alkaline magmas: An experimental study of stability, phase relationships, and the role of epidote in magmatic evolution. Am Mineral 81:462-474
Schreyer W, Fransolet AM, Abraham K (1986) A miscibility gap in trioctahedral Mn-Mg-Fe chlorites: Evidences from the Lienne Valley manganese deposit, Ardennes, Belgium. Contrib Mineral Petrol 94: 333-342
Scott AK, Scott AG (1985) Geology and genesis of uranium-rare earth deposits at Mary Kathleen, North Queensland. Australasian Inst Mining Metall Proc 290:79-89
Semenov EI (1958) Relationship between composition of rare earths and composition and structures of minerals. Geochemistry 5:574-586
Semenov EI, Barinski RL (1958) The composition characteristics of the rare-earths in minerals. Geokhimiia, Akademiia nauk SSSR 4:314-333 (in Russian)
Semenov EJ, Upendran R, Subramanian V (1978) Rare earth minerals of carbonatites of Tamil Nadu. J Geol Soc India 19:550-557
Shannon RD (1976) Revised effective ionic radii and systematic studies of interatomic distances in halides and chalcogenides. Acta Crystallogr Sect A 32:751-767
Shepel AB, Karpenko MV (1969) Mukhinite, a new vanadian of epidote. Doklady Akad Nauk SSSR 185/6: 1342-1345 (in Russian)
Smith HA, Barreiro B (1990) Monazite U-Pb dating of staurolite grade metamorphism in pelitic schists. Contrib Mineral Petrol 105:602-615
Smith MP, Henderson P, Jeffries T (2002) The formation and alteration of allanite in skarn from the Beinn an Dubhaich granite aureole, Skye. Eur J Mineral 14:471-486
Smith WL, Franck ML, Sherwood AM (1957) Uranium and thorium in the accessory allanite of igneous rocks. Am Mineral 42:367-378
Smulikowski W, Kozlowski A (1994) Distribution of cerium, lanthanum and yttrium in allanites and associated epidotes of metavolcanic rocks of Hornsund area, Vestspitsbergen. Neues Jahrbuch fur Mineralogie–Abhandlungen 166:295-324
Söhnge PG (1945) The structure, ore genesis and mineral sequence of the cassiterite deposits in the Zaaiplaats tin mine, Potgietersrust district, Transvaal. Trans Geol Soc South Africa 47:157-181
Sokolova EV, Nadezhina TN, Pautov LA (1991) Crystal structure of a new natural silicate of manganese from the epidote group. Soviet Physics - Crystallography 36:172-174
Sorensen SS (1991) Petrogenetic significance of zoned allanite in garnet amphibolites from a paleo-subduction zone: Catalina Schist, southern California. Am Mineral 76:589-601
Sorensen SS, Grossman JN (1989) Enrichment of trace elements in garnet amphibolites from a paleosubduction zone: Catalina Schist, southern California. Geochim Cosmochim Acta 53:3155-3177
Sorensen SS, Grossman JN (1993) Accessory minerals and subduction zone metasomatism: a geochemical comparison of two mélanges (Washington and California, U.S.A.). Chem Geol 110:269-297
Spandler C, Hermann J, Arculus R, Mavrogenes J (2003) Redistribution of trace elements during prograde metamorphism from lawsonite blueschist to eclogite facies; implications for deep subduction-zone processes. Contrib Mineral Petrol 146:205-222
Sverdrup TL, Bryn KØ, Saebø PC (1959) Contrib the mineralogy of Norway. No. 2. Bastnäsite, a new mineral for Norway. Norsk Geologisk Tidsskrift 39:237-247
Tarassoff P and Gault RA (1994) The Orford Nickel Mine, Quebec, Canada. Mineral Record 25:327-345
Tempel H-G (1938) Der Einfluss der seltenen Erden und einiger anderer Komponenten auf die physikalisch-optischen Eigenschaften innerhalb der Epidot-Gruppe. Chemie der Erde 11:525-551 (in German)
Thomson T (1810) Experiments on allanite, a new mineral from Greenland. Trans R Soc Edinburgh 8(6): 371-386

Treolar PJ (1987) Chromian muscovites and epidotes from Outokumpu, Finland. Mineral Mag 51:593-599
Treolar PJ, Charnley NR (1987) Chromian allanite from Outokumpu, Finland. Can Mineral 25:413-418
Tribuzio R, Messiga B, Vannucci R, Bottazzi P (1996) Rare earth element redistribution during high-pressure-low-temperature metamorphism in ophiolitic Fe-gabbros (Liguria, northwestern Italy: implications for light REE mobility in subduction zones. Geology 24:711-714
Tulloch AJ (1986) Comment on "Implications of magmatic epidote-bearing plutons on crustal evolution in the accreted terranes of northwestern North America" and "Magmatic epidote and its petrologic significance". Geology 14:186-187
Ueda T (1955) The crystal structure of allanite, $OH(Ca,Ce)_2(Fe^{III}Fe^{II})Al_2OSi_2O_7SiO_4$. Memoirs of the College of Science, University of Kyoto Series B22/2:145-163
Ueda T (1957) Studies on the metamictization of radioactive minerals. Memoirs of the College of Science, University of Kyoto, Series B24/2:81-120
Ueda T, Korekawa M (1954) On the metamictization. Memoirs of the College of Science, University of Kyoto Series B21/2:151-162
van Marcke de Lummen G (1986) Tin-bearing epidote from skarn in the Land's End aureole, Cornwall, England. Can Mineral 24:411-415
Vance ER, Routcliffe P (1976) Heat treatment of some metamict allanites. Mineral Mag 40:521-523
Vazquez JA, Reid MR (2001) Timescales of magmatic evolution by coupling core-to-rim ^{238}U-^{230}Th ages and chemical compositions of mineral zoning in allanite from the youngest Toba Tuff. EOS Trans, Am Geophys Union, 82/47, Fall Meeting Supplement, Abstract V32D-1019
Vazquez JA, Reid MR (2003) The protracted history of magmatic evolution recorded by zoning in allanites. EOS Trans, Am Geophys Union, 84/46, Fall Meeting Supplement, Abstract V11F-08
von Blanckenburg F (1992) Combined high-precision chronometry and geochemical tracing using accessory minerals applied to the Central-Alpine Bergell intrusion (Central Europe). Chem Geol 100:19-40
Vyhnal CR, McSween HY Jr, Speer JA (1991) Hornblende chemistry in southern Appalachian granitoids: implications for aluminum hornblende thermobarometry and magmatic epidote stability. Am Mineral 76:176-188
Wakita H, Rey P, Schmitt RA (1971) Abundances of 14 rare earth elements and 12 other elements in Apollo 12 samples: five igneous and one breccia rocks and four soils. 2nd Lunar Science Conference, Supplement 2 (2):1319-1329. Geochim Cosmochim Acta
Ward CD, McArthur JM, Walsh JN (1992) Rare earth element behaviour during evolution and alteration of the Dartmoor granite, SW England. J Petrology 33:785-815
Watson MD, Snyman CP (1975) The geology and the mineralogy of the fluorite deposits at the Buffalo fluorspar mine on Buffelsfontein, 347KR, Naboomspruit district. Trans Geol Soc South Africa 78:137-151
Weber WJ (1990) Radiation-induced defects and amorphization in zircon. J Mater Res 5:2687-2697
Weber WJ, Ewing RC, Catlow CRA, Diaz de la Rubia T, Hobbs LW, Kinoshita C, Matzke H, Motta AT, Nastasi M, Salje EKH, Vance ER, Zinkle SJ (1998) Radiation effects in crystalline ceramics for the immobilization of high-level nuclear waste and plutonium. J Mater Res 13(6):1434-1484
Weiss S (2002) Allanit aus alpinen Klüften (I). Lapis 9:29-43 (in German)
Weiss S, Parodi GC (2002) Allanit aus alpinen Klüften (II). Lapis, 10, 24-28 (in German)
Williams GH (1893) Piedmontite and scheelite from the ancient rhyolite of South Mountain, Pennsylvania. Amer J Sci 46:50-57
Wing B, Ferry JM, Harrison TM (2003) Prograde destruction and formation of monazite and allanite during contact and regional metamorphism of pelites: petrology and geochronology. Contrib Mineral Petrol 145: 228-250
Wood SA (1990) The aqueous geochemistry of rare earth elements and yttrium. 2. Theoretical predictions of speciation in hydrothermal solutions to 350°C at saturated water pressure. Chem Geol 88:99-125
Wood SA, Ricketts A (2000) Allanite-(Ce) from the Eocene Casto Granite, Idaho: Response to Hydrothermal Alteration. Can Mineral 38:81-100
Yang JJ and Enami M (2003) Chromian dissakisite-(Ce) in a garnet lherzolite from the Chinese Su-Lu UHP metamorphic terrane: Implications for Cr incorporation in epidote minerals and recycling of REE into the Earth's mantle. Am Mineral 88:604-610
Zakrzewski MA, Lustenhouwer WJ, Nugteren HJ, Williams CT (1992) Rare-earth mineral yttrian zirconolite and allanite-(Ce) and associated minerals form Koberg mine, Bergslagen, Sweden, Mineral Mag 56: 27-35
Zdorik TB, Kupriyanova II, Kumskova NM (1965) Crystalline orthite from some metasomatic formations in Siberia. Mineraly SSSR 15:208-214, Izd. Nauka, Moscow (in Russian)
Zen E-an, Hammarstrom JM (1984) Magmatic epidote and its petrologic significance. Geology 12:515-518

Zen E-an, Hammarstrom JM (1986) Reply on the comments on "Implications of magmatic epidote-bearing plutons on crustal evolution in accreted terranes of northwestern North America" and "Magmatic epidote and its petrologic significance" by A.J. Tulloch and by R.H. Moench. Geology 14:188-189

Zenzén N (1916) Determinations of the power of refraction of allanites. Acta Universitatis Upsaliensis, Bulletin of the Geological Institute 15:61-76

Zhirov KK, Bandurkin GA, Lavrentiev YuG (1961) To the geochemistry of rare-earth elements in pegmatites of north Karelia. Geokhimiya 11:995-1004 (in Russian)